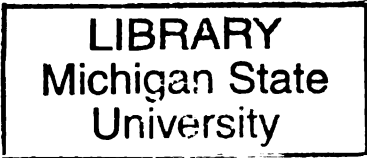


2
010



This is to certify that the
dissertation entitled

**CHARACTERIZATION OF THE *FREMYELLA DIPLOSIPHON*
PHOTORECECTOR RcaE AND ITS ROLE IN
COMPLEMENTARY CHROMATIC ADAPTATION**

presented by

Juliana Rose Bordowitz

has been accepted towards fulfillment
of the requirements for the

Doctoral degree in Cell and Molecular Biology

Major Professor's Signature

10/19/2009

Date

CHARACTERIZATION OF THE *FREMYELLA DIPLOSIPHON* PHOTORECEPTOR
RcaE, AND ITS ROLE IN COMPLEMENTARY CHROMATIC ADAPTATION

By

Juliana Rose Bordowitz

A DISSERTATION

Submitted to
Michigan State University
in partial fulfillment of the requirements
for the degree of

DOCTOR OF PHILOSOPHY

Cell and Molecular Biology

2009

ABSTRACT

CHARACTERIZATION OF THE *FREMYELLA DIPLOSIPHON* PHOTORECEPTOR RcaE AND ITS ROLE IN COMPLEMENTARY CHROMATIC ADAPTATION

By

Juliana Rose Bordowitz

Fremyella diplosiphon is a freshwater filamentous cyanobacterium that possesses the ability to sense and adapt to changes in ambient light. In a process called complementary chromatic adaptation (CCA), which is predominantly responsive to red light (RL) and green light (GL), the cyanobacterium enhances its photosynthesis by altering the phycobiliprotein composition of its light-harvesting antennae. RcaE, a phytochrome-class photoreceptor, is required for CCA to occur (Kehoe and Grossman, 1996, *Science*, 273:1409-12). In addition to the pigmentation phenotype associated with CCA, early micrograph studies showed that wild-type (WT) *F. diplosiphon* displays different cell morphologies under GL and RL conditions (Bennett and Bogorad, 1973, *J Cell Biol*, 58:419-35).

Microscopic and biochemical analyses confirmed that WT *F. diplosiphon* strains maintain distinct RL and GL morphologies. Further, analyses of an RcaE null mutant strain (FdBk14) showed that RcaE regulates filament length and cell shape in response to RL and GL. Light-shifting experiments demonstrated that RcaE regulation of light-dependent morphology is photoreversible. Lysozyme-sensitivity experiments with WT and FdBk14 strains established a light-dependent alteration in cell wall integrity associated with the observed morphology differences, thus establishing that RcaE-regulated changes in cellular morphology are correlated with modifications of cell wall structure or composition. Identification and mRNA expression analyses of the cell-

shape-determining *mre* genes from *F. diplosiphon* demonstrated that *mre* expression is RcaE-regulated. RT-PCR analyses showed that the expression of *mre* genes was down-regulated in the FdBk14 strain, indicating that RcaE controls expression of the gene encoding bacterial actin MreB, a cytoskeletal component involved in the regulation of cell shape in many prokaryotic systems.

Sequence analysis of RcaE indicates similarity to plant phytochromes in its N-terminus, as well as to two-component histidine kinases in its C-terminus (Kehoe and Grossman, 1996). In addition, RcaE contains conserved GAF, PAS and Hbox domains which have been associated with chromophore attachment, signal sensing, and phospho-transfer, respectively (Kehoe and Gutu, 2006, *Annu Rev Plant Biol*, 57:127-50). To determine the role of these domains in RcaE's regulation of CCA, a mutational analysis approach was taken. Mutation of residues within the GAF domain resulted in defects in both pigmentation and cellular morphology. Mutating a cluster of conserved residues within the PAS domain showed that this domain was essential for GL-regulated cellular morphology. Further, mutating a conserved histidine within the Hbox domain confirmed that this residue contributes to the *in vivo* biochemical activity of RcaE, as both pigmentation and morphology were affected. These studies established that the GAF, PAS and Hbox domains all contribute to the regulation of CCA. Therefore, the analyses in this dissertation work have contributed significantly towards understanding the molecular basis of the photoregulation of cellular morphology in *F. diplosiphon*, as well as advanced our knowledge of the biochemical mechanisms utilized by RcaE in its regulation of CCA.

This dissertation is dedicated to the memory of P.F. Bordowitz for his encouragement and inspiration, and to D.R.Weldon and W.F.Weldon for their immeasurable support.

ACKNOWLEDGMENTS

It cannot go unmentioned that earning a PhD takes more than just the drive and desire of the pursuant. Many people over the last 5 years have been very instrumental in this journey for me, and I'd like to acknowledge and thank them here.

First and foremost, I'd like to thank my advisor, Dr. Beronda Montgomery-Kaguri, for giving me the opportunity to work on such an interesting project. Throughout the last 4 ½ years her enthusiasm and support has never wavered. When I started in Beronda's lab, I had very little experience working with cyanobacteria; her patience during my transition from plant to cyanobacterial work gave me the confidence I needed to proceed from my rotation into my thesis project. Beronda's open-door policy and mentoring has fostered my progression from student to scientist, and prepared me well for my post-doctoral venture. I'm extremely grateful for her infinite optimism, and for making her lab such a positive place to evolve into a scientist.

I'd also like to thank the core members of the lab: Melissa Whitaker, Sankalpi Warnasooriya, and Bagmi Pattanaik. Without them, everyday life in the lab would have been boring! Over the years, we have had innumerable conversations about experimental design, data analyses, and final data representation. This has been a critical part of my development as a scientist, and I greatly appreciate having had the opportunities to share my ideas and receive thoughtful and constructive feedback. I also appreciate our constant reminders to each other of the "be positive" lab motto... such encouragement has made days of negative results bearable! And, in the midst of all the science, we always managed to laugh, which is what has made the BMK lab so much fun to be a part of.

In addition, I was also fortunate to have worked with a number of amazing undergrads while completing my thesis work. Whether they were MSU students, or summer interns, Michaela TerAvest, Tashiba Nelson, Taina Theodore, and Adrienne Williams have all contributed to many protocol optimizations and head scratching moments. I appreciate the opportunity to have mentored such enthusiastic students, and wish them all the best of luck with their futures!

To my fellow CMB colleagues, who started this journey with me—you have become my “Michigan family”. I’d especially like to thank Laura Lamb, Charlie Miller, Aaron DeWard, Eric Marrotte, and Sebla Kutluay—many nights we spent studying in the BPS fishbowl. From the infamous 801 study groups as first year students, to preparing for our prelims, and finally to practicing our defense talks; we have always been there for each other, and there is no way I would have gotten through this without your support! Along the way, we established friendships that I know will last a lifetime! I’d also like to say thank you to fellow CMB’er and best friend, Danielle Nevarez for being the most awesome roommate ever, and for being a part of this journey since our college days back at the University of Arizona! Finally, to Aaron McBride, Wanessa Wight, and Jamie Kooper, who are also fellow CMB’ers— thanks for always being available for practice talks, and participating in CMB social events!

Finally, I’d like to thank those in my family who have continued to encourage me through all of this! It has been hard being all the way across the country, but having their support has meant the world to me. I’d especially like to thank my little sister Donna, and my little brother Bobby, who have had to deal with my absence since I went away for college. While I know they would have preferred me to be closer to home, their love and

understanding have helped me to focus on achieving my goals. And, if it weren't for my family in Hobart, IN, the homesickness would have been unbearable! Thank you Uncle Mike and Aunt Deb for giving me a place to call "home"! Thank you for making me a part of all the holidays and big family moments over the last 5 years. And, thank you Allie, Paige and Claire for being the best little cousins in the world, and sharing your mom and dad with me!

TABLE OF CONTENTS

LIST OF TABLES	x
LIST OF FIGURES	xi
KEY TO ABBREVIATIONS.....	xiii
CHAPTER ONE	
Introduction/Literature Review.....	1
1.1 Importance of Photoperception.....	2
1.2 <i>Fremyella diplosiphon</i> and Complementary Chromatic Adaptation	2
1.3 Phytochrome-like Photoreceptor RcaE.....	5
1.4 Phytochromes.....	5
1.5 Phytochrome Signaling.....	7
1.6 Two-Component Systems.....	9
1.6.1 Histidine Kinases	10
1.6.2 Response Regulators.....	12
1.7 The RcaE-Mediated CCA Signaling Pathway.....	13
1.7.1 A Complex Phosphorelay Cascade.....	13
1.7.2 Transcriptional Regulation of PBP Operons.....	14
1.7.3 The CCA Signaling Model	16
1.8 The Biochemical Role(s) of RcaE in CCA Signaling.....	16
1.8.1 GAF Domains	17
1.8.2 PAS Domains.....	20
1.8.3 Hbox Domains	21
1.9 Research Aims	21
REFERENCES	25
CHAPTER TWO	
RcaE Regulates Cell and Filament Morphology	29
2.1 Introduction.....	30
2.2 Methods.....	32
2.3 Results.....	41
2.3.1 Characterization of the light-dependent cell and filament morphologies of wild-type and RcaE-deficient cells.....	41
2.3.2 RcaE regulates cellular morphology in <i>F. diplosiphon</i> during CCA.....	45
2.4 Discussion	55
REFERENCES	57
CHAPTER THREE	
RcaE Controls the Expression of Cell-Shape-Determining Genes.....	60
3.1 Introduction.....	61
3.2 Methods.....	62
3.3 Results.....	69

3.3.1 Light-dependent cell wall alteration	69
3.3.2 Effect of A22 on <i>F. diplosiphon</i> cell lengths and widths	72
3.3.3 <i>F. diplosiphon</i> contains an <i>mreBCD</i> operon.....	76
3.3.4 Verification of <i>mreB</i> copy number in <i>F. diplosiphon</i>	77
3.3.5 Light-regulated <i>FdmreBCD</i> gene expression	80
3.4 Discussion	81
REFERENCES	86
CHAPTER FOUR	
<i>In vivo</i> Biochemical Characterization of RcaE.....	88
4.1 Introduction.....	89
4.2 Methods.....	92
4.3 Results.....	96
4.3.1 CCA Pigmentation Response.....	96
4.3.2 Phycobiliprotein Accumulation	100
4.3.4 Cellular Morphology Response	106
4.4 Discussion	112
REFERENCES	116
CHAPTER FIVE	
Conclusions/Perspectives.....	118
5.1 Light-Dependent Regulation of Cellular Morphology in <i>F. diplosiphon</i>	119
5.2 Biochemical Characterization of RcaE.....	122
5.3 Perspectives.....	124
REFERENCES	128
APPENDICES	129
APPENDIX A1	
Sequencing of <i>F. diplosiphon</i> shuttle vector pPL2.7.....	130
APPENDIX A2	
Determining Imaging Parameters for <i>F. diplosiphon</i> PBP	
Autofluorescence	135
APPENDIX A3	
Homology Modeling of <i>F. diplosiphon</i> GAF-PAS Domain.....	140
REFERENCES	145

LIST OF TABLES

Table 2.1. Median filament lengths and numbers of cells of <i>F. diplosiphon</i> strains under GE-WL or RE-WL	42
Table 2.2. Median filament lengths and numbers of cells of <i>F. diplosiphon</i> strains under broad-band GL or RL	46
Table 3.1. Primers used for isolation and identification of <i>F. diplosiphon mreBCD</i> operon, generation of probes for Southern blot analyses, and RT PCR analyses.....	67
Table 3.2. Predicted number of restriction enzyme sites for <i>mreB</i> and <i>cpeB</i> in <i>F. diplosiphon</i> genome.....	79
Table 4.1. Primers used for RcaE cloning and mutagenesis	94
Table 4.2. Median cell lengths for SF33, FdBk14, and FdBk14 transformed with RcaE mutant variants in GL and RL.....	109
Table A1.1. Primers used for sequencing <i>F. diplosiphon</i> shuttle vector pPL2.7	133
Table A2.1. Spectral emission collections after excitation with 488, 543, and 633 nm laser lines.....	137

LIST OF FIGURES

Images in this dissertation are presented in color

Figure 1.1. Characteristics of Complementary Chromatic Adaptation in WT <i>Fremyella diplosiphon</i>	4
Figure 1.2. Depiction of RcaE: A Phytochrome-related Photoreceptor	6
Figure 1.3. Simplified Model of a Two-Component System.....	11
Figure 1.4. Simplified Model for CCA Signaling Pathway	15
Figure 1.5. Sequence Alignment of GAF Domains	18
Figure 2.1. Range of Filament Lengths of <i>F. diplosiphon</i> Strains Grown Under Broad-band GL or RL.....	38
Figure 2.2. Cell Morphologies of the WT and SF33 <i>F. diplosiphon</i> Strains in GE-WL and RE-WL	42
Figure 2.3. Morphological Differences Between <i>F. diplosiphon</i> Strains in Broad-band GL and RL	46
Figure 2.4. Complementary Chromatic Adaptation in Wild-type <i>F. diplosiphon</i> Strains, FdBk14, and FdBk14 transformants	47
Figure 2.5. Phycobiliprotein Ratios and Immunoblot Analysis of RcaE Accumulation in WT and SF33 Strains, the FdBk14 mutant, and FdBk14 transformants	48
Figure 2.6. Phycobiliprotein Autofluorescence of <i>F. diplosiphon</i> Strains in Broad-band GL and RL	50
Figure 2.7. Median Cell lengths and Cell Morphologies of <i>F. diplosiphon</i> Strains in Light-shifting Experiments.....	53
Figure 3.1. Lysozyme-sensitivity Assays for <i>F. diplosiphon</i> Strains	71
Figure 3.2. <i>F. diplosiphon</i> Morphological Difference Between A22-treated Strains in GL and RL	74
Figure 3.3. Cell Length and Width Responses of <i>F. diplosiphon</i> to Treatment with MreB Inhibitor A22.....	75

Figure 3.4. Organization of <i>mreBCD</i> Operon in <i>F. diplosiphon</i> Genome.....	78
Figure 3.5. BLASTn (nt database) Results of Cloned <i>FdmreBCD</i> Operon Components	78
Figure 3.6. <i>F. diplosiphon mreB</i> Southern Blot Analysis.....	79
Figure 3.7. mRNA Expression Analyses of <i>F. diplosiphon mre</i> Genes	82
Figure 4.1. Depiction of Newly Constructed RcaE Mutants	95
Figure 4.2. CCA Pigmentation Analyses in SF33, FdBk24, and RcaE Mutants	98
Figure 4.3. Chl <i>a</i> and Phycobiliprotein Levels in SF33, the FdBk14 Mutant, and FdBk14 Transformed with RcaE Mutant Variants	101
Figure 4.4. Phycobiliprotein Ratios and Immunoblot analysis of RcaE in SF33, the FdBk14 mutant, and FdBk14 Transformed with RcaE Mutant Variants	104
Figure 4.5. Morphological Differences Between of SF33, FdBk14, and FdBk14 Transformed with RcaE Mutant Variants in GL and RL.....	108
Figure A1.1 <i>F. diplosiphon</i> Shuttle Vector pPL2.7	134
Figure A2.1. Spectral Emission Collection of SF33 GL-grown Cells after Excitation with 543 nm laser.....	138
Figure A2.2. Spectral Emission Collection of SF33 RL- grown Cells after Excitation with 543 nm laser.....	139
Figure A3.1. Secondary Structure Predictions of RcaE GAF-PAS Domains.....	143
Figure A3.2. PyMOL images of DrCBD and Homology Modeled RcaE GAF-PAS domains	144

KEY TO ABBREVIATIONS

A22	MreB inhibitor
A ₇₅₀	absorbance at 750 nm
A ₈₀₀	absorbance at 800 nm
Ala	alanine
AP	allophycocyanin
At	<i>Arabidopsis thaliana</i>
ATP	adenosine triphosphate
ATPase	adenosine triphosphatase
attB1/2	Gateway® cloning sites
BG-11	blue green medium
bps	base pairs
C or Cys	cysteine
CBD	chromophore-binding domain
CCA	complementary chromatic adaptation
CDP-Star	chemiluminescent substrate for alkaline phosphatase
cDNA	complementary DNA
chl <i>a</i>	chlorophyll a
CLSM	confocal laser scanning microscope
Cph1	cyanobacterial phytochrome 1
C-terminus	carboxy-terminus
D or Asp	aspartate

DIC	differential interference contrast
DIG	digoxigenin
Dim	dimerization domain
DNA	deoxyribonucleic acid
EDTA	ethylenedinitrilotetraacetic acid
Fd	<i>Fremyella diplosiphon</i>
FdBk14	rcaE null mutant strain
FdR	<i>F. diplosiphon</i> red mutants
GAF	cGMP-specific and –stimulated phosphodiesterases, <i>Anabena</i> adenylate cyclases and <i>E. coli</i> FhlA
gDNA	genomic DNA
GE-WL	green-enriched white light
GL	green light
Gro-Lux	F20T12/GRO Gro-Lux fluorescent bulbs for RE-WL
H or His	histidine
Hbox	sub-domain of his-kinase domain
HK	histidine kinase
Hpt	histidine containing phosphotransfer domain
HRP	horseradish peroxidase
IQR	interquartile range
Kan	kanamycin
kb	kilobases
mRNA	messenger RNA
nt	nucleotides

N-terminus	amino-terminus
OD	optical density
PAS	<i>Drosophila</i> <u>P</u> ER (period clock protein), mouse <u>A</u> RNT (aryl hydrocarbon receptor nuclear transporter), and <i>Drosophila</i> <u>S</u> IM (single-minded protein)
PBP	phycobiliprotein
PBS	phycobilisome
PC (PCi)	inducible phycocyanin
PCc	constitutive phycocyanin
PCR	polymerase chain reaction
PDVF	polyvinylidene flouride immobilin-P transfer membrane
PE	phycoerythrin
Pfam	protein families database
Pfr	far-red-light absorbing phytochrome
PG	peptidoglycan
phy	phytochrome
PIF3	phytochrome-interacting factor 3
PIFs	phytochrome-interacting factors
PL/AQ	F20T12/PL/AQ wide-spectrum fluorescent bulbs for GE-WL
PKS1	phytochrome kinase substrate 1
Pr	red-light absorbing phytochrome
PS II	photosystem II reaction center
PYP	photactive yellow protein
qRT-PCR	quantitative real time polymerase chain reaction

Rca	regulator of chromatic adaptation
RE-WL	red-enriched white light
RFU	relative fluorescence units
RL	red light
RNA	ribonucleic acid
RR	response regulator
RT-PCR	reverse transcription –polymerase chain reaction
SDS-PAGE	sodium dodecoylsulfate polyacrylamide gel electrophoresis
Syn	<i>Synechocystis</i>
TCS	two-component system
TE buffer	tris-EDTA buffer
TM	thylakoid membrane
Tyr or Y	tyrosine
WL	white light
WT	wild-type

CHAPTER ONE

Introduction/Literature Review

1.1 Importance of Photoperception

Sensing light is one of the most indispensable abilities for organisms that depend on light for photosynthesis. Hence, the developmental changes that occur upon light perception are amongst the most important adaptive responses that photosynthetic organisms possess. It is critical that such organisms maintain a way to perceive light, in order to maximize its utilization for their survival. Not only does light provide energy derived from photosynthesis, but it also acts as signals which are important input factors in adaptive mechanisms required for survival.

For example, plants have highly developed mechanisms which allow them to monitor and perceive different wavelengths, quality, and periodicity of light (reviewed in Franklin and Whitelam, 2004; Matthews, 2006). The ability to do so allows these sessile organisms to adapt to a given environment, and proceed with their growth and developmental processes. This ability is a biological process known as photomorphogenesis and enables photosynthetic organisms to respond and adapt in order to optimally thrive in changing environmental light conditions. Like plants, photosynthetic cyanobacteria also possess the ability to alter their growth in response to changes in their light environment. One particular process is called complementary chromatic adaptation (CCA), and the model organism in which it is studied (*Fremyella diplosiphon*), was the major focus of this work.

1.2 *Fremyella diplosiphon* and Complementary Chromatic Adaptation

Fremyella diplosiphon is a freshwater, filamentous cyanobacterium (also referred to as *Calothrix* sp. strain PCC 7601). *F. diplosiphon* possesses the ability to sense and

acclimate to changes in its ambient light environment via a process called CCA (Tandeau de Marsac, 1977). This process, which is predominantly responsive to red light (RL) and green light (GL), is the most well-studied photomorphogenic process in cyanobacteria. During CCA, a cyanobacterium enhances its photosynthesis by altering the phycobiliprotein composition of its light-harvesting antennae in order to efficiently utilize the light in its environment.

In *F. diplosiphon*, the light-harvesting complex is the phycobilisome (PBS), which is composed primarily of three phycobiliproteins: allophycocyanin (AP; λ_{\max} of 650 nm), phycoerythrin (PE; λ_{\max} of 560 nm), and phycocyanin (PC; λ_{\max} of 620 nm) (reviewed in Tandeau de Marsac 1983; Stowe-Evans and Kehoe, 2004). AP and several associated linker proteins make up the core of the structure, while PE and PCi (inducible PC) are contained within the light-harvesting rods (Figure 1.1A). Immediately proximal to the AP core proteins is a set of constitutive PC proteins (PCc), which like AP, do not change accumulation during CCA. When wild-type (WT) *F. diplosiphon* cells are grown under RL conditions, the rods of PBSs accumulate PCi (hereafter PC), the RL-induced phycobiliprotein, yielding a blue-green color phenotype (Figure 1.1B and C, left), and a more rounded cellular morphology (Figure 1.1D, left; Bennett and Bogorad, 1973). Under GL conditions, the rods of the PBSs accumulate PE, the GL-induced phycobiliprotein, yielding a red color phenotype (Figure 1.1B and C, right), with an elongated, brick-like cellular morphology (Figure 1.1D, right; Bennett and Bogorad, 1973). CCA allows for this RL-GL reversible responsiveness (Tandeau de Marsac 1977; Stowe-Evans and Kehoe, 2004).

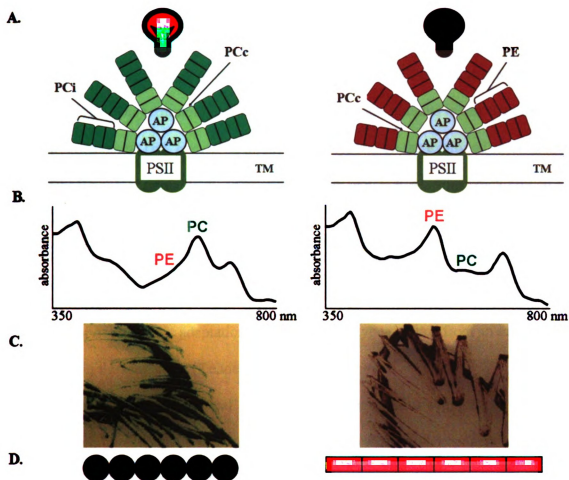


Figure 1.1. Characteristics of Complementary Chromatic Adaptation in WT *Fremyella diplosiphon*. **A.** PBS composition under RL (left) and GL (right) conditions. The PBS core is comprised of AP, and associated linker proteins. The inner rods of the PBS are comprised of PCc. Under RL conditions the outer PBS rods accumulate the RL-inducible PBP PCi, while under GL conditions they accumulate the GL-inducible PBP PE. **B.** Whole-cell absorbance spectral scans illustrating the maximum absorbance peaks of PBP accumulation under RL (left) and GL (right) conditions. **C.** Cellular pigmentation response to RL (left) and GL (right). Under RL conditions, cells are green, while under GL conditions cells are brick-red. **D.** Morphological response to RL (left) and GL (right), adapted from Bennett and Bogorad, 1973. Cells grown in RL are more rounded and compact, while cells grown in GL are more elongated and brick-like in shape.

1.3 Phytochrome-like Photoreceptor RcaE

In a screen for CCA pigmentation mutants, a strain designated FdBk14 was isolated, which exhibits a black phenotype under both RL and GL conditions (Kehoe and Grossman, 1996). The terminology used for describing color mutants in this organism is based first on the name (Fd, *Fremyella diplosiphon*), second on the exhibited color of the mutant, (Bk, Black), and finally on isolate number (14, isolate #14). This black mutant accumulates both PE and PC, regardless of the light conditions under which it is grown (Kehoe and Grossman, 1996; Terauchi *et al.*, 2004). Using a genetic complementation approach, a gene was identified that is required for the RL-GL responsiveness and named *rcaE*, regulator of chromatic adaptation; the black phenotype resulted from an insertional mutation within the *rcaE* gene (Kehoe and Grossman, 1996).

Sequence analysis of the RcaE protein revealed similarities with plant phytochrome photoreceptors in its N-terminus, as well as with two-component histidine kinases in its C-terminus (Figure 1.2; Kehoe and Grossman, 1996). Further, protein families database (Pfam; Bateman *et al.*, 2004) analysis confirmed the presence of additional conserved domains which are associated with chromophore attachment, signal sensing, and protein-protein interactions (Kehoe and Gutu, 2006) and will be discussed in more detail in section 1.8.

1.4 Phytochromes

Photoreceptors are light-sensitive proteins which are involved in the sensing of and responses to light. One of the most well studied families of photoreceptors is the phytochrome family (phys). Classically, phys are red/far-red reversible photoreceptors in

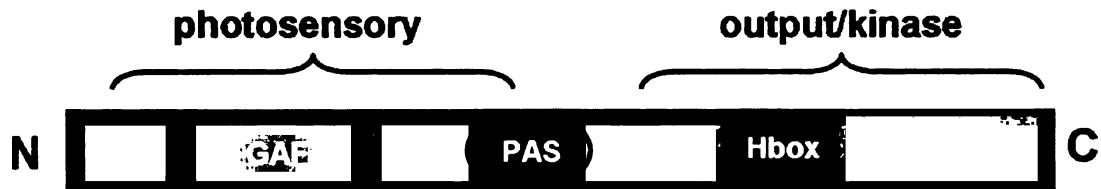


Figure 1.2. Depiction of RcaE: A Phytochrome-related Photoreceptor. Sequence analysis of RcaE shows N-terminal similarity to the photosensory regions of phytochromes, whereas the C-terminal end shows similarity to bacterial output/kinase domains. Further Pfam analyses of this 655 amino acid protein, with a predicted molecular weight of 74 kDa, confirms the presence of distinct conserved domains. GAF: chromophore-binding domain present in phytochromes (Pfam PF01590). PAS: domain involved in signaling proteins; signal sensor domain (Pfam PF00989). H-box: motif found in the histidine kinase domain; phospho-acceptor site (Pfam PF00512)

higher plants that are involved in light perception and photomorphogenic responses (reviewed in Chen *et al.*, 2004; Schepens *et al.*, 2004; Rockwell *et al.*, 2006). These light-dependent responses span the entire life cycle of the plant and range from seed germination, to seedling development and flowering, and finally senescence (reviewed in Franklin *et al.*, 2005; Matthews, 2006).

Originally, phys were thought to be present in only plants and algae; however, during studies on CCA in cyanobacteria, Kehoe and Grossman (1996) discovered the first prokaryotic phytochrome-like protein, RcaE, in *F. diplosiphon*. This discovery motivated the search for similar proteins throughout sequenced organisms and it is now known that they exist not only in plants and cyanobacteria, but in bacteria and fungi as well (Karniol *et al.*, 2005; Lariguet and Dunand, 2005; Montgomery and Lagarias, 2002).

Because of the prevalence of phys in plants, bacteria, and fungi, it has been proposed that higher plant phys evolved from a cyanobacterial precursor, the progenitor of chloroplasts in plants. Overall sequence conservation amongst the phylogenetic classes of phys strongly indicates a conserved function (Vierstra, 2003; Montgomery and Lagarias, 2002). More distinctly, the presence of phy-like proteins in photosynthetic prokaryotes and their sequence similarity to plant phys indicates that the mechanisms of light perception and signal output may be similar.

1.5 Phytochrome Signaling

Phy structure and function have been the topic of many reviews (Franklin *et al.*, 2005; Matthews, 2006; Rockwell *et al.*, 2006). Of particular interest is the existence of multiple copies of phys in some species, including higher plants. The prevalence of phy

gene families indicates strong functional importance; multiple gene copies most often indicate critical functions. For example, the model organism *Arabidopsis thaliana* has five phy, phyA-phyE, which have been shown to have unique as well as redundant roles in plant growth and development (reviewed in Schepens *et al.*, 2004; Franklin and Whitelam, 2004; Matthews, 2006). However, the existence of a gene family makes studies to determine distinct phy function somewhat difficult.

The phy apoprotein (non-chromophorylated) is encoded by nuclear gene(s) (e.g., *A. thaliana* *PHYA-PHYE*); the translated messenger RNA is then exported to the cytosol, the apoprotein is transcribed and then assembles with the light-absorbing, plastid synthesized linear tetrapyrrole (bilin) to become a functional phy (holoprotein). The phy apoprotein requires the covalent attachment of a linear tetrapyrrole prosthetic group in order to become photoactive and maintain photochemical function (Hanzawa *et al.*, 2002 and Gyula *et al.*, 2003). Traditionally, phys exist in two photo-interconvertible forms: the inactive red-light absorbing (Pr) and the active far-red-light absorbing (Pfr). When the inactive Pr form absorbs red light, the chromophore undergoes a conformational change and the molecule converts to the active Pfr isoform. This phenomenon is a photoreversible process; the ability of the bilin chromophore to undergo photoisomerization is what allows holophytochromes to absorb different light wavelengths and thus differ in the response to red light and far-red light (reviewed in Chen *et al.*, 2004 and Rockwell *et al.*, 2006).

Although decades of research have gone into understanding how plant phys function, the complete signaling mechanism still remains unclear. Sequence comparisons strongly indicate that they may act as light-regulated kinases, based on the large

conservation of histidine-kinase related domains (Chen *et al.*, 2004, and Karniol *et al.*, 2005). Additionally, identification of phy interacting factors (PIFs) and insight into their roles as transcriptional regulators (reviewed in Gyula *et al.*, 2003), has helped strengthen the postulated serine/threonine kinase activity of phys. More specifically, the identification and characterization of phy-dependent phosphorylation of PIF3 (Al-Sady *et al.*, 2006), and phytochrome kinase substrate 1 (PKS1; Fankhauser *et al.*, 1999) indicates the requirement for phosphotransfer to occur in order to elicit the phy-mediated photomorphogenic responses. Despite the unknowns, it is clear that upon photoconversion of phys and translocation into the plant nucleus, their associated signal transduction cascades are activated.

Studies with cyanobacteria and other prokaryotic systems have begun to aid in the understanding of how light-regulated signaling in these organisms might occur. For example, the study of CCA in *F. diplosiphon* has provided a model system for such mechanisms, since a phenotype is easily observed, and genes can be easily assessed via genetic manipulation. Understanding how CCA is regulated in *F. diplosiphon* will allow the function of the proteins involved in signaling to be assessed. Hence, continuation of the prokaryotic research will undoubtedly yield valuable information that could increase our understanding of the signaling mechanisms utilized by phytochrome-class photoreceptors in general.

1.6 Two-Component Systems

Bacteria often utilize two-component systems (TCS) to adapt to changes in their environment. Typically, each TCS is composed of a signal sensor, most often a histidine kinase (HK), and a signal transmitter, i.e. a response regulator (RR) that transmits the

signal and often results in transcriptional regulation. These systems work via a phosphoryl transfer cascade that is tightly regulated by specific domains and/or residues within these domains (see Figure 1.3). The organization and function of domains in these proteins will be addressed in the following sections.

1.6.1 Histidine Kinases

Each prototypical HK contains specific conserved domains/motifs that function in signal sensing, molecule dimerization, and histidine kinase activity. All of these activities are crucial for the function of the sensor molecule in order to relay the signal to the RR. Typically the N-terminal portion of the HK contains the input domain (sensor domain) which controls the activity of the transmitter domain. The sensor domain is the portion of the molecule which senses the environmental stimuli. The C-terminal transmitter module contains specific motifs including a dimerization domain (Dim), a histidine-containing phosphotransfer domain (Hpt), and a kinase/phosphatase ATP binding domain (reviewed in Parkinson and Kofoed, 1992; Chieri Tomomori and Ikura, 2003).

The Hpt domain of HKs contain a conserved His residue, which is phosphorylated by the ATP binding domain. The kinase/phosphatase domain is the core domain of HKs. This domain is multifunctional because it is responsible for autophosphorylation of HK dimers, and for phosphorylation/dephosphorylation of the conserved Asp residue in the downstream RR. This feature is what allows many HKs to act as bi-functional enzymes—i.e., it allows HKs to act as both a kinase and a phosphatase. To facilitate the activity of this domain along with the Hpt domain, the Dim domain brings these other domains together in close proximity, which enables multiple reactions during the signal

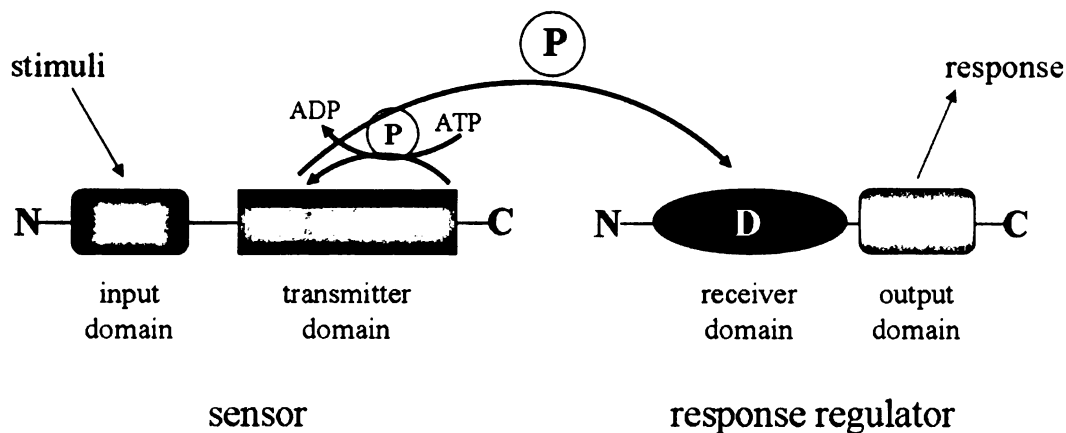


Figure 1.3. Simplified Model of a Two-Component System. Bacterial two-component systems are comprised of a sensor molecule (left) and a response regulator (right). The input domain of the sensor molecule senses the environmental stimuli, which triggers the transmitter domain to utilize ATP and auto-phosphorylate at the conserved His residue (H), in turn activating phosphoryl transfer (arrows with circled P) to the response regulator. The conserved Asp residue (D) in the receiver domain accepts the transferred phosphate, allowing the output domain to activate a response. N and C indicate amino- and carboxy-terminal ends, respectively. Figure adapted from Parkinson and Kofoid, 1992.

relay to occur simultaneously (reviewed in Chieri Tomomori and Ikura, 2003).

While HKs and TCS are most prevalent in bacteria (Parkinson and Kofoid, 1992), hybrid HKs in eukaryotes and the discovery of similar, yet more complex molecules and related signaling systems (e.g. phytochrome signaling) have begun to be identified in many bacteria as well as higher organisms (Vierstra, 2003). By applying what has been discovered in bacterial systems, such complex systems may begin to be elucidated. For example, the discovery of conserved motifs in the C-terminal histidine kinase domain of RcaE suggests that RcaE likely functions in a TCS in order to initiate expression of the genes responsible for CCA (Kehoe and Grossman, 1997).

1.6.2 Response Regulators

The second part of TCS is the signal transmitters—i.e., RRs. Typically RRs are comprised of a receiver domain and an output domain (see Figure 1.3). The receiver domain contains the conserved aspartate residue (D), which is required for accepting the phosphate transferred from a cognate HK (reviewed in Parkinson and Kofoid, 1992; Chieri Tomomori and Ikura, 2003). The RR output domain (e.g. DNA binding domain), is responsible for initiating the downstream response, which may result in transcriptional regulation (reviewed in Parkinson and Kofoid, 1992). In fact, most RRs that contain DNA-binding domains are characterized as DNA-binding transcription factors (Parkinson and Kofoid, 1992).

Although the domain architecture of RRs can vary (Parkinson and Kofoid, 1992), the conserved aspartate residue must be present in order to receive the phosphate from the HK, and thus be part of a TCS. Evaluation of the variation in RRs domain architecture (as well as HKs) has revealed recognizable systems that have more complex signal relays

which incorporate these kinds of molecules (reviewed in Vierstra, 2003). For example, the *F. diplosiphon* RRs RcaF and RcaC in the CCA signaling pathway have very different domain architecture (see section 1.7.1).

1.7 The RcaE-Mediated CCA Signaling Pathway

1.7.1 A Complex Phosphorelay Cascade

The current proposed model for RcaE signaling in CCA has arisen from the identification of RcaE as well as downstream RR components (Kehoe and Grossman, 1996; Kehoe and Grossman, 1997; Chiang *et al.*, 1992). The pathway is a complex phosphorelay system, based on the presence of two RR components. The two RRs that have been identified in this signaling pathway have been well characterized. The first RR, RcaF, is directly downstream of RcaE, both in the *F. diplosiphon* genome as well as in the proposed signaling pathway (Kehoe and Grossman, 1997). RcaF was identified in an attempt to isolate and characterize CCA signaling components. In this screen, pigmentation mutants were identified that exhibited insertional mutagenesis in the gene *rcaF* (Kehoe and Grossman, 1997). Further analyses of the mutants obtained in this study revealed that mutations in both the C-terminal portion of RcaE (the HK portion) as well as the receiver domain of RcaF resulted in the inability to maintain CCA (i.e., red phenotype under RL). Because of the similarity of RcaF to the Spo0F and CheY RRs, and the fact that it does not contain an output domain, its role was proposed to be purely for phospho-acceptance from RcaE and thus phospho-transfer to the cognate RR RcaC (Kehoe and Grossman, 1997).

The more canonical RR in this pathway, RcaC, was originally identified and characterized for its ability to complement previously isolated FdR mutants (Chiang *et al.*, 1992). Sequence analysis indicated that RcaC is a protein analogous to those involved in bacterial two-component systems. RcaC contains two receiver domains which each contain conserved aspartate residues. In between the receiver domains, resides a prototypical histidine phosphate transfer (HPt) domain, which is flanked by a DNA-binding domain (Chiang *et al.*, 1992; Kehoe and Grossman, 1997).

Mutational analyses of the conserved aspartate residues revealed that these residues are indeed required for proper CCA regulation (Li and Kehoe, 2005). This work, along with the identification of RcaF (Kehoe and Grossman, 1997), suggests that a phosphorylation event is required for RL-induced gene regulation, while likely a dephosphorylation event occurs during GL-induced gene regulation. In addition, the newly characterized DNA-binding domain has been shown to be involved in the down-stream transcriptional regulation of light-regulated operons (Li *et al.*, 2008).

1.7.2 Transcriptional Regulation of PBP Operons

The regulation of CCA in *F. diplosiphon* has been shown to occur largely by the transcription of the operons which encode components of the PBPs. These operons lie downstream of RcaE and RRs RcaF and RcaC in the signaling pathway. Detailed analyses of transcript regulation have shown that under GL conditions, transcription of *cpeBA* (which encodes PE) and *cpeCDE* (which encodes the PE linkers) is activated, but remains inactive under RL conditions. Further, under RL conditions, transcription of *cpcB2A2H2ID2* (referred to as *cpcB2A2*), which encodes the RL-inducible PC and associated linkers (*H2I2D2*) is activated, but remains inactive under GL conditions

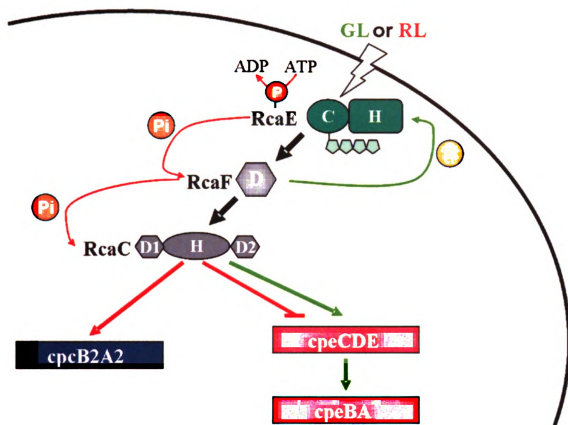


Figure 1.4. Simplified Model for CCA Signaling Pathway. RcaE is involved in a complex phosphorelay system with RcaF, a CheY-related RR lacking an output domain, and RcaC, a complex RR with a DNA-binding domain. Under RL conditions (red arrows), RcaE is proposed to act as a kinase, resulting in the phosphorylation of RcaF and RcaC, thus leading to the induction of the PC_i operon *cpcB2A2*, encoding the PC and PC linkers, and repression of the *cpeCDE* and *cpeBA* operons, encoding the PE linkers and PE, respectively. Under GL conditions (green arrows), RcaE is proposed to act as a phosphatase that dephosphorylates RcaF and results in the induction of the PE operons (*cpeCDE* and *cpeBA*).

(Conley *et al.*, 1985; Oelmüller *et al.*, 1985; Federspiel and Grossman, 1990).

Additionally, transcriptional activators RcaA, RcaB and CpeR have also been identified and characterized. These regulators are required for the expression of the *cpeBA* operon (Sobczyk *et al.*, 1993; Cobley *et al.*, 2002; Sieb and Kehoe, 2002).

1.7.3 The CCA Signaling Model

Based on the previously described molecular and genetic characterizations of RcaF and RcaC, as well as the detailed transcriptional profiling of the light-inducible operons described above, a current model exists to explain the CCA signaling mechanism (reviewed in Kehoe and Gutu, 2006; Montgomery, 2008). In RL conditions (indicated by the red arrows in Figure 1.4), RcaE is thought to act as a kinase, utilizing ATP, and transferring a phosphate to RcaF, which is then transferred to RcaC. This cascade activates transcription of the *cpcB2A2* operon, encoding the PC proteins and associated linkers, while repressing the *cpeCDE* and *cpeBA* operons. Under GL conditions (indicated by the green arrows in Figure 1.4), RcaE is thought to function as a phosphatase, removing a phosphate from RcaF, thereby maintaining RcaC in an unphosphorylated state, activating expression of the *cpeCDE* and *cpeBA* operons and allowing transcription of the PE linkers and proteins respectively (recently reviewed in Montgomery, 2008).

1.8 The Biochemical Role(s) of RcaE in CCA Signaling

Although much has been done in terms of the identification and molecular characterization of the CCA signaling pathway, the biochemical role of RcaE itself

remains to be elucidated. Detailed analyses of the conserved domains within RcaE may provide insight into its role as a photoreceptor for this signaling pathway. The conserved domains of RcaE and their potential functions will be discussed below.

1.8.1 GAF Domains

One of the conserved domains identified in the N-terminal region of RcaE is a GAF domain (Pfam PF 01590; reviewed in Kehoe and Gutu, 2006). These domains are defined as such because of their presence in cGMP-specific and -stimulated phosphodiesterases, *Anabena* adenylate cyclases and in *E. coli* FhlA (Bakal and Davies, 2000). GAF domains are found in phytochromes and contain conserved cysteine residues required for chromophore attachment (Montgomery and Lagarias, 2002). Sequence analysis and alignment reveal that GAF domains occur in the chromophore-binding domains of phytochromes, and that specific residues in these domains are highly conserved (Figure 1.5). This conservation suggests an important role for these residues in chromophore attachment and/or the photochemical activity attributed to chromophore configuration.

Mutation studies of the conserved cysteine residue C198 within the RcaE GAF domain (Figure 1.5, box #1) have implicated its importance in chromophore attachment (Terauchi *et al.*, 2004). However, a C198A variant, which was hypothesized to lack light-sensing capability, fully complements the FdBk14 mutant in RL but not in GL (Terauchi *et al.*, 2004). This suggests that in RL RcaE function is dependent upon associated proteins, or that there is another intramolecular chromophore attachment site that functions for RL sensing.

229 **KVRE**LTGGYDRVMMAK**FHE**DDDHGEVVS**EVTK**PK**GLE**RYLGLHYPA**TDI**EQAR**FLF**TKNK**RV** 280 290 300 310 320 330
 263 **SVAR**DLTGYDRVNVV**KFHE**DEHGEVVA**ESKR**DDLE**SY**IGLHYPA**TDI**EQAS**RF**LKQNR**RV** **At PhyA**
 124 **EVQR**ILLQADRA**LIV**HVL**PD**GTG**KT**SESVL**PD**Y**PT**LM**DL**EF**Q**EV**F**EQ**E**Y**Q**LL**YA**QGR**RV** **At PhyB**
 163 **EVRR**MTGGFDRV**MLV**FR**DE**NNHG**DI**AE**DK**RDD**M**K**RY**LG**LHY**EP**Q**EV**F**EQ**E**Y**Q**LL**YA**QGR**RV** **Fd RecA**
 163 **TVRE**LLTGFDRV**MLV**K**FA**PDATGE**VI**AE**K**ARR**EG**LHA**F**LGH**RF**PAS**DI**PAQ**AR**AL**Y**TR**HL**L**R** **Syn Cph1**
 340 350 360 370 380 390
 289 **MIVD**CNA**KKH**AR**V**--L**Q**DE**K**L**S**F**D**L**T**L**G**ST**IR**AP**H**CH**L**Q**Y**MAN**ND**SI**AS**LV**MA**V**V**VE**E** **At PhyA**
 323 **MIVD**CNA**TF**V**L**V--**V**Q**D**DR**L**T**Q**S**R**CL**V**GS**T**LR**A**EP**H**CH**S**Q**Y**MAN**NG**S**IAS**L**MA**V**I**NG**N** **At PhyB**
 184 **A**L**AD**DV**H**D**F**T**A**GL**A**--**V**Q**D**DR**L**T**Q**S**R**CL**V**GS**T**LR**A**EP**H**CH**S**Q**Y**MAN**NG**S**IAS**L**MA**V**I**NG**N** **Fd RecA**
 223 **V**L**RD**V**Y**GV**AV**PL**TP**AV**N**ST**NR**AV**D**L**T**ES**IL**RS**A**Y**H**CH**L**T**Y**L**KN**KG**V**GA**S**L**T**IS**L**IK**D**GH **Syn Cph1**
 223 **L**T**AD**TR**AA**AV**PL**D**P**V**L**N**P**Q**T**NA**PT**PL**G**GA**V**LR**AT**SP**K**HN**Q**Y**L**R**N**KG**V**GS**LS**VS**V**VG**G**Q **Dr BphP**

Figure 1.5 Sequence Alignment of GAF Domains. Sequence alignment of a portion of GAF domains in *Arabidopsis* (At) phytochromes A and B, *F. diplosiphon* (Fd) *Synechocystis* (Syn) Cph1, and *Deinococcus radiodurans* (Dr) BphP, with conserved residues highlighted in yellow. Boxed in red: (1) conserved Cys residue required for chromophore attachment; (2) conserved Tyr residue involved in chromophore photochemistry, as discussed in text.

Further, mutations of residues in GAF domains of proteins from *Calothrix*, *Anabaena*, *Arabidopsis*, and *Synechocystis* have indicated their importance for chromophore-binding specificity (Hanzawa *et al.*, 2002; Quest and Gartner, 2004) and chromophore conformation (Fischer and Lagarias, 2004; Fischer *et al.*, 2005). As discussed in section 1.5, the ability of the chromophore to undergo photoisomerization is what allows it to absorb different wavelengths of light, and elicit photomorphogenic responses. Therefore, mutating residues in the GAF domain is likely to affect the function of a phy, if not the function of the chromophore itself. For example, a mutation of a conserved tyrosine (Y; Figure 1.5, box #2) to a histidine (H) in the GAF domain of the *Synechocystis* (*Syn*) photoreceptor Cph1 inhibits the photoisomerization process (Fischer and Lagarias, 2004).

The conformation of the mutated Cph1 chromophore is “locked” in the Pr form, disabling the conversion to the Pfr form upon absorption of red light and yielding a fluorescent molecule (Fischer and Lagarias, 2004). Since this tyrosine residue is highly conserved, the same group tested whether the photochemical function was conserved in phytochromes of *Arabidopsis*, *Synechocystis*, and *Pseudomonas aeruginosa* by producing the same mutations in each organism. Based on a fluorescence phenotype, which results from the inability to convert to the Pfr form, they discovered that indeed the function of the tyrosine residue was conserved between plants and cyanobacteria. In a saturated mutational analysis of this tyrosine residue in *Syn* Cph1, all amino acid substitutions resulted in reduced photoconversion (Fischer *et al.*, 2005).

These results show that this tyrosine residue regulates the conformation of the chromophore. Thus, the photochemistry of these plant and cyanobacterial bilin molecules

is essential to the signaling initiated by light perception. Interestingly, this tyrosine residue is also conserved in RcaE's GAF domain (Figure 1.5, box #2). To date, the function of this residue has yet to be addressed, however, based on the results from Fischer *et al.*, 2005, it is highly likely that the function is also conserved.

1.8.2 PAS Domains

Another conserved domain identified in the photosensory region of RcaE is a PAS domain (Pfam PF 00989; Kehoe and Gutu, 2006). PAS domains were originally identified because of the presence of repetitive sequences in the *Drosophila* PER (period clock protein), the mouse ARNT (aryl hydrocarbon receptor nuclear transporter), and the *Drosophila* SIM (single-minded protein) proteins (Zhulin *et al.*, 1997). It is now recognized that PAS proteins are found throughout all kingdoms of life and function in signal sensing, ligand binding, and protein-protein interactions (Bakal and Davies, 2000; Ponting and Aravind, 1997; Taylor and Zhulin, 1992). Furthermore, recent structural analysis suggests that PAS domains are similar to GAF domains and may have similar functions (Wagner *et al.*, 2005).

Since PAS domains are typically involved in signal sensing and protein-protein interactions, it is possible that this region of RcaE could be involved in sensing the signal that initiates the CCA signaling cascade. The PAS domain could also be a potential site for additional chromophore attachment or binding of an associated protein(s). This is not an uncommon occurrence, for example, the PYP bacterial blue-light photoreceptor is a PAS protein which has a 4-hydroxycinnamyl chromophore attached to it (Pellequer *et al.*, 1998; reviewed in Taylor and Zhulin, 1999).

1.8.3 Hbox Domains

The conserved domain identified in the C-terminal output/kinase region of RcaE is an Hbox domain (Pfam PF 00512; Kehoe and Gutu, 2006). These domains are motifs which are conserved in kinase domains of HKs. As discussed in section 1.6.1, the conserved histidine residue functions as the phospho-acceptor site during phosphorelay cascades. It is also the site for autophosphorylation in HK dimers, which is important for signal activation.

Various studies have shown that mutation of the conserved histidine in HKs inhibits response to stimuli, thus disrupting the signaling cascade (reviewed in Vierstra, 2003). Since RcaE contains a conserved histidine residue in this domain (H430), it is likely that it could be crucial to RcaE activity and, in turn, CCA signaling. Interestingly, recent studies on light-regulated changes in RcaC abundance have indicated that functional RcaE is required, and more specifically, its HK domain as well as the conserved H430 residue (Li and Kehoe, 2008). However, the role of this particular residue in RcaE's regulation of CCA has yet to be fully determined.

1.9 Research Aims

In addition to the pigmentation phenotype associated with CCA and the signaling components, early micrograph studies showed that WT *F. diplosiphon* displays different cell morphologies under GL and RL conditions (Bennett and Bogorad, 1973). Under RL conditions the cells are small and round and the filaments are short in length. Under GL conditions the cells have a brick-like shape, and the filaments are longer (revisit Figure 1.1D). Studies to compare the difference between the *rcaE* null mutant, FdBk14, in both

light conditions with WT cells would provide insight into RcaE's role in the regulation of cell and filament morphology. Microarray studies with wild type cells have implicated RcaE in the control of the expression of genes other than phycobiliprotein-encoding genes, providing support that phycobiliprotein accumulation is not the only pathway affected (Stowe-Evans and Kehoe, 2004). Therefore, an aim of the research presented in this dissertation is to elucidate the role of RcaE in the control of *F. diplosiphon* cellular morphology. This is the focus of chapters 2 and 3.

Since RcaE is one of the major factors in the CCA signaling pathway and has yet to be fully characterized, elucidating the physiological and biochemical function of this protein will provide insight into the molecular mechanisms which are involved in the biliprotein-regulated photomorphogenesis in photosynthetic organisms. The FdBk14 mutant displays an observable CCA pigmentation defect (revisit section 1.3); the ability to utilize genetic complementation in *F. diplosiphon* allows *in vivo* characterization of such color mutants. Therefore, an additional aim of the research presented in chapter 4 of this dissertation is to determine the roles of the previously mentioned conserved domains identified in RcaE in its biochemical activity, by using mutation and complementation analyses, which will be discussed in more detail below.

Since the photochemistry of some phytochromes has been linked to specific conserved residues in the GAF domain, this domain serves as a candidate for identifying residue(s) with a similar function in RcaE. Mutational analysis of a conserved tyrosine residue in GAF domains has implicated its importance for the photochemical process of the *Synechocystis* Cph1 phytochrome, as well as the *Arabidopsis* PhyA and PhyB phytochromes (Fischer and Lagarias, 2004; Fischer *et al.*, 2005). As discussed in

sections 1.5 and 1.8.1, this residue is essential for the proper configuration of the chromophore during photoconversion. Studying mutations of this residue in RcaE (see chapter 4) will aid in characterizing the photochemistry of the photoreceptor during CCA, and further solidify the hypothesis that this function is evolutionarily conserved.

The kinase activity of RcaE has yet to be thoroughly studied, although apoRcaE exhibits some kinase activity (Montgomery, unpublished). Therefore it is necessary to further establish the activity of the wild type protein. Additionally, mutational analysis of residues, particularly the conserved histidine (H430) in the H-box domain will allow the biochemical function of RcaE to be assessed *in vivo*. Since the H-box domain is located in the conserved histidine kinase portion of RcaE, characterization of mutant(s) in this domain (see chapter 4) will elucidate the phosphorylation event needed to initiate CCA.

It is predicted that the PAS region of RcaE is involved in sensing the signal that initiates the light-signaling cascade. It could also be a potential site for chromophore attachment or binding of associated protein(s). Mutational analysis of this conserved domain will determine if it is involved in light sensing. It is also likely that the PAS domain of RcaE could be a sensor for other environmental signals such as oxygen levels (Taylor and Zhulin, 1999). Hence, mutating the PAS domain may disrupt its ability to bind ligands or signal molecules which allow RcaE to sense such environmental changes; the mutation(s) would therefore alter the output. Thus, characterization of this domain (see chapter 4) could suggest a possible link between the CCA signaling cascade and other cellular responses to external stimuli.

The aims described above offer a detailed approach to understanding how RcaE regulates CCA. Utilizing a mutational analysis approach will allow the working model

for RcaE signaling to be tested. Characterizing the light-regulated biochemical function of this photoreceptor will aid in understanding how related photosynthetic organisms sense and respond to their light environments. Finally, by characterizing the cellular morphology of the FdBk14 mutant as well as the RcaE mutant variants, novel roles may be discovered which could implicate RcaE's involvement in cross talk with non-photosynthetic signaling pathways.

REFERENCES

1. **Al-Sady, B., W. Ni, S. Kircher, E. Schafer, and P. H. Quail.** 2006. Photoactivated phytochrome induces rapid PIF3 phosphorylation prior to proteasome-mediated degradation. *Mol Cell* **23**:439-46.
2. **Aravind, L., and C. P. Ponting.** 1997. The GAF domain: an evolutionary link between diverse phototransducing proteins. *Trends Biochem Sci* **22**:458-9.
3. **Bateman, A., L. Coin, R. Durbin, R. D. Finn, V. Hollich, S. Griffiths-Jones, A. Khanna, M. Marshall, S. Moxon, E. L. Sonnhammer, D. J. Studholme, C. Yeats, and S. R. Eddy.** 2004. The Pfam protein families database. *Nucleic Acids Res* **32**:D138-41.
4. **Bennett, A., and L. Bogorad.** 1973. Complementary chromatic adaptation in a filamentous blue-green alga. *J Cell Biol* **58**:419-35.
5. **Chen, M., J. Chory, and C. Fankhauser.** 2004. Light signal transduction in higher plants. *Annu Rev Genet* **38**:87-117.
6. **Chiang, G. G., M. R. Schaefer, and A. R. Grossman.** 1992. Complementation of a red-light-indifferent cyanobacterial mutant. *Proc Natl Acad Sci U S A* **89**:9415-9.
7. **Chieri Tomomori, H. K., and Mitsuhiro Ikura.** 2003. The Histidine Kinase Family: Structures of Essential Building Blocks, p. 12-24. *In* M. I. a. R. Dutta (ed.), *Histidine Kinases in Signal Transduction*. Academic Press, Elsevier Science, San Diego.
8. **Cobley, J. G., A. C. Clark, S. Weerasurya, F. A. Queseda, J. Y. Xiao, N. Bandrapali, I. D'Silva, M. Thounaojam, J. F. Oda, T. Sumiyoshi, and M. H. Chu.** 2002. CpeR is an activator required for expression of the phycoerythrin operon (cpeBA) in the cyanobacterium *Fremyella diplosiphon* and is encoded in the phycoerythrin linker-polypeptide operon (cpeCDESTR). *Mol Microbiol* **44**:1517-31.
9. **Conley, P. B., P. G. Lemaux, and A. R. Grossman.** 1985. Cyanobacterial light-harvesting complex subunits encoded in two red light-induced transcripts. *Science* **230**:550-3.
10. **Fankhauser, C., K. C. Yeh, J. C. Lagarias, H. Zhang, T. D. Elich, and J. Chory.** 1999. PKS1, a substrate phosphorylated by phytochrome that modulates light signaling in *Arabidopsis*. *Science* **284**:1539-41.

11. **Federspiel, N. A., and A. R. Grossman.** 1990. Characterization of the light-regulated operon encoding the phycoerythrin-associated linker proteins from the cyanobacterium *Fremyella diplosiphon*. *J Bacteriol* **172**:4072-81.
12. **Fischer, A. J., and J. C. Lagarias.** 2004. Harnessing phytochrome's glowing potential. *Proc Natl Acad Sci U S A* **101**:17334-9.
13. **Fischer, A. J., N. C. Rockwell, A. Y. Jang, L. A. Ernst, A. S. Waggoner, Y. Duan, H. Lei, and J. C. Lagarias.** 2005. Multiple roles of a conserved GAF domain tyrosine residue in cyanobacterial and plant phytochromes. *Biochemistry* **44**:15203-15.
14. **Franklin, K. A., V. S. Lerner, and G. C. Whitelam.** 2005. The signal transducing photoreceptors of plants. *Int J Dev Biol* **49**:653-64.
15. **Franklin, K. A., and G. C. Whitelam.** 2004. Light signals, phytochromes and cross-talk with other environmental cues. *J Exp Bot* **55**:271-6.
16. **Gyula, P., E. Schafer, and F. Nagy.** 2003. Light perception and signalling in higher plants. *Curr Opin Plant Biol* **6**:446-52.
17. **Hanzawa, H., T. Shinomura, K. Inomata, T. Kakiuchi, H. Kinoshita, K. Wada, and M. Furuya.** 2002. Structural requirement of bilin chromophore for the photosensory specificity of phytochromes A and B. *Proc Natl Acad Sci U S A* **99**:4725-9.
18. **Houmard, J., and N. T. de Marsac.** 1988. Complementary Chromatic Adaptation: Physiological Conditions and Action Spectra. *Methods Enzymol* **167**:808-47.
19. **Karniol, B., J. R. Wagner, J. M. Walker, and R. D. Vierstra.** 2005. Phylogenetic analysis of the phytochrome superfamily reveals distinct microbial subfamilies of photoreceptors. *Biochem J* **392**:103-16.
20. **Kehoe, D. M., and A. R. Grossman.** 1997. New classes of mutants in complementary chromatic adaptation provide evidence for a novel four-step phosphorelay system. *J Bacteriol* **179**:3914-21.
21. **Kehoe, D. M., and A. R. Grossman.** 1996. Similarity of a chromatic adaptation sensor to phytochrome and ethylene receptors. *Science* **273**:1409-12.
22. **Kehoe, D. M., and A. Gutu.** 2006. RESPONDING TO COLOR: The Regulation of Complementary Chromatic Adaptation. *Annu Rev Plant Biol* **57**:127-50.
23. **Lariguet, P., and C. Dunand.** 2005. Plant photoreceptors: phylogenetic overview. *J Mol Evol* **61**:559-69.

24. **Li, L., R. M. Alvey, R. P. Bezy, and D. M. Kehoe.** 2008. Inverse transcriptional activities during complementary chromatic adaptation are controlled by the response regulator RcaC binding to red and green light-responsive promoters. *Mol Microbiol* **68**:286-97.
25. **Li, L., and D. M. Kehoe.** 2008. Abundance changes of the response regulator RcaC require specific aspartate and histidine residues and are necessary for normal light color responsiveness. *J Bacteriol* **190**:7241-50.
26. **Li, L., and D. M. Kehoe.** 2005. In vivo analysis of the roles of conserved aspartate and histidine residues within a complex response regulator. *Mol Microbiol* **55**:1538-52.
27. **Mathews, S.** 2006. Phytochrome-mediated development in land plants: red light sensing evolves to meet the challenges of changing light environments. *Mol Ecol* **15**:3483-503.
28. **Montgomery, B. L.** 2008. Shedding new light on the regulation of complementary chromatic adaptation. *Central European Journal of Biology* **3**:351-358.
29. **Montgomery, B. L., and J. C. Lagarias.** 2002. Phytochrome ancestry: sensors of bilins and light. *Trends Plant Sci* **7**:357-66.
30. **Oelmuller, R., A. R. Grossman, and W. R. Briggs.** 1988. Photoreversibility of the Effect of Red and Green Light Pulses on the Accumulation in Darkness of mRNAs Coding for Phycocyanin and Phycoerythrin in *Fremyella diplosiphon*. *Plant Physiol* **88**:1084-1091.
31. **Parkinson, J. S., and E. C. Kofoid.** 1992. Communication modules in bacterial signaling proteins. *Annu Rev Genet* **26**:71-112.
32. **Pellequer, J. L., K. A. Wager-Smith, S. A. Kay, and E. D. Getzoff.** 1998. Photoactive yellow protein: a structural prototype for the three-dimensional fold of the PAS domain superfamily. *Proc Natl Acad Sci U S A* **95**:5884-90.
33. **Ponting, C. P., and L. Aravind.** 1997. PAS: a multifunctional domain family comes to light. *Curr Biol* **7**:R674-7.
34. **Quest, B., and W. Gartner.** 2004. Chromophore selectivity in bacterial phytochromes: dissecting the process of chromophore attachment. *Eur J Biochem* **271**:1117-26.
35. **Rockwell, N. C., Y. S. Su, and J. C. Lagarias.** 2006. Phytochrome structure and signaling mechanisms. *Annu Rev Plant Biol* **57**:837-58.
36. **Schepens, I., P. Duek, and C. Fankhauser.** 2004. Phytochrome-mediated light signalling in *Arabidopsis*. *Curr Opin Plant Biol* **7**:564-9.

37. **Seib, L. O., and D. M. Kehoe.** 2002. A turquoise mutant genetically separates expression of genes encoding phycoerythrin and its associated linker peptides. *J Bacteriol* **184**:962-70.
38. **Sobczyk, A., G. Schyns, N. Tandeau de Marsac, and J. Houmard.** 1993. Transduction of the light signal during complementary chromatic adaptation in the cyanobacterium *Calothrix* sp. PCC 7601: DNA-binding proteins and modulation by phosphorylation. *Embo J* **12**:997-1004.
39. **Stowe-Evans, E. L., and D. M. Kehoe.** 2004. Signal transduction during light-quality acclimation in cyanobacteria: a model system for understanding phytochrome-response pathways in prokaryotes. *Photochem Photobiol Sci* **3**:495-502.
40. **Tandeau de Marsac, N.** 1977. Occurrence and nature of chromatic adaptation in cyanobacteria. *J Bacteriol* **130**:82-91.
41. **Tandeau de Marsac, N.** 1983. Phycobilisomes and Complementary Chromatic Adaptation in Cyanobacteria. *Bulletin de L' Institut Pasteur* **81**:210-254.
42. **Taylor, B. L., and I. B. Zhulin.** 1999. PAS domains: internal sensors of oxygen, redox potential, and light. *Microbiol Mol Biol Rev* **63**:479-506.
43. **Terauchi, K., B. L. Montgomery, A. R. Grossman, J. C. Lagarias, and D. M. Kehoe.** 2004. RcaE is a complementary chromatic adaptation photoreceptor required for green and red light responsiveness. *Mol Microbiol* **51**:567-77.
44. **Vierstra, R. D.** 2003. Cyanophytochromes, Bacteriophytochromes, and Plant Phytochromes: Light-Regulated Kinases Related to Bacterial Two-Component Regulators, p. 273-295. *In* M. I. a. R. Dutta (ed.), *Histidine Kinases in Signal Transduction*. Academic Press, Elsevier Science, San Diego.
45. **Vierstra, R. D., and S. J. Davis.** 2000. Bacteriophytochromes: new tools for understanding phytochrome signal transduction. *Semin Cell Dev Biol* **11**:511-21.
46. **Wagner, J. R., J. S. Brunzelle, K. T. Forest, and R. D. Vierstra.** 2005. A light-sensing knot revealed by the structure of the chromophore-binding domain of phytochrome. *Nature* **438**:325-31.
47. **Yeh, K. C., S. H. Wu, J. T. Murphy, and J. C. Lagarias.** 1997. A cyanobacterial phytochrome two-component light sensory system. *Science* **277**:1505-8.
48. **Zhulin, I. B., B. L. Taylor, and R. Dixon.** 1997. PAS domain S-boxes in Archaea, Bacteria and sensors for oxygen and redox. *Trends Biochem Sci* **22**:331-3.

CHAPTER TWO

RcaE Regulates Cell and Filament Morphology

This chapter contains previously published work:

Bordowitz, J.R and Montgomery, B.L. (2008) Photoregulation of Cellular Morphology during Complementary Chromatic Adaptation Requires Sensor-Kinase-Class Protein RcaE in *Fremyella diplosiphon*. *J. Bacteriol.* 2008 **190: 4069-4074.**

2.1 Introduction

Complementary chromatic adaptation (CCA) is a light-dependent acclimation process used by some cyanobacteria that results in optimal growth and development in response to changes in the ambient light environment (reviewed by Kehoe and Gutu, 2006). This process is most readily identified by cells changing in color from brick red to blue-green due to variations in the prevalence of green or red wavelengths in ambient light, respectively. These pigmentation changes result from reconfiguration of the light-harvesting complexes and allow cyanobacteria to finely-tune light absorption to the predominant wavelengths of ambient light and thereby maximize photosynthesis (Campbell, 1996). CCA has been most extensively characterized in the cyanobacterium *Fremyella diplosiphon* (also called *Calothrix sp.* PCC 7601).

The pigmentation changes that are characteristic of CCA are controlled by the phytochrome-related photoreceptor RcaE in *F. diplosiphon* (Kehoe and Grossman, 1997, Terauchi *et al.*, 2004). RcaE is a sensor-kinase-class protein that contains an N-terminus related to the chromophore-binding domain of phytochromes and a C-terminal histidine kinase domain (Herdman *et al.*, 2000; Kehoe and Grossman, 1996). Higher plant phytochromes are red/far-red reversible photoreceptors that control numerous aspects of light-dependent growth and development, including seed germination, flowering, and senescence (reviewed by Chen *et al.*, 2004; Wang 2005). RcaE has been shown to exist as a chromophorylated biliprotein that is required for responsiveness to green light (GL) and red light (RL) (Kehoe and Grossman, 1996; Terauchi *et al.*, 2004). RcaF and RcaC are response regulators that are proposed to act downstream of RcaE; together these three components are predicted to form a complex phosphorelay that regulates the

transcriptional changes necessary for altered pigmentation during CCA (Kehoe and Grossman, 1997; Kehoe and Gutu, 2006).

The characterized CCA response in *F. diplosiphon* consists of changes in cell and filament morphologies, in addition to the readily observable pigmentation changes that arise in varying light conditions (Bennett and Bogorad, 1973). RL-grown vegetative cells of the *F. diplosiphon* UTEX481 wild-type (WT) strain are smaller and more rounded in shape than the longer, cylindrical vegetative cells that are observed under green-enriched fluorescent illumination (Bennett and Bogorad, 1973). UTEX481 WT filaments are shorter in RL than in green-enriched fluorescent light: filaments grown in green-enriched fluorescent light were ~9.2 times longer than and contained about 4 times as many cells as RL-grown cells (Bennett and Bogorad, 1973). Light-dependent filament length changes in *F. diplosiphon* slightly precede the changes observed in the levels of phycobiliproteins – e.g., in response to RL illumination, the lengths of filaments previously adapted to green-enriched light decreased just prior to a measurable decrease in GL-inducible PE content and an inverse increase in RL-inducible PC content (Bennett and Bogorad, 1973).

The regulation of light-dependent hormogonia differentiation, a distinct photomorphogenic response in *F. diplosiphon*, has been shown to occur via a regulatory process different from the photoregulation of phycobiliprotein levels that is characteristic of CCA in this organism (Damerval *et al.*, 1991). The differentiation of hormogonia and heterocysts has been attributed to differential excitation of the photosystems by GL and RL, which differs from their effect on CCA (Campbell, 1996). This study investigates whether the CCA-associated changes in vegetative cell and filament morphologies are

controlled by the Rca system or a distinct photoregulatory system. This work examines the molecular basis of the observed light-dependent morphological changes through microscopic and biochemical analyses of WT and RcaE-deficient *F. diplosiphon* strains.

2.2 Methods

2.2.1 Strains and culture conditions

The wild-type *F. diplosiphon* used in these experiments refers to the shortened-filament strain (SF33) of *F. diplosiphon* (Cobley *et al.*, 1993). FdBk14, an *rcaE* null mutant was previously described (Kehoe and Grossman, 1996). The strains were grown in BG-11 (Fluka; Sigma-Aldrich) with 20 mM HEPES, pH 8.0, (hereafter BG-11/HEPES) at 28°C, shaking at 175 rpm either with or without 20 $\mu\text{g mL}^{-1}$ Kanamycin (Kan₂₀). Broad-band monochromatic red light (RL) illumination was provided by CVG Sleeved Rosco Red 24 (General Electric F20T12/R24) fluorescent tubes and green light (GL) illumination by CVG Sleeved Rosco Green 89 (General Electric F20T12/G78) fluorescent tubes (Standard Electric Co.). Light intensities were measured using a LI-250A Light Meter (LI-COR, Lincoln, NE) equipped with a Quantum sensor (LI-COR). To determine cell culture densities, absorbance at 750 nm (A_{750}) was measured using a SpectraMax M2 microplate reader (Molecular Devices, Sunnyvale, CA).

2.2.2 Plasmids and Transformations

Shuttle vector pPL2.7 (Chiang *et al.*, 1992b) was converted to Gateway[®]-ready vector pPL2.7GWC as follows: pPL2.7 was digested with *HpaI* and treated with calf

intestinal alkaline phosphatase. The linearized pPL2.7 vector was then ligated with Gateway[®] conversion reading frame cassette A (Invitrogen Corporation, Carlsbad, CA).

The primers 5' FLRcaE-GWC

(5'GGGGACAAGTTTGTACAAAAAAGCAGGCTATGAGGGATTTTGGACGCTG
AGTG) and 3' FLRcaE-GWC

(5'GGGGACCACTTTGTACAAGAAAGCTGGGTTCATTGGATATTGGCGTACT
CAAG) with introduced attB1 and attB2 sites (underlined) respectively, were used to

amplify *rcaE* with its native promoter by PCR. The PCR product was recombined into pDONRTM/Zeo (Invitrogen) using the BP ClonaseTM II enzyme (Invitrogen) according to

the manufacturer's instructions. Following selection of transformants in the presence of zeocin and verification of *rcaE* sequence, the construct was recombined with

pPL2.7GWC using the LR ClonaseTM II enzyme (Invitrogen) according to the manufacturer's instructions to produce pPL2.7GWC-natRcaE.

Shuttle vector pPL2.7 (Chiang *et al.*, 1992b) was used as a vector only control in these experiments, since the Gateway[®] converted version (described above) contains a *ccdB* suicide cassette, which does not allow for Kan selection of transformants (see Appendix A1). RcaE constructs were transformed into FdBk14 cells via electroporation as described (Kehoe and Grossman, 1998) with the following exceptions: after transformation, 50 mL cultures were recovered in constant RL ($\sim 60 \mu\text{mol m}^{-2} \text{s}^{-1}$) for 2-3 weeks during Kan selection. After the recovery period, 10 mL of each culture were sub-cultured into flasks containing 40 mL of fresh BG-11/HEPES media supplemented with

Kan₂₀ for RL and GL growth. RL-grown cultures were maintained at 19-20 $\mu\text{mol m}^{-2} \text{s}^{-1}$, while the GL-grown cultures were maintained at 9-10 $\mu\text{mol m}^{-2} \text{s}^{-1}$.

2.2.3 Spectral Analysis

Complementation of mutant strains was observed spectrophotometrically as previously described (Terauchi *et al.*, 2004). At an A₈₀₀ ~0.10 whole-cell absorbance spectra from 400 nm to 750 nm were obtained in a SpectraMax M2 microplate.

2.2.4 Chl *a* and phycobiliprotein quantification

Chlorophyll *a* (chl *a*) and phycobiliproteins were extracted and analyzed as previously described (Kahn *et al.*, 1997; Tandeau de Marsac and Houmard, 1988), with the following exceptions: During incubation in extraction buffers, samples were gently shaken on a platform rotator. For spectral analysis, supernatants (200 μL) were loaded in triplicates into a flat-bottom 96-well plate (Corning Plastics, Corning, NY) and absorbance values read using a SpectraMax M2 microplate reader. Absorbance values were used to calculate concentrations using previously determined equations (Tandeau de Marsac and Houmard, 1988; see below). The levels of phycobiliproteins are reported as the grand average of three independent experiments and normalized to their respective levels of chl *a*. Standard deviations of the ratios are reported.

EQUATIONS

$$\text{Chl } a = ((A_{665} \times 13.9 \times (\text{weight}/0.8)/1.5))/1000$$

$$\text{PC} = ((A_{620} - (0.7 \times A_{650}))/7.38)$$

$$AP = ((A_{650} - (0.19 \times A_{620}))/5.65)$$

$$PE = ((A_{565} - (2.8 \times PC) - (1.34 \times AP))/12.7)$$

Standard Deviations (with Ratio: $R=X/Y$):

$$SD = \sqrt{\left(\frac{SDX}{avgX}\right)^2 + \left(\frac{SDY}{avgY}\right)^2}$$

Where: SD is standard deviation

avg is average (mean)

X is PE, PC or AP

Y is Chl *a*

2.2.5 Protein extraction and immunoblot analyses

Soluble protein extracts were obtained from 20-30 mL cultures of *F. diplosiphon* grown in RL or GL to an A_{750} of ~ 1.0 as previously described (Balabas *et al.*, 2003).

Total protein concentrations were determined spectrophotometrically in a flat-bottom 96-well plate (Corning Plastics, Corning, NY) using the microtiter plate procedure of the Bio-Rad Protein Assay Kit according to the manufacturer's instructions (Bio-Rad, Hercules, CA) and a SpectraMax M2 microplate reader. Clarified lysates were then concentrated using chloroform/methanol precipitation and resuspended in 250 mM Tris-HCl pH 6.8, 15% glycerol (v/v), 5.6 % SDS, 0.005% 2-mercaptoethanol, 0.0025 % bromophenol blue (1X SDS-PAGE sample buffer). Concentrated protein samples were run on a 4-12.5% SDS-PAGE gel (Laemmli, 1970) and transferred to Immobilon-P PDVF membrane (Millipore, Billerica, MA).

After transfer, membrane blots were blocked in 10 mM Tris pH 7.5, 150 mM NaCl, 0.05% Tween-20, 3% BSA for 1 hour at room temperature. Membranes were then incubated with an anti-RcaE antibody (Terauchi *et al.*, 2004) overnight at 4°C with gentle shaking. Membranes were then probed with an HRP-conjugated anti-rabbit secondary antibody according to the manufacturer's instructions (Pierce Biotechnology, Inc., Rockford, IL). Antibody was detected using ECL Advance chemiluminescent substrate from Amersham (Piscataway, NJ), SuperSignal[®] West Dura Extended Duration chemiluminescent substrate from Pierce (Rockford, IL), or SuperSignal[®] West Pico chemiluminescent substrate from Pierce (Rockford, IL), as indicated, on a Kodak Image Station 2000MM Multimodal Imaging System (Eastman Kodak Company, Rochester, NY) using a black excitation filter and an open emission filter at 0% bulb intensity.

2.2.6 Microscopy

Slides of immobilized *F. diplosiphon* cells were prepared according to a procedure adapted from Reize and Melkonian, 1989. Cells at a final OD of ~ 0.1 in 1.2% UltraPure™ L.M.P agarose (Invitrogen) in BG-11/HEPES were pipetted into a vacuum lubricant-enclosed square onto 1.0-mm thick 3"x 1½" Propper bev-l-edge[®] pre-cleaned twin-frost[®] microslides (Long Island City, NY). A 24 x 50 mm coverslip (Corning, Lowell, MA) was placed over the suspension and slides were fixed at 4°C prior to imaging. The immobilized live cells were visualized with an inverted Axiovert 200 Zeiss LSM 510 Meta confocal laser scanning microscope (CLSM: Carl Zeiss MicroImaging,

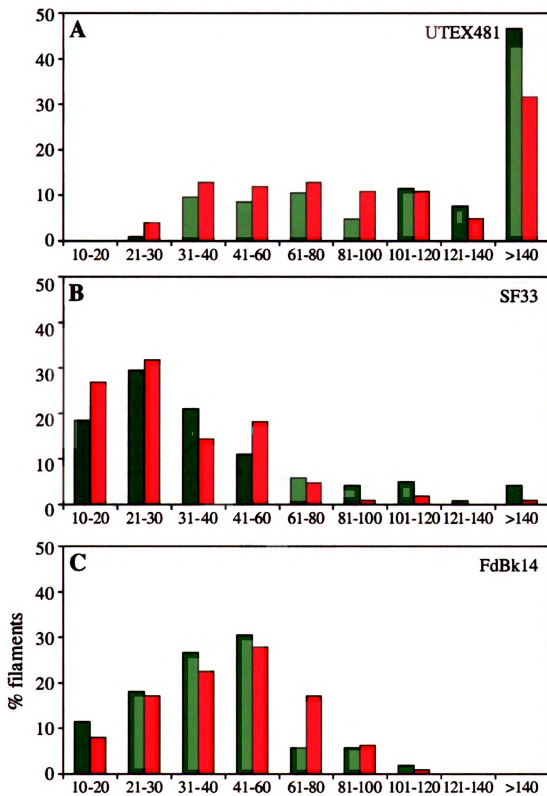
Thornwood, NY) using differential interference contrast (DIC) optics and fluorescence excitation/emission filters. A 40x/1.3NA oil immersion Plan-Neofluar objective lens or 63x/1.4NA oil immersion Plan-Apo objective lens was used for imaging as indicated. DIC imaging was performed using the 488-nm laser. Population scanning was done via Z-series at 5- μm intervals to optimize for large data pools. Filament length and cell size measurements were made by utilizing the calibrated measurement tools of the Zeiss LSM Image Browser (LSMib). Filament lengths were graphed into 10 μm intervals, displaying a non-Gaussian distribution (Figure 2.3). Data were subjected to two-tailed Mann-Whitney U-tests in order to determine statistical significance.

Initial phycobiliprotein autofluorescence was detected using settings adapted from previously published methods (Sinha *et al*, 2002). After spectral imaging of WT GL- and RL-grown cells to further refine the parameters for detection of autofluorescence (Appendix A2), autofluorescence was collected using a 543-nm laser for excitation and emission collected using a 560- to 615-BP filter and 640- to 753-nm Meta detector for GL-grown cells and with a 615-nm LP filter for RL-grown cells. Images were acquired from the CLSM microscope using the LSM FCS Zeiss 510 Meta AIM imaging software.

2.2.7 Light Shifting Experiments

Light shifting experiments consisted of transferring GL-grown cells to RL growth conditions and vice versa. Prior to shifting, the cultures were normalized to $A_{750} \sim 0.1$ and allowed to recover in broad-band GL or RL for ~ 5 hrs. One set of flasks was kept in constant light conditions as a control, while another set was shifted to the opposite condition. Cell samples were collected and prepared for DIC imaging 24 hrs post shift,

Figure 2.1. Range of filament lengths of *F. diplosiphon* strains grown under broad-band GL or RL. Percentage of GL- and RL-grown filaments measuring the indicated length (μm) for each strain: UTEX481 (A), SF33 (B), Fdbk14 (C), FdBk14 transformed with: pPL2.7RcaE (D), and pPL2.7 (E). Number of filaments counted for each strain is as indicated in Table 2.2



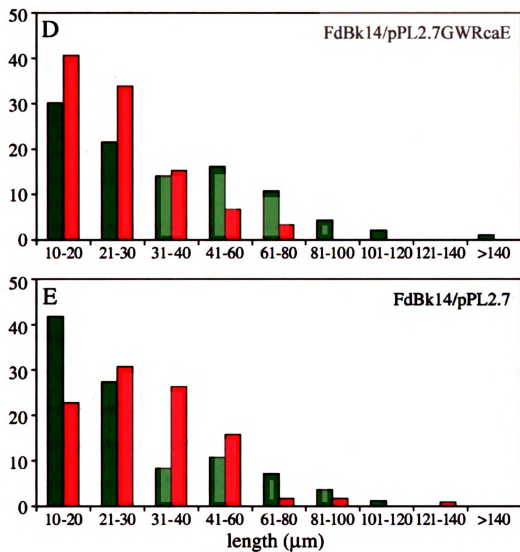


Figure 2.1 continued

using confocal microscopy as described above. Cultures were returned to their original light conditions 48 hrs after the initial shift, and cells were imaged 24 hrs later. Samples were also collected for whole-cell spectral scans at each time point. All sample collection was done under illumination identical to that of the final growth condition.

2.3 Results

2.3.1 Characterization of the light-dependent cell and filament morphologies of wild-type and RcaE-deficient cells

Cell cultures were grown under green- and red-enriched fluorescent illumination in order to reexamine cell and filament morphologies previously reported for *F. diplosiphon* UTEX481 WT cells (Bennett and Bogorad, 1973) and to determine these properties for SF33 cells. SF33 is a shortened-filament mutant strain derived from UTEX481 WT (Cobley *et al.*, 1993). The shortened-filament phenotype results in the formation of colonies when SF33 is grown on plates, which facilitates genetic manipulation of the strain. SF33 is a hormogonium- and heterocyst-deficient strain (Herdman *et al.*, 2000). However, SF33 shows normal CCA regulation of PBP gene expression (Cobley *et al.*, 1993). Thus, this strain was used for comparative studies of the photoregulation of vegetative cellular morphology in *F. diplosiphon*. Transmitted light, DIC, and PBS autofluorescent images were gathered to assess cell size and shape, filament length, and the number of cells per filament.

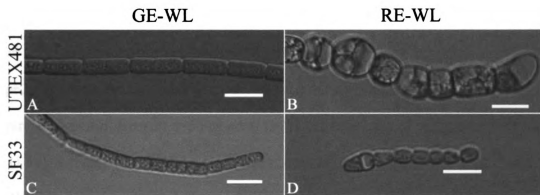


Figure 2.2. Cell Morphologies of the WT and SF33 *F. diplosiphon* strains in GE-WL and RE-WL. Representative optical slices from a Z-series of DIC images of WL-adapted filaments of UTEX481 (A and B) and SF33 (C and D) were captured at a 40X oil immersion lens objective. Bars, 10 μ m.

Strain	Filament length (μ m) under:		No. of cells/filament under:		No. of examined filaments grown under:	
	GE-WL	RE-WL	GE-WL	RE-WL	GE-WL	RE-WL
UTEX481**	212.9	53.4	17	5	20	23
SF33**	52.4	23.3	12	5	26	27

Table 2.1. Median filament lengths and numbers of cells of *F. diplosiphon* strains under GE-WL or RE-WL. **, $P < 0.001$; two-tailed Mann-Whitney U test. The probability score indicates that the difference in filament length between GE-WL- and RE-WL-grown cultures was highly statistically significant. GE-WL was from PL/AQ wide-spectrum fluorescent bulbs. RE-WL was from Gro-Lux fluorescent bulbs.

Observed cell shapes for UTEX481 were analogous to those previously reported: under green-enriched white light (GE-WL) growth conditions, cells were elongated in shape, whereas red-enriched white light (RE-WL) exposure resulted in round cells (Figure 2.2A and B; Bennett and Bogorad, 1973). The median filament length was 212.9 μm (17 cells/filament) and 52.4 μm (12 cells/filament) for UTEX481 and SF33 under GE-WL, respectively (Table 2.1). The length of individual UTEX481 cells under these conditions was very similar to that previously reported, whereas the filament length was about half that described (Bennett and Bogorad, 1973). Under RE-WL, UTEX481 filaments had a median length of 52.4 μm , a length nearly identical to that reported by Bennett and Bogorad (1973); while SF33 filaments were 23.3 μm (Table 2.1). Both strains exhibited significantly longer filaments under green-enriched growth as compared to red-enriched growth.

Having established the response of the cells under green- and red-enriched fluorescent illumination, cells were then grown under broad-band GL or RL, which have been identified as the colors that result in maximal CCA, to get more insight specifically into the impact of these colors of light on the full CCA response in *F. diplosiphon*. As noted for GE-WL, GL-grown UTEX481 cells were elongated and brick-like in shape, whereas RL-grown cells were rounded in shape (Figure 2.3A and B). However, RL-grown UTEX481 cells were not as round or as vacuolated as those grown under RE-WL (compare Figures 2.2B and 2.3B; Bennett and Bogorad, 1973). The filaments of UTEX481 cultures grown under GL were significantly longer than the filaments of cultures grown under RL, i.e. 130 μm vs. 94.5 μm (Table 2.2).

Similar to UTEX481, a significant difference in SF33 cell shape and filament length between GE-WL and RE-WL conditions was observed (Figure 2.2C and D; Table 2.1). The difference in cell shape, however, was less obvious for broad-band GL vs. RL growth. SF33 cells were approximately the same length in GL as they were in RL, though cell shape was slightly more rounded under RL conditions (compare Figures 2.3C and D). The major observed difference was the impact of GE-WL vs. broad-band GL on SF33 cell shape, which could be a fluence effect or may be due to the impact of additional wavelengths of light present in the GE-WL. GL-grown SF33 filaments were significantly longer than RL-grown filaments. In GL, the median length of SF33 filaments was 32.9 μm , with 7 cells per filament, whereas RL-grown filaments had a median length of 26.9 μm , with 5 cells per filament (Table 2.2). Notably, broad-band light conditions yielded considerably shorter filaments than green- or red-enriched light, particularly under GL.

In comparison to the UTEX481 and SF33 morphologies described above, the FdBk14 mutant strain displayed markedly different and novel filament and cell morphologies. The filaments tended to be longer and less rigid in structure than those of the parental SF33 strain (Figures 2.3E and F; Table 2.2). The filaments curled in the focal plane and were composed of round, bubble-like cells in both RL and GL conditions. The number of cells per filament for FdBk14 cultures was nearly identical under both light conditions and there was no statistically significant difference between the median filament lengths under GL and RL (Table 2.2).

2.3.2 *RcaE* regulates cellular morphology in *F. diplosiphon* during CCA

To determine whether the discernible difference in shape between SF33 and *RcaE*-deficient FdBk14 cells correlated with *RcaE* activity, *rcaE* under control of its native promoter was introduced into the FdBk14 cell line and the impact of *RcaE* accumulation on cell size, shape, and filament morphology was assessed. Whole-cell spectral analyses show that complementation of the FdBk14 cell line with *RcaE* restores light-dependent PBP absorption peaks seen in both UTEX481 and SF33 (compare Figures 2.4D to B and C), while the FdBk14/pPL2.7 vector only control (Figure 2.4E) resembles the FdBk14 mutant scan. Immunoblot analyses demonstrated accumulation of *RcaE* in the complemented cells (Figure 2.5, lower panel).

Recovery of light-dependent PBP accumulation in the FdBk14/pPL2.7GWR*RcaE* transformants indicated that the *RcaE* accumulating in these cells was functional: grown under RL these cells exhibited low PE/PC ratios, whereas under GL they had high PE/PC ratios, similar to SF33 cells grown in identical conditions (Figure 2.5, upper panel). The accumulation of this functional *RcaE* also was correlated with complementation of the rounded cell shape phenotype of the *RcaE*-null mutant (Figure 2.2G and 2.2H). Although the levels of *RcaE* detected for UTEX481 and SF33 cells are noticeably different, the levels of *RcaE* accumulating in these cells did not seem to be correlated with differences in the cells' ability to regulate PE/PC ratios in response to light.

Whereas this observation does not preclude the differences in *RcaE* accumulation being associated with different cellular shape phenotypes, it is unlikely for this to be the case given the major phenotypic differences observed between GL-grown UTEX481 and

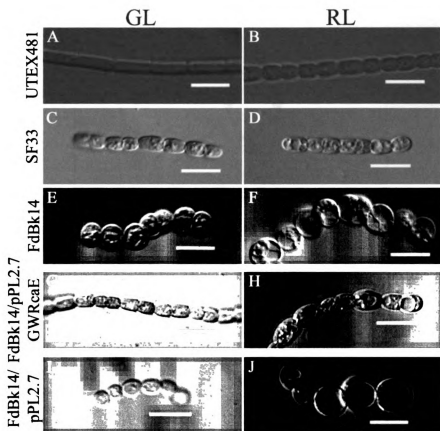


Figure 2.3. Morphological differences between *F. diplosiphon* strains in broad-band GL and RL. Representative optical slices from a Z-series of DIC images of GL- and RL-adapted filaments of UTEX481 (A and B), SF33 (C and D), FdBk14 (E and F), FdBk14/pPL2.7GWRcaE (G and H), and FdBk14/pPL2.7 (I and J) were captured at a 40X oil immersion lens objective. Bars, 10 μ m.

Strain	Filament length (μ m) under:		No. of cells/filament under:		No. of examined filaments grown under:	
	GL	RL	GL	RL	GL	RL
UTEX481*	130.4	94.6	10	8	105	101
SF33*	32.0	26.9	7	5	119	104
FdBk14	37.9	44.3	8	7	105	111
FdBk14/pPL2.7GWRcaE**	30.0	22.1	7	4	94	118
FdBk14/pPL2.7	23.0	30.1	4	4	84	114

Table 2.2. Median filament lengths and numbers of cells of *F. diplosiphon* strains under broad-band GL or RL. *, $P < 0.05$, and **, $P < 0.001$; two-tailed Mann-Whitney U test. The probability scores indicate that the differences in filament length between GL- and RL-grown cultures were statistically significant and highly statistically significant, respectively.

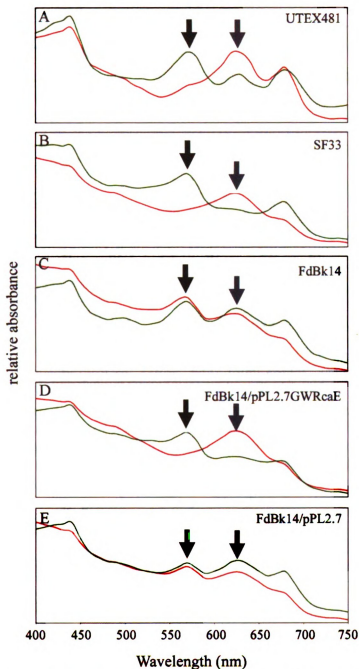


Figure 2.4. Complementary chromatic adaptation in wild type *F. diplosiphon* strains, FdBk14, and FdBk14 transformants. Whole cell absorbance spectra of GL- and RL- grown cells: UTEX481 (A), SF33 (B), FdBk14 (C), FdBk14 transformed with: pPL2.7RcaE (D), and pPL2.7 (E). The scan shown for each strain is representative of three or more independent transformations. Cultures were grown in RL or GL, as indicated by line color. Black arrows, PE absorption maxima, grey arrows, PC absorption maxima.

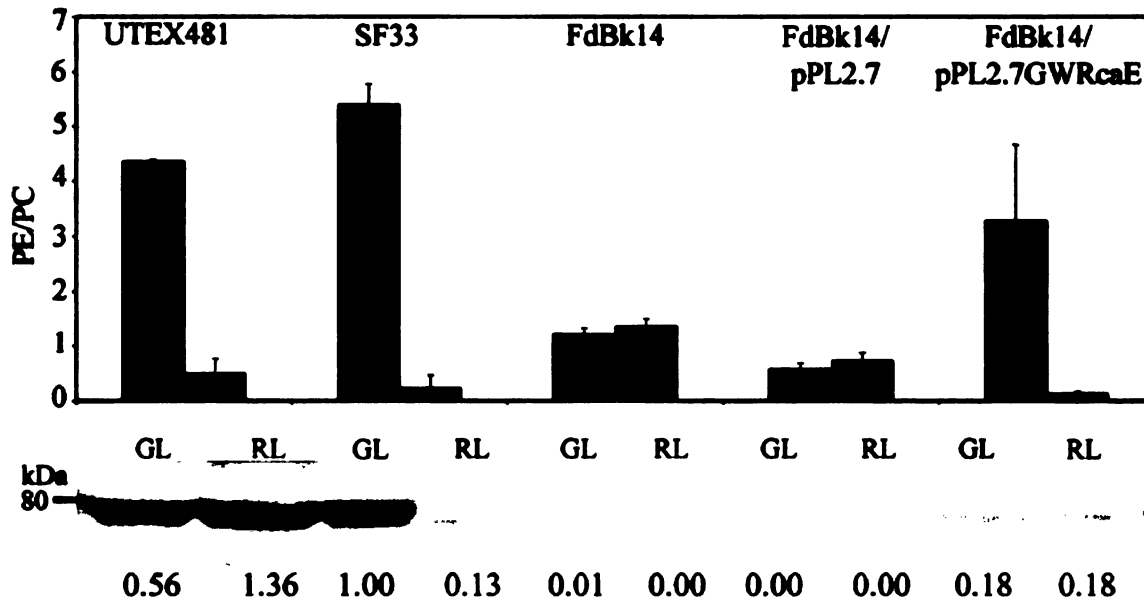


Figure 2.5. Phycobiliprotein ratios and immunoblot analysis of RcaE accumulation in WT and SF33 strains, the FdBk14 mutant, and FdBk14 transformants. Upper panel, PE/PC ratios for *F. diplosiphon* strains. The colors of the bars indicate the colors of the illumination under which the cells were grown, and the bars represent the averages (\pm standard deviations) of results from three independent experiments. Lower panel, immunoblot results for RcaE accumulation in WT cells and FdBk14 cells either untransformed or transformed with pPL2.7 or pPL2.7GWRcaE during growth in GL or RL. A molecular mass marker is indicated to the left.

SF33 cells. In these strains, the levels of RcaE were much more similar, as was the size and shape of RL-grown UTEX481 and SF33 cells, which had a much greater difference in the levels of RcaE accumulation. Notably, the shape of complemented cells was similar to the cell phenotype observed for SF33 cells. GL-grown cells were more cylindrical, whereas RL-grown cells were more rounded in shape, also analogous to those shapes observed for UTEX481.

GL-grown FdBk14/pPL2.7GWRcaE filaments had a median length of 30.0 μm with 7 cells per filament, and RL-grown filaments had a median length of 22.1 μm with 4 cells per filament (Table 2.2). Thus, the filaments were significantly longer in GL as compared to RL, which is consistent with the patterns observed for both the SF33 and UTEX481 strains. The FdBk14/pPL2.7 vector control cells were very similar to the FdBk14 parental line with regard to the round cell shape as expected (Figure 2.3 I and J). Notably, the filament lengths were not significantly different under GL and RL conditions, but were shorter than the FdBk14 strain (Table 2.2). Vector-control cells did not show complementation of the PBP accumulation levels under red and green illumination: PE/PC ratios were similar in GL and RL, as observed for the parental FdBk14 line (Figure 2.5).

Confocal-scanning analyses enabled detection of autofluorescence from the phycobilisomes, and, thereby, to gain a more detailed view of the filament and cell structure. It also was vital to be able to visualize autofluorescence to ensure that slide preparation had not harmed the cells. For GL-grown filaments, autofluorescence was observed using a band pass filter of 560-615 nm (Figure 2.6, left, indicated by pink color), correlating with the accumulation of GL-inducible PE, as well as autofluorescence

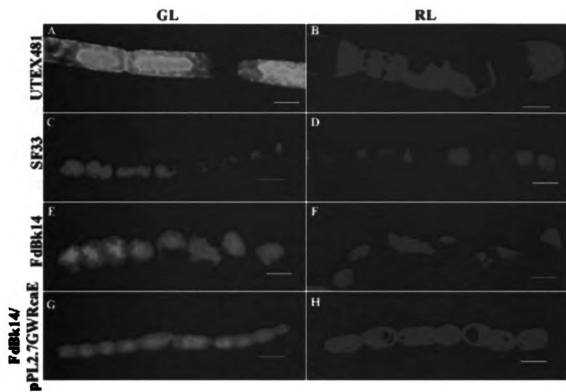


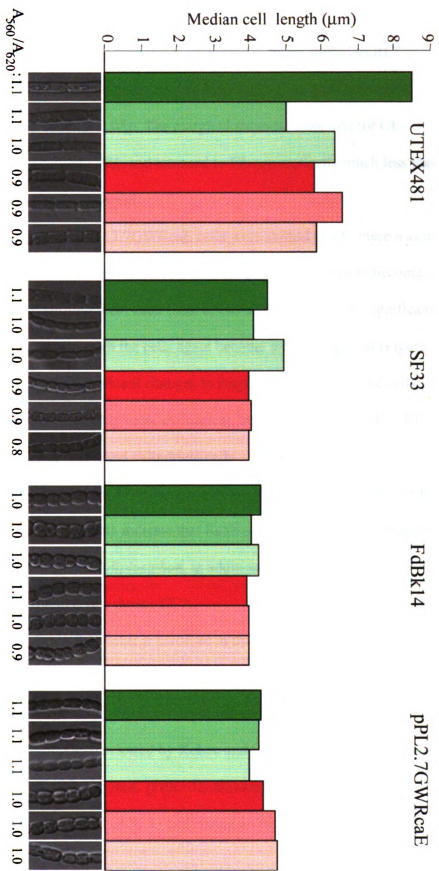
Figure 2.6. Phycobiliprotein autofluorescence of *F. diplosiphon* strains in broadband GL and RL. Maximum-projection images from a Z series of images of GL- and RL-adapted filaments of UTEX481 (A and B), SF33 (C and D), FdBk14 (E and F), and FdBk14/pPL2.7GWRcaE (G and H) were collected at a 63X oil immersion lens objective with a 2.5X zoom setting. Bars, 5 μ m.

from AP using the meta scanning filter from 640-753 nm (Figure 2.6, left, indicated by blue color). In RL-grown filaments, autofluorescence was observed using a 615-nm long pass filter (Figure 2.6, right, indicated by blue color), which correlates with the accumulation of PC, as well as PCc and AP. In the autofluorescent images, the differences in cellular morphology between WT and RcaE-deficient strains were more apparent.

To explore further whether the light-dependent changes in cell shape were under direct control of RcaE, the impact of shifting cells from one light condition to another on cellular morphology was examined. In these experiments, the change in shape observed for WT cells was largely photoreversible and preceded light-dependent acclimation of phycobiliprotein levels (Figure 2.7). Cells of GL-grown UTEX481 cultures, shortened significantly when shifted to RL ($p < 0.001$, two-tailed Mann Whitney U test) and elongated significantly when shifted back to GL ($p < 0.001$), while the ratio of A_{560} to A_{620} , an estimation of PE to PC content, remained basically constant. Conversely, UTEX481 cells of RL-grown cultures elongated significantly when shifted to GL ($p < 0.01$) and shortened significantly when shifted back to RL ($p = 0.013$), again with constant A_{560}/A_{620} ratios.

Notably, whereas SF33 cells exhibited a significant response when being shifted from GL to RL ($p = 0.011$) and back ($p < 0.001$), these cells did not display significant changes in cell length in response to RL-grown cells being shifted to GL ($p \geq 0.05$) and back ($p \geq 0.05$). Although no significant changes in length were observed, cells shifted from RL to GL were observably more cylindrical, whereas those shifted from GL to RL

Figure 2.7. Median cell lengths and cell morphologies of *F. diplosiphon* strains in light-shifting experiments. Upper panel, bars represent the median cell lengths (in micrometers) calculated for a data set of at least 100 cells measured for UTEX481, SF33, FdBk14 and 50-100 cells for pPL2.7GWRcaE. Cultures were maintained in constant green (■) or red (■) light or shifted from GL to RL (■) before being shifted back to GL (■) or shifted from RL to GL (■) before being shifted back to RL (■). Lower panel, representative optical slices from a Z-series of DIC images collected at a 40X oil immersion lens objective with a 3X zoom setting. Numbers below the images are the ratios of A_{560} to A_{620} and are reported as an estimation of the ratios of PE to PC.



were more rounded, as observed for all other strains (Figure 2.7, lower panel). GL-grown FdBk14 cells showed only marginally significant responses to being shifted to RL ($p=0.014$) and back ($p=0.03$) and no significant response when RL-grown cells were shifted to GL ($p\geq 0.05$) and back ($p\geq 0.05$). The marginal response observed for GL-grown FdBk14 cells being shifted to RL and returned to GL are markedly much less than the response observed for the SF33 parent.

When GL-grown FdBk14/pPL2.7GWRcaE cells were shifted to RL, there was no statistically significant change in length ($p\geq 0.05$), though the cells did seem to become a bit more rounded. Further, shifting them back from to GL also resulted in no significant difference in length ($p\geq 0.05$), although the cells again become more cylindrical (Figure 2.7). Interestingly, although no significant changes in length were observed, the cells shifted from RL to GL were observably more cylindrical, but upon shifting back to RL, there seems to be a mixture of round and cylindrical cells. This indicates that the morphology is changing, however not as noticeably (or quickly) as what was seen for the WT strains. Taken together, these data indicate that RcaE controls the light-dependent changes in cellular morphology in *F. diplosiphon*, in addition to the steady-state acclimation of phycobiliprotein levels during CCA.

As these results indicate that RcaE is involved in the photoregulation of cell and filament morphologies in *F. diplosiphon*, it was further investigated whether this RcaE-dependent morphological response was being transmitted via the known RcaE-RcaF-RcaC signal transduction pathway (reviewed by Kehoe and Gutu, 2006). Examination of the cell shapes of *rcaF* (FdR101) and *rcaC* (FdR102) mutants that were isolated as pigmentation mutants after heatshock of SF33 cells using an established protocol (Alvey

et al., 2003) was conducted in order to determine whether they exhibited phenotypes similar to the RcaE-deficient FdBk14 mutant. Because *rcaF* and *rcaC* mutants exhibit constitutive accumulation of GL-inducible PE either in GL or RL growth conditions (Chiang *et al.*, 1992; Kehoe and Grossman, 1997) and thus the Rca pathway is likely fixed in the GL mode in these mutants, the observation that cells of the FdR101 and FdR102 mutants grown in either GL or RL were nearly identical in appearance to GL-grown SF33 cells was not unexpected (Bordowitz and Montgomery, unpublished).

2.4 Discussion

In summary, these results indicate that RcaE has a regulatory role in the light-dependent changes in cell shape and filament morphologies in *F. diplosiphon*. The photoreceptor RcaE had already been shown to regulate the light-dependent phycobiliprotein changes that occur as a part of CCA (Kehoe and Grossman, 1997; Terauchi *et al.*, 2004). Although light-dependent changes in vegetative cell morphology previously had been noted to respond to RL and GL illumination (Bennett and Bogorad, 1973), the molecular basis of the photoregulation of cell and filament morphologies for *F. diplosiphon* had not been determined definitively, though it was proposed to be directly or indirectly controlled by a photoreceptor(s) (Bennett and Bogorad, 1973). Thus, the finding that RcaE is the photoreceptor responsible for regulating these responses represents a novel role for the phytochrome-like protein RcaE in this organism and provides a molecular link for the pigmentation and morphological aspects of CCA first documented over 30 years ago.

Phytochromes previously have been implicated in the regulation of development and cellular morphology in a range of organisms from prokaryotes to eukaryotes. Such phytochrome-associated regulation of development includes growth responses, cell shape and filament morphology, sexual development, and cell elongation and expansion (Adamec *et al.*, 2005; Blumenstein *et al.*, 2005; Diakoff and Scheibe, 1975; Kakiuchi *et al.*, 2001; Lazaroff and Schiff, 1962; Robinson and Miller, 1970; Wang, 2005). Thus, the association of RcaE activity with the light-dependent regulation of vegetative cell shape and filament morphology in *F. diplosiphon* described here is not serendipitous for a phytochrome-related protein.

The regulation of PBP accumulation during CCA is largely dependent upon the Rca system. An inability to induce the RL-dependent cellular phenotype in *rcaF* and *rcaC* mutants suggests that functional RcaF and RcaC are required for correct regulation of cell shape in *F. diplosiphon*, at least in response to RL (Bordowitz and Montgomery, unpublished). Such red mutants have previously been thought to disrupt phosphorelay from the kinase-active state of RcaE and thus exhibit phenotypes associated with RcaF and RcaC in their unphosphorylated states (Kehoe and Grossman, 1997). Collectively, these results suggest that RcaE regulates cell shape and filament length via the downstream effectors RcaF and RcaC in response to RL. Whether the kinase activity of RcaE and subsequent phosphorelay to RcaF and RcaC are required absolutely for the photoregulation of cell and filament morphologies and if additional effectors are required for responsiveness to GL are questions currently under investigation.

REFERENCES

1. **Adamec, F., D. Kaftan, and L. Nedbal.** 2005. Stress-induced filament fragmentation of *Calothrix elenkinii* (cyanobacteria) is facilitated by death of high-fluorescence cells. *J. Phycol.* **41**:835-839.
2. **Alvey, R. M., J. A. Karty, E. Roos, J. P. Reilly, and D. M. Kehoe.** 2003. Lesions in phycoerythrin chromophore biosynthesis in *Fremyella diplosiphon* reveal coordinated light regulation of apoprotein and pigment biosynthetic enzyme expression. *Plant Cell* **15**:2448-63.
3. **Balabas, B. E., B. L. Montgomery, L. E. Ong, and D. M. Kehoe.** 2003. CotB is essential for complete activation of green light-induced genes during complementary chromatic adaptation in *Fremyella diplosiphon*. *Mol. Microbiol.* **50**:781-93.
4. **Bennett, A., and L. Bogorad.** 1973. Complementary chromatic adaptation in a filamentous blue-green alga. *J. Cell. Biol.* **58**:419-35.
5. **Blumenstein, A., K. Vienken, R. Tasler, J. Purschwitz, D. Veith, N. Frankenberg-Dinkel, and R. Fischer.** 2005. The *Aspergillus nidulans* phytochrome FphA represses sexual development in red light. *Curr. Biol.* **15**:1833-1838.
6. **Campbell, D.** 1996. Complementary chromatic adaptation alters photosynthetic strategies in the cyanobacterium *Calothrix*. *Microbiology* **142**:1255-1263.
7. **Campbell, D., J. Houmard, and N. T. De Marsac.** 1993. Electron transport regulates cellular differentiation in the filamentous cyanobacterium *Calothrix*. *Plant Cell* **5**:451-463.
8. **Chen, M., J. Chory, and C. Fankhauser.** 2004. Light signal transduction in higher plants. *Annu. Rev. Genet.* **38**:87-117.
9. **Chiang, G. G., M. R. Schaefer, and A. R. Grossman.** 1992. Complementation of a red-light-indifferent cyanobacterial mutant. *Proc. Natl. Acad. Sci. U. S. A.* **89**:9415-9.
10. **Chiang, G. G., M. R. Schaefer, and A. R. Grossman.** 1992. Transformation of the filamentous cyanobacterium *Fremyella diplosiphon* by conjugation or electroporation. *Plant Physiol. Biochem.* **30**:315-325.
11. **Cobley, J. G., E. Zerweck, R. Reyes, A. Mody, J. R. Seludo-Unson, H. Jaeger, S. Weerasuriya, and S. Navankasattusas.** 1993. Construction of shuttle plasmids which can be efficiently mobilized from *Escherichia coli* into the chromatically adapting cyanobacterium, *Fremyella diplosiphon*. *Plasmid* **30**:90-105.

12. **Damerval, T., G. Guglielmi, J. Houmard, and N. T. De Marsac.** 1991. Hormogonium differentiation in the cyanobacterium *Calothrix*: A photoregulated developmental process. *Plant Cell* **3**:191-201.
13. **Diakoff, S., and J. Scheibe.** 1975. Cultivation in the dark of the blue-green alga *Fremyella diplosiphon*. A photoreversible effect of green and red light on growth rate. *Physiol. Plant.* **34**:125-128.
14. **Herdman, M., T. Coursin, R. Rippka, J. Houmard, and N. Tandeau de Marsac.** 2000. A new appraisal of the prokaryotic origin of eukaryotic phytochromes. *J. Mol. Evol.* **51**:205-13.
15. **Kahn, K., D. Mazel, J. Houmard, N. Tandeau de Marsac, and M. R. Schaefer.** 1997. A role for cpeYZ in cyanobacterial phycoerythrin biosynthesis. *J. Bacteriol.* **179**:998-1006.
16. **Kakiuchi, Y., T. Takahashi, A. Murakami, and T. Ueda.** 2001. Light irradiation induces fragmentation of the plasmodium, a novel photomorphogenesis in the true slime mold *Physarum polycephalum*: action spectra and evidence for involvement of the phytochrome. *Photochem. Photobiol.* **73**:324-329.
17. **Kehoe, D. M., and A. R. Grossman.** 1997. New classes of mutants in complementary chromatic adaptation provide evidence for a novel four-step phosphorelay system. *J. Bacteriol.* **179**:3914-21.
18. **Kehoe, D. M., and A. R. Grossman.** 1996. Similarity of a chromatic adaptation sensor to phytochrome and ethylene receptors. *Science* **273**:1409-12.
19. **Kehoe, D. M., and A. R. Grossman.** 1998. Use of molecular genetics to investigate complementary chromatic adaptation: advances in transformation and complementation. *Methods Enzymol* **297**:279-290.
20. **Kehoe, D. M., and A. Gutu.** 2006. Responding to color: The regulation of complementary chromatic adaptation. *Annu. Rev. Plant. Biol.* **57**:127-50.
21. **Laemmli, U. K.** 1970. Cleavage of structural proteins during the assembly of the head of bacteriophage T4. *Nature* **227**:680-685.
22. **Lazaroff, N., and J. Schiff.** 1962. Action spectrum for developmental photo-induction of the blue-green alga *Nostoc muscorum*. *Science* **137**:603.
23. **Reize, I. B., and M. Melkonian.** 1989. A new way to investigate living flagellated/ciliated cells in the light microscope: immobilization of cells in agarose. *Bot. Acta* **102**:145-151.

24. **Robinson, B. L., and J. H. Miller.** 1970. Photomorphogenesis in the blue-green alga *Nostoc commune* 584. *Physiol. Plant.* **23**:461-472.
25. **Sinha, R. P., P. Richter, J. Faddoul, M. Braun, and D. P. Hader.** 2002. Effects of UV and visible light on cyanobacteria at the cellular level. *Photochem. Photobiol. Sci.* **1**:553-9.
26. **Tandeau de Marsac, N., and J. Houmard.** 1988. Complementary chromatic adaptation: physiological conditions and action spectra. *Methods Enzymol.* **167**:318-328.
27. **Terauchi, K., B. L. Montgomery, A. R. Grossman, J. C. Lagarias, and D. M. Kehoe.** 2004. RcaE is a complementary chromatic adaptation photoreceptor required for green and red light responsiveness. *Mol. Microbiol.* **51**:567-77.
28. **Wang, H.** 2005. Signaling mechanisms of higher plant photoreceptors: A structure-function perspective. *Curr. Top. Dev. Biol.* **68**:227-261.

CHAPTER THREE

RcaE Controls the Expression of Cell-Shape-Determining Genes

This chapter contains work submitted as:

Bordowitz, J.R and Montgomery, B.L. (2009) RcaE impacts cell wall structure and controls the expression of genes encoding cell-shape-determining proteins during regulation of cellular morphology in *Fremyella diplosiphon*.

3.1 Introduction

Bacteria display a wide range of cellular morphologies and can modify their shape in response to environmental changes (reviewed in Daniel and Errington, 2003; Shih and Rothfield, 2006; Cabeen and Jacobs-Wagner, 2007). Therefore, regulation of cell shape is important to the function and survival of cells. In bacteria, cell shape is determined by factors involved in the synthesis of the peptidoglycan (PG) layer, which provides strength and rigidity of the cell wall (reviewed in Daniel and Errington, 2003; Osborn and Rothfield, 2007). Over the past decade, much work has gone into identifying and characterizing the cytoskeletal components involved in determining bacterial cell shape (reviewed in Osborn and Rothfield, 2007). Many of the identified factors include actin and tubulin homologs, which prove to be crucial for maintaining PG structure (reviewed in Shih and Rothfield, 2006). However, the role these elements have in the regulation of cell shape remains to be elucidated.

Results presented in the previous chapter demonstrate that the light-dependent morphology of *F. diplosiphon* is regulated by the phytochrome-like photoreceptor RcaE. Little is known about factors involved in regulation of cell shape in cyanobacteria. However, one component that has been recently identified to have a role in the regulation of cell shape and morphology in the filamentous cyanobacterium *Anabaena* sp. PCC 7120 (*Anabaena*) is MreB (Hu *et al.*, 2007). When *mreB* was disrupted in this organism, cell shape was severely impacted; the WT rod-shaped cells become spherical, and nearly doubled in their width.

MreB is an actin-like ATPase bacterial homologue of eukaryotic F-actin; it is filamentous and forms helical structures along the long axis of the cell (Jones *et al.*,

2001). These filaments are localized beneath the bacterial cell membrane (reviewed in Cabeen and Jacobs-Wagner, 2007). MreB (and its counterparts) has been shown to be involved in the regulation of cell shape in many bacterial species, including *Escherichia coli*, *Caulobacter crescentus*, and *Bacillus subtilis* (reviewed in Carballido-López, 2006; Shih and Rothfied, 2006; Divakaruni *et al.*, 2007). In all of these organisms, mutants of *mreB* result in the shift from a rod-shaped (or crescent) cell to a spherical cell. Thus, MreB activity is associated with rod-shaped cells and its absence with spherical cells (reviewed in Cabeen and Jacobs-Wagner, 2007).

The spherical cellular shape observed for the RcaE-deficient FdBk14 mutant strain of *F. diplosiphon* compared to the WT SF33 strain (Bordowitz and Montgomery 2008), resembles the morphology of *mreB* mutants. Therefore, it is hypothesized that cell wall composition and the activity of components such as MreB may be under light- and/or RcaE-dependent regulation in this organism. Hence, the work presented here aims to characterize the impact of RcaE activity on cell wall integrity, as well as to identify and characterize the regulation of an operon encoding cell-shape determining Mre proteins in *F. diplosiphon*.

3.2 Methods

3.2.1 Strains and culture conditions

The *F. diplosiphon* strains used in these experiments are the shortened-filament strain (SF33) of *F. diplosiphon* (Cobley *et al.*, 1993), FdBk14, an *rcaE* null mutant previously described (Kehoe and Grossman, 1996), and UTEX481 (obtained from The Culture Collection of Algae (UTEX)). For comparative studies, FdBk14 was

transformed with pPL2.7 (Cobley *et al.*, 1993) or with pPL2.7GWRcaE (Bordowitz and Montgomery, 2008). The strains were grown in BG-11 (Fluka; Sigma-Aldrich) with 10 mM HEPES, pH 8.0 (hereafter BG-11/HEPES), at 28°C, shaking at 175 rpm with or without 20 µg/mL kanamycin (Kan₂₀) in monochromatic RL or GL, as described in Bordowitz and Montgomery, 2008.

3.2.2 Isolation of *F. diplosiphon* genomic DNA and total RNA

Genomic DNA (gDNA) was isolated from *F. diplosiphon* cultures using a phenol-chloroform based method adapted from a previously described protocol (Wu *et al.*, 2000). Cells were lysed in TE buffer (pH 8.0) in the presence of glass beads using vortexing. The gDNA was extracted with phenol/chloroform (1:1 vol/vol), precipitated with 100% ethanol in the presence of 0.3 M NaOAc (pH 4.5), and then resolubilized in TE buffer (pH 8.0). Isolated gDNA was treated with RiboShredderTM RNase Blend (Epicentre Biotechnologies, Madison, WI) in order to digest contaminating RNA.

Total RNA was isolated from 50 mL cultures grown in either RL or GL, as previously described (Seib and Kehoe, 2002). The concentration and purity of purified DNA and RNA was determined spectrophotometrically using an Agilent 8453 spectrophotometer (Agilent Technologies, Inc., Santa Clara, CA).

3.2.3 Lysozyme sensitivity assays

F. diplosiphon cultures were normalized to $A_{750} \sim 0.6$ and centrifuged at 4,500 rpm for 10 min. Cell pellets were re-suspended in 50 mM Tris-HCl (pH 8.0), 50 mM

NaCl, 10 mM EDTA (pH 8.0), 250 mM sucrose (i.e., STES buffer), with 5 mg/mL lysozyme (Roche) and incubated in darkness, shaking gently on a platform rocker. For each strain, at each time point, three 1 mL samples were spun down at 13,000 rpm for 5 min. The zero time point was taken immediately after initial cell pellet re-suspension. For quantification, supernatants (200 μ L) were loaded in triplicate into a flat-bottom 96-well plate (Corning Plastics, Corning, NY) and fluorescence values read using a SpectraMax M2 microplate reader with excitation at 590 nm and fluorescence emission collected at 642 nm. Total fluorescence is shown as relative fluorescence units (RFU) and results indicate representative data from at least four independent experiments.

3.2.4 A22 treatment

F. diplosiphon cultures were normalized to $A_{750} \sim 0.1$ and allowed to recover in broad-band GL or RL for ~ 5 hrs in 6-well Corning plates (Corning Life Sciences, Lowell, MA). In order to increase the likelihood of cell wall penetration with the inhibitor, cultures were incubated in the dark, as has been described for *F. diplosiphon* transformations (Kehoe and Grossman, 1998). Cultures were then treated with either 10 μ g/mL of MreB inhibitor A22 (Calbiochem, EMD Chemicals, Inc., Gibbstown, NJ) dissolved in methanol or an equal volume of 100% methanol as a control. Cell samples were collected after 24 hrs of treatment, and prepared for differential interference contrast (DIC) and autofluorescence imaging using confocal microscopy as described (Bordowitz and Montgomery, 2008). The lengths and widths of 50 cells were measured for each strain, under each light condition, for all treatments. Data represent the grand median lengths and widths (\pm standard deviation) from 6 independent experiments, after removal

of statistical outliers. Statistical outliers were determined by calculating the interquartile range (IQR) of the data sets for each strain, using the first and third quartiles. A conservative approach was taken by determining an extreme outlier to be outside three times the interquartile range from the first or third quartile. Data sets that contained 50% or more of such outliers were excluded.

3.2.5 Identification and cloning of *F. diplosiphon mreBCD operon*

Primers 5'mreB and 3'mreB (for sequence, see Table 3.1) were designed against the *Anabaena* PCC7120 *mreB* gene (*all0087*), and used to amplify *FdmreB* from isolated gDNA. The initial 1.6 kb fragment isolated was gel purified via QIAquick[®] PCR Purification kit (Qiagen) and cloned into the pCR2.1TOPO vector (Invitrogen Corporation, Carlsbad, CA). Sequencing analysis confirmed an identifiable *mreB* open reading frame, along with a partial *mreC* fragment. Inverse *mreB* primers 5'mreB-r and 3'mreB-r along with those designed for the *Anabaena mreC* (*all0086*) i.e., 5'mreC and 3'mreC were used to amplify *FdmreC* from isolated gDNA. To determine the genomic context of *mreB*, inverse PCR was performed essentially as described (Sambrook and Russell, 2001). Primers 5'mreB-r, 3'mreB-r, 5'mreC-r, 3'mreC-r, 5'mreD, 3'mreD, 3'mreD-r, 5'mreB-intgen1-r, 5'mreB-intgen2-r, and 5'mreB-intgen3-r were used in successive cycles of inverse PCR to identify the flanking genes. BLASTn analyses confirmed identification of genes and sequences were deposited into GenBank as accession number GQ472772.

3.2.6 Production of probes for Southern analyses

Primers FdmreBintF and FdmreBintR were designed against an internal sequence of the identified *mreB* gene, to yield a ~560 bp fragment after PCR amplification, FdmreBint. The fragment was isolated via QIAquick[®] Gel Extraction kit (Qiagen) and subjected to digoxigenin (DIG) labeling as suggested by the manufacturer using the DIG-High Prime DNA Labeling and Detection Starter Kit II (Roche). The *cpeB* positive control gene was also amplified using *cpeB*-PCR1 and *cpeB*-PCR2 primers, and the PCR product was purified and labeled as described above. Non-labeled PCR products were cloned into the pCR2.1TOPO vector (Invitrogen) and sequences confirmed using the M13 priming sites.

3.2.7 Southern blot analyses

SF33 gDNA (10 µg) was digested overnight (~17 hrs) with *Bam*HI, *Hind*III, *Cl*aI or *Taq*I restriction enzymes (Invitrogen). These enzymes were predicted to cut 0, 1, 1 and 4 times within the *FdmreB* gene and 0, 1, 0, and 1 times within the *FdcpeB* gene, respectively (Table 3.2). After electrophoresis on a 0.8% agarose gel at 60V for 4-5 hrs, transfer to Hybond-N nylon membrane (Amersham, Piscataway, NJ) was carried out for 1.5-3 hrs as described previously (Piotr Chomczynski, 1992). Nucleic acids were cross-linked to the membrane using UV-Stratalinker 2400 (Sratagene, Cedar Creek, TX). Pre-hybridization was carried out at 47°C for 30 min using solutions provided by the DIG-High Prime DNA Labeling and Detection Starter Kit II (Roche) and 500 µg/mL purified salmon sperm DNA (Invitrogen). Hybridization was carried out overnight at the same temperature using 100 ng/mL of DIG labeled probe and 500µg/mL purified salmon sperm DNA (Invitrogen). DIG detection was carried out following the manufacturer's

primer name	sequence 5'-3'	purpose
5'mreB	GTGGGGCTTTT TAGG	cloning/sequencing
3'mreB	CTACATATTT CGAGATCGT	cloning/sequencing
5'mreB-r	CCTAAAAAGCCCCAC	cloning/sequencing
3'mreB-r	ACGATCTCGAAATATGTAG	cloning/sequencing
5'mreC	ATAGATGGTTATCTTACG	cloning/sequencing/RT-PCR
3'mreC	GGTTTTCGGGTTTTGGAT	cloning/sequencing
5'mreC-r	CGTAAGATAACCATCTAT	inverse PCR/sequencing
3'mreC-r	TACCAAAACCCGAAACC	inverse PCR/sequencing
5'mreD	ATGAAGATGCCTGCATTT	cloning/sequencing/RT-PCR
3'mreD	TTAAGATTGCTCGAACAA	cloning/sequencing
3'mreD-r	TTGTTGAGCAATCTTAA	inverse PCR/sequencing
5'mreB-intgen1-r	TTAATAAACTCTTTAG	inverse PCR/sequencing
5'mreB-intgen2-r	GCGGTAGCAGTCCGC	inverse PCR/sequencing
5'mreB-intgen3-r	GTTCTTATGGATGAG	inverse PCR/sequencing
mreBintF	AGGTATTGTACTCCA	probe/RT-PCR
mreBintR	ATGAAGAAAGTTCATAAT	probe
mreBRTRV1	TCATGTTGCCAGTTGGTTCAG	RT-PCR
mreCRTRV2	ACCAATGGTCAGCGCTACGT	RT-PCR
mreDintR	CAAGGCAATAGAAATAAA	RT-PCR
ribo23sintF	AGCTTCATTGTCAAGAAG	RT-PCR
ribo23sintR	GCGACCCACTCTCGTGGG	RT-PCR
cpeB-PCR1	GTTCTATATTGTCTTGTTCAGGG	probe
cpeB-PCR2	AAACTGTGTTGGATGTCAATCTG	probe

Table 3.1. Primers used for isolation and identification of *F. diplosiphon mreBCD* operon, generation of probes for Southern blot analyses, and RT-PCR analyses.

guidelines, with the exception of stringency wash temperature optimizations. The CDP-Star (Roche) chemiluminescence was visualized on a Kodak Image Station 2000MM Multimodal Imaging System (Eastman Kodak Company, Rochester, NY) using a black excitation filter and an open emission filter at 0% bulb intensity for the time indicated. Band sizes were determined by standard curve analyses using DIG-labelled DNA ladder II (Roche).

3.2.8 Semi-quantitative RT-PCR amplification analyses

Purified RNA was isolated from WT and FdBk14 mutant cells grown in RL and GL as described above. Purified RNA was then treated with TURBO DNA-free kit (Ambion, Austin, TX) to remove genomic DNA according to the manufacturer's instructions. Reverse transcription was conducted with 1 µg of RNA using the Reverse Transcription System (Promega Corporation, Madison, WI), as suggested by manufacturer. Semi-quantitative polymerase chain reaction (PCR) amplification was performed using 1 µL of cDNA product, GoTaq® Green master mix (Promega) as directed by manufacturer, and primer sets (for sequences see Table 3.1) designed for each gene of interest, i.e., *mreB* (*mreBintF* and *mreBRTRV1*), *mreC* (*5'mreC* and *mreCRTRV2*), *mreD* (*5'mreD* and *mreDintR*), as well as the 23S ribosomal control gene (*ribo23sintF* and *ribo23sintR*). The general program was: denaturation at 94°C for 1 min, then 30 (gene specific) or 25 (ribosomal) cycles of 94°C for 30 s, annealing at the indicated temperature for 30 s, and extension at 68°C for the indicated time (s), followed by an additional cycle of 68°C for 1min, ending with a hold at 4°C. The gene specific

annealing temperatures were: 46°C (*FdmreB*), 48°C (*FdmreC*), 46°C (*FdmreD*) and 51°C (23S ribosomal). Gene-specific extension times were 25 s (*FdmreB*), 20 s (*FdmreC*), 25 s (*FdmreD*), and 40 s (23S ribosomal). The PCR products were analyzed by agarose gel electrophoresis, gels imaged and bands quantified using Quantity One 1-D Software (Bio-Rad Laboratories, Inc., Hercules, CA).

3.3 Results

3.3.1 Light-dependent cell wall alteration

Upon the discovery of the FdBk14 mutant morphology (Bordowitz and Montgomery, 2008), it was proposed that such a difference in cell shape may have a link to cell wall integrity. In Hu *et al.*, (2007), it was reported that MreB mutants of *Anabaena* displayed a round morphology, similar to the phenotype observed for FdBk14, as opposed to the more elongated rod shaped WT cells of *Anabaena*. In the same study, the authors showed that the mutant also released more PBPs after treatment with lysozyme. These results indicated that the round morphology was correlated with a higher susceptibility to treatment with the cell-wall degrading enzyme. To determine whether the spherical shape of FdBk14 cells is associated with a change in cell wall structure or integrity relative to the SF33 parental strain, similar lysozyme-sensitivity assays were performed in order to quantify relative cell sensitivity in GL- and RL-grown cultures.

During a lysozyme-sensitivity time course, it was quite noticeable that, overall, RL-grown cells were more susceptible to lysozyme treatment; these cells released PBPs before their GL counterparts (Figure 3.1A). These results indicate that, indeed, an altered

cell wall is associated with a more rounded morphology, as RL-grown cells tend to be more round in their shape, compared to the cylindrical shape of GL-grown cells (Bordowitz and Montgomery, 2008). Also, the time course shows that there is an initial linear relationship between 0'-20' and 20'-40', before the total PBP fluorescence for each strain reaches a threshold. After calculating the rates (slopes) of the line between these time points (data not shown), it is notable that indeed the RL-grown cells have faster PBP release than those in GL. Additionally, when comparing FdBk14 to SF33, the mutant cells (irrespective of light condition) release of PBPs is initially ~3 times faster than SF33.

By comparing the total PBP release of WT strains after a threshold was reached (at 120'), the results indicate that overall, RL grown cells show higher total fluorescence (Figure 3.1B). The higher PBP release in RL vs. GL in these strains is extremely significant ($p=0.0005$ or $p<0.0001$ for UTEX481 and SF33, respectively). When comparing the WT strains, it is clear that UTEX481 releases more PBPs than SF33. This could be due to the difference in cell size; i.e., the UTEX481 cells are larger than the SF33 cells (Bordowitz and Montgomery, 2008), and therefore may contain more PBS than SF33 cells. In contrast, the FdBk14 mutant displays significantly lower ($p\leq 0.005$) PBP release in RL than in GL. Notably, however, the FdBk14 has higher fluorescence under both light conditions, than its parental strain SF33—2.3 and 1.2 times higher for GL and RL respectively. Thus, regardless of light condition, functional RcaE seems to be needed for lysozyme resistance.

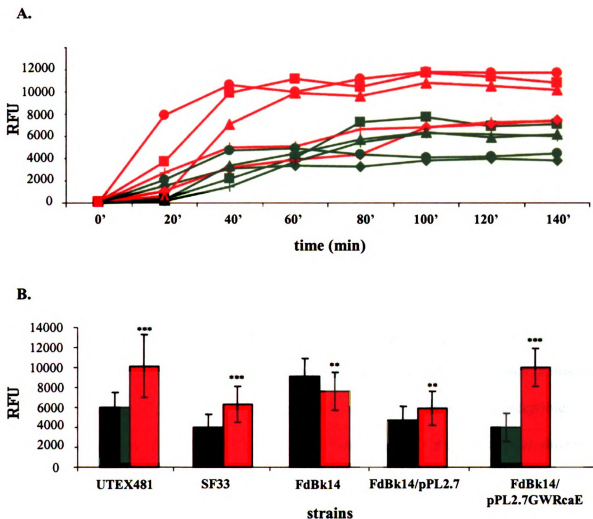


Figure 3.1. Lysozyme-sensitivity assays for *F. diplosiphon* strains. Phycobiliprotein (PBP) release was measured after treatment with 5 mg/mL lysozyme. Total PBP fluorescence was measured in supernatants of cells at an emission of 642 nm after excitation at 590 nm. A) Release of PBPs over time: UTEX481 (■) SF33 (◆), FdBk14 (▲), pPL2.7 (+) and RcaE (●); color of lines indicate growth condition. Graph is a representative time course from 4 independent experiments. B) Total PBP fluorescence after 120 min incubation with lysozyme. Color of bars indicates growth condition. Data represent the mean (\pm standard deviations) of at least 4 independent experiments. ***, $p \leq 0.0005$, and **, $p \leq 0.005$, indicate significant difference between GL vs. RL values, as determined using unpaired two-tailed t-test.

To further investigate RcaE's role in lysozyme susceptibility, FdBk14 was complemented with full length RcaE. The above-mentioned GL vs. RL difference in lysozyme sensitivity observed for WT strains was restored in FdBk14 cells complemented with a WT copy of *rcaE*, but not in cells transformed with an empty vector. Taken together, these results indicate first, that RL grown cells, which are more round in their shape, are more susceptible to lysozyme treatment, and hence may be altered in their cell wall composition. Second, the FdBk14 mutant in general, is more susceptible than the SF33 parent, which further indicates that the rounded cell morphology is linked to an altered cell wall composition.

3.3.2 Effect of A22 on F. diplosiphon cell lengths and widths

After establishing a light-dependent cell wall alteration in *F. diplosiphon*, a link to *mreB* was investigated by testing whether or not *F. diplosiphon* cells were susceptible to a known MreB inhibitor, A22 (Gitai *et al.*, 2005; Bean *et al.*, 2009). As has been shown for many bacteria, treatment of cells with this inhibitor results in morphologies that mimic an *mreB* mutant, i.e. A22-treated cells become more rounded in shape compared to their WT counterparts (Gitai *et al.*, 2005; Bean *et al.*, 2009). *F. diplosiphon* cultures grown under GL or RL conditions were normalized at $A_{750} \sim 0.1$ and then treated for 24 hours with either an empty vehicle (methanol) or 10 $\mu\text{g/mL}$ of A22.

Both the UTEX481 and SF33 cells exhibited visual morphological responses in GL and RL when treated with A22, compared to the methanol control treatment (compare Figure 3.2A and C to B and D; E and G to F and H). The length of UTEX481 cells shortened significantly after treatment (Figure 3.3A) under both light conditions; cells

were ~8% and ~10% shorter in GL and RL respectively ($p < 0.01$ and $p < 0.001$). In addition to the change in length, these cells also significantly widened by ~5% in GL ($p < 0.001$; Figure 3.3B). The SF33 cells also decreased in length under both light conditions, ~3% in GL, and ~6% in RL (Figure 3.3A). In contrast with UTEX481, SF33 cells decreased significantly in width, ~7% in GL ($p < 0.01$; Figure 3.3B). A22 treatment of FdBk14 cells elicited smaller effects with a limited observable impact on cellular morphology (Figure 3.2I - L). The length of FdBk14 cells was not significantly altered under GL or RL (Figure 3.3A); however, the width of FdBk14 cells was marginally reduced in both GL and RL (Figure 3.3B).

The FdBk14 mutant cells were affected only slightly by the A22 inhibitor—i.e., there were only slight changes in cell and width. Since MreB activity is inhibited by A22, these results indicate that the FdBk14 mutant either lacks MreB, or at least contains lower levels of it. By contrast, the length and width of both UTEX481 and SF33 cells were affected. These results suggest that *mreB* is playing a role in the difference in cell morphology between the WT strains UTEX481, SF33 and the FdBk14 mutant strain. If the presence of *mreB* is required for the more elongated cells, such as was seen in the WT strains, then this could explain why there were more significant (albeit slight) changes in the WT cells when treated with A22, than there were in the FdBk14 mutant cells, which are already round in shape. These results suggest that there may be differential expression of *mreB* not only in the WT versus mutant strains, but also possibly in GL versus RL, since cells are more elongated in GL than in RL (Bennett and Bogorad, 1973; Bordowitz and Montgomery, 2008).

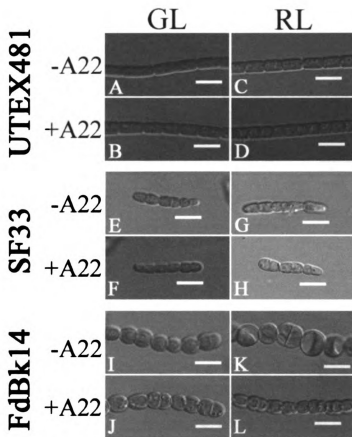


Figure 3.2. *F. diplosiphon* morphological differences between A22-treated strains in GL and RL. Representative optical slices from a Z-series of DIC images of GL- and RL-adapted filaments of UTEX481 (A-D), SF33 (E-H), and FdBk14 (I-L) treated for 24 h with methanol only (-A22) or with MreB inhibitor A22 at a concentration of 10 $\mu\text{g}/\text{mL}$ (+A22) after normalizing cultures to $A_{750} \sim 0.1$. Images were captured with a 40X oil immersion lens objective, with 2X zoom. Bars, 10 μm .

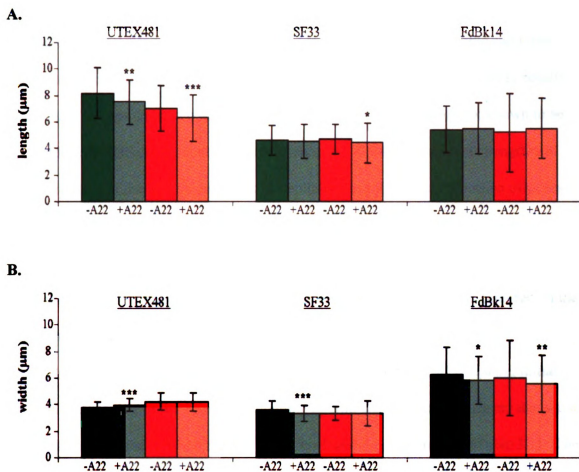


Figure 3.3. Cell length and width responses of *F. diplosiphon* to treatment with MreB inhibitor A22. Cultures were grown with 10 µg/mL of inhibitor (+A22) or with an equal volume of 100% methanol used as a vehicle control (-A22) for 24 h after normalizing cultures to $A_{750} \sim 0.1$. Data represent median lengths (A) or widths (B) of at least 175 cells for 6 independent experiments. Bars indicate color of light for growth conditions. *, $p < 0.05$, **, $p < 0.01$, and ***, $p < 0.001$, indicate marginal, statistical, and highly statistical significance respectively, as determined using two-tailed Mann-Whitney U-test.

3.3.3 *F. diplosiphon* contains an *mreBCD* operon

Since it is evident that there is likely cell-wall component(s) being affected in the morphological differences occurring during CCA, identification of possible candidates which could be involved in this phenomenon was pursued. Previous microarray results from *F. diplosiphon* indicated differential regulation of 17 novel genes not known to be associated with PBS components (Stowe-Evans *et al.*, 2004). These data strengthened the prediction that the photoreceptor RcaE could be controlling the expression of genes associated with cell wall composition, given both the morphological differences, as well as the results gathered from the lysozyme-sensitivity assays. Based on what is known about cell-shape determining factors (discussed in section 3.1), focus was centered on the cell-shape determining gene *mreB*.

As there was no publicly available genome sequence for *F. diplosiphon*, initial isolation and cloning of the *FdmreB* containing operon was done using primers that were designed based on the *Anabaena* (PCC7120) *mreB* and *mreC* sequences (Table 3.1). The isolated clones contained a fragment with sequence homologous to *mreB* (BLASTn), as well as a partial fragment homologous to *mreC* (BLASTn). After further cloning, inverse PCR, and sequence analysis, an entire *FdmreBCD* operon was identified (Figure 3.4). BLASTn analyses of the 1,044 bp *FdmreB* sequence identified matches to genes encoding rod-shape determining proteins, MreB, and MreB-like sub families of various other cyanobacteria (Figure 3.5A). These same analyses on the 816 bp *FdmreC*, and 618 bp *FdmreD* yielded similar results (Figure 3.5B and C, respectively). In all cases, the newly identified *F. diplosiphon* genes share highest homology to their *Nostoc* and *Anabaena* counterparts.

3.3.4 Verification of *mreB* copy number in *F. diplosiphon*

In order to determine *mreB* gene copy number in *F. diplosiphon*, Southern blot analysis was utilized. A non-radioactive approach was taken, and DNA probes were designed, PCR- amplified, and labeled with digoxigenin (DIG), a steroid hapten, to label the probes for hybridization and subsequent chemiluminescence detection, as described in the methods section (3.2.7). Restriction enzymes were chosen which produced 5' overhangs, and which were predicted to have 0, 1, or multiple cut sites within the *FdmreB* gene (Table 3.2). As an experimental control the *FdcpeB* gene was used, which has been previously confirmed as a single copy gene (Grossman *et al.*, 1986).

The *Bam*HI enzyme, which was predicted not to cut within the *mreB* gene, yielded a single, large smear (Figure 3.6, left panel), while *Hind*III (predicted to cut once) consistently yielded two bands (Figure 3.6, right panel). *Cla*I, which was also predicted to cut once, showed only one band. However, one of the bands for this enzyme was predicted to be about 86 bps, so it is quite likely that this size was not resolved well enough during electrophoresis, hence no detection on the blot. Unfortunately, *Taq*I, which was predicted to cut *mreB* four times, showed only two distinguishable bands (somewhat smeared) at best. Again, this could most likely be due to the fact that four out of the five bands were all predicted to be less than 100 bps in size.

As previously stated, these same enzymes were used for Southern analysis on the *cpeB* gene, a gene which encodes the β -subunit of PE (Grossman *et al.*, 1986). The band

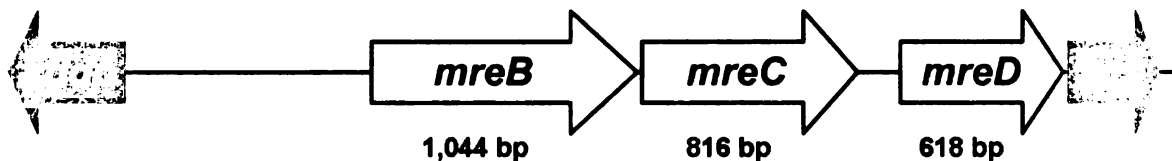


Figure 3.4. Organization of *mreBCD* operon in *F. diplosiphon* genome. Cloning and sequencing analyses confirm that *mreB*, *mreC*, and *mreD* are located in an operon, downstream of an open reading frame encoding an RNA-directed DNA polymerase (*rddp*) and upstream of an open reading frame encoding a gene with limited similarity to an exodeoxyribonuclease (*orf*). The *mreBCD* genes are ~1.0 kb, 816 bp, and 618 bps in size, respectively.

A.

Accession	Description	e value	identity
CP001037.1	<i>N. punctiforme</i> PCC 73102; cell shape determining protein, MreB/Mrl family	0.0	88%
BA000019.2	<i>Nostoc sp.</i> PCC 7120 DNA; rod shape-determining protein	0.0	83%
CP000117.1	<i>A. variabilis</i> ATCC 29413; rod shape-determining protein MreB	0.0	82%
CP000393.1	<i>T. erythraeum</i> IMS101; rod shape-determining protein MreB	0.0	74%
CP000951.1	<i>Synechococcus sp.</i> PCC 7002; cell shape determining protein, MreB/Mrl family	2.0E-168	74%
CP001291.1	<i>Cyanothece sp.</i> PCC 7424; cell shape determining protein, MreB/Mrl family	7.0E-155	73%

B.

Accession	Description	e value	identity
CP001037.1	<i>N. punctiforme</i> PCC 73102; Rod shape-determining protein MreC	1.0E-155	76%
CP000117.1	<i>A. variabilis</i> ATCC 29413; rod shape-determining protein MreC	5.0E-136	74%
BA000019.2	<i>Nostoc sp.</i> PCC 7120 DNA; rod shape-determining protein	1.0E-130	74%
CP000393.1	<i>T. erythraeum</i> IMS101; rod shape-determining protein MreC	4.0E-11	65%

C.

Accession	Description	e value	identity
CP001037.1	<i>N. punctiforme</i> PCC 73102; conserved hypothetical protein	2.0E-126	76%
CP000117.1	<i>A. variabilis</i> ATCC 29413; conserved hypothetical protein	1.0E-111	78%
BA000019.2	<i>Nostoc sp.</i> PCC 7120 DNA; all0001 all0085	1.0E-111	78%
CP001344.1	<i>Cyanothece sp.</i> PCC 7425; rod shape-determining protein MreD	2.0E-27	68%
CP001287.1	<i>Cyanothece sp.</i> PCC 8801; rod shape-determining protein MreD	5.0E-21	66%

Figure 3.5. BLASTn (nt database) results of cloned *FdmreBCD* operon components. Tables indicate the highest scoring hits for A.) *FdmreB*, B.) *FdmreC*, and C.) *FdmreD*

gene	size (bp)	enzyme	No. of cuts	sites (bp)
<i>mreB</i>	1008	<i>Bam</i> HI	0	n/a
		<i>Hind</i> III	1	228
		<i>Cla</i> I	1	86
		<i>Taq</i> I	4	8, 86, 203, 819
<i>cpeB</i>	555	<i>Bam</i> HI	0	n/a
		<i>Hind</i> III	1	512
		<i>Cla</i> I	0	n/a
		<i>Taq</i> I	1	527

Table 3.2. Predicted number of restriction enzyme sites for *mreB* and *cpeB* in *F. diplosiphon* genome. Cut sites were predicted based on gene products obtained with primers described in Table 3.1.

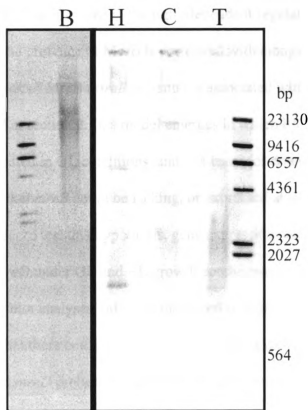


Figure 3.6. *F. diplosiphon mreB* Southern blot analysis. 10 µg of gDNA was digested overnight (~17 h) with *Bam*HI (B), *Hind*III (H), *Cla*I (C), or *Taq*I (T). Chemiluminescent detection of *mreB* DNA probe after hybridization to N-nylon membrane. Sizes of detected bands were calculated based on standardization with the DNA ladder.

patterns resulting from digestion with each of the enzymes matched with the expected number (Table 3.2), given a single copy (data not shown), hence the DIG-labeled probe and protocol proved to be a suitable technique for detection. After comparing the results from the *FdmreB* analyses and the *FdcpeB* analyses, it appears that *mreB* exists as a single copy with in the *F. diplosiphon* genome.

3.3.5 Light-regulated *FdmreBCD* gene expression

Given the lysozyme sensitivity and A22 treatment results, it was logical to predict MreB (and/or *mreBCD*) to be involved in the light-dependent regulation of cell shape in *F. diplosiphon*. Since the presence of MreB is correlated with elongated (rod-shaped) cell morphology, and lack of MreB (*mreB* mutants) is associated with rounder cell morphology (discussed in section 3.1), a model emerges in which it is predicted that (1) *mreB* could be up-regulated in GL conditions, and at a basal (or down-regulated) level in RL conditions, and (2) that *mreB* could be lacking, or expressed at lower levels, in the FdBk14 mutant. In order to test this hypothesis, gene expression analyses was conducted for *mreB*, *mreC*, and *mreD* under GL and RL growth conditions.

Initial Northern blot analyses indicated that *mreB* is indeed up-regulated in GL (data not shown), and that there could be lower levels in the FdBk14 mutant. Further analyses with *mreC* and *mreD* probes indicated that MreB, C and D could be co-regulated. In order to verify these preliminary results, a semi-quantitative reverse transcription- polymerase chain reaction (RT-PCR) approach was taken. RT was done on total RNA collected from UTEX481, SF33 and FdBk14 (as described in section 3.2.8) grown in GL and RL.

RT-PCR analyses indicated that *mreB* is expressed quite well in the UTEX481 cells, with higher expression under GL conditions than RL conditions (Figure 3.7A and B). These results correlate with the more elongated cell shape previously observed under GL (Bennett and Bogorad, 1973; Bordowitz and Montgomery, 2008), and the hypothesis that *mreB* may be expressed higher in GL-grown cells. RT-PCR analyses also indicated that *mreB* expression is distinctly lower in the FdBk14 cells than in the SF33 cells under both GL ($p=0.0546$) and RL ($p=0.0017$) conditions (Figure 3.7A and B). Notably, *mreB* was expressed at fairly high levels in SF33 cells grown under both GL and RL conditions (Figure 3.7A and B). Expression levels of *mreC* and *mreD* were also assessed; both of these genes were expressed at lower levels than *mreB* in UTEX481 and SF33 (compare Figure 3.7 A, C, D). Additionally, the expression of these two genes was considerably lower in the FdBk14 mutant than in UTEX481 and SF33 (compare Figure 3.7 A, C, and D).

Taken together, these results indicate that functional RcaE is required for WT *mre* gene expression in *F. diplosiphon*. Since *mre* genes are more highly expressed in SF33 cells than in the FdBk14 mutant, these results correlate very nicely with the mutant morphology and the known function of MreB. This also indicates RcaE-dependent *mreB* expression in *F. diplosiphon* and a novel function for this photoreceptor.

3.4 Discussion

To summarize, the work presented in this chapter has shown that there is a light-dependent alteration in cell wall integrity that is associated with the difference in *F.*

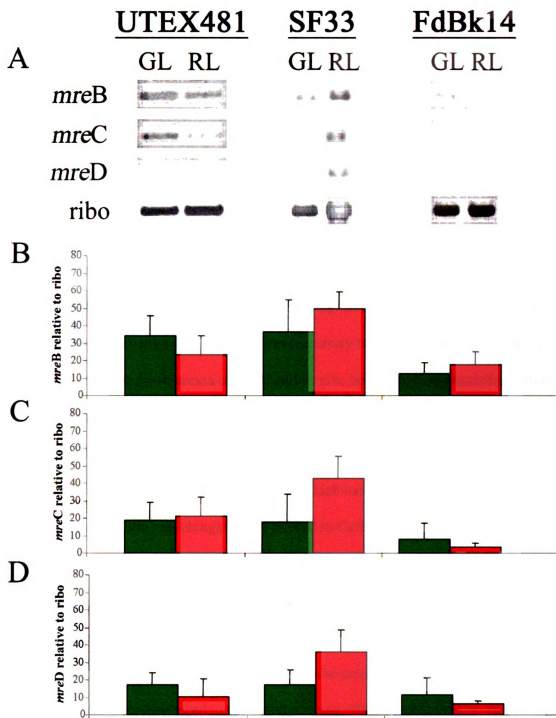


Figure 3.7. mRNA expression analyses of *F. diplosiphon* *mre* genes. Comparative mRNA expression analyses were conducted for *mreB*, *mreC*, and *mreD* using RT-PCR analysis for RNA isolated from UTEX481, SF33, or FdBk14 cells grown under GL and RL conditions. mRNA expression analyses of the 23S ribosomal gene (ribo) were used as a control. A.) Agarose gel electrophoresis analyses of PCR products from a representative RT-PCR reaction. B.) *mreB*, C.) *mreC* and D.) *mreD* average mRNA values (\pm standard deviation) were calculated from at least 3 independent experiments. Color of bar indicates growth condition.

diplosiphon cell morphology. Cells that are more rounded in shape, i.e. RL-grown UTEX481 and SF33, or the spherical FdBk14 mutant, are more susceptible to lysozyme treatment. By contrast, cells that are more cylindrical or rod-like in shape, i.e., GL-grown UTEX481 and SF33 cells seem to be more resistant to lysozyme. This increased susceptibility indicates that there is an altered cell wall composition associated with the rounded cellular morphology of the FdBk14 mutant, and that this change in composition could be what causes the change from a rigid rod-shaped cell to a sphere.

With the discovery of RcaE-dependent cellular morphology (Bordowitz and Montgomery, 2008), and microarray results indicating the regulation of 17 novel genes during CCA (Stowe-Evans *et al.*, 2004), it was necessary to focus on the identification of factors which could be downstream of RcaE and/or also be involved in regulating cellular morphology. Since the lysozyme-sensitivity assays established the possibility of an altered cell wall composition, and A22 treatment affected WT cellular lengths and widths, emphasis was placed on the *mre* system, which has been identified in many bacteria to be involved in cell elongation (reviewed in Carballido-López, 2006; Shih and Rothfield, 2006). Cloning and sequencing analyses confirmed the presence of an *mreBCD* operon in *F. diplosiphon* (Figure 3.4), with further Southern analysis indicating existence of *mreB* as a single copy in the genome (Figure 3.6).

The bacterial actin MreB has been shown to be present in rod-shaped cells, while absent in spherical cells (reviewed in Carballido-López, 2006). Additionally, the MreB inhibitor, A22, has been shown to mimic the morphology of cells lacking *mreB*, i.e., round cells in *Caulobacter* and *E. coli* (Gitai *et al.*, 2005; Karczmarek *et al.*, 2007). Treating *F. diplosiphon* UTEX481 and SF33 cells with A22 resulted in reduced length in

both GL and RL conditions (Figure 3.3A), and an increased width in GL conditions (Figure 3.3B). Since these results show that A22 has a significantly larger impact on cellular morphology of GL-grown cells, it is clear that functional MreB is present in *F. diplosiphon*. Further, MreB activity can be linked to the more elongated, brick-shaped cells which are observed under GL-growth conditions.

In order to link MreB activity and the photoregulation of cellular morphology in *F. diplosiphon*, the expression of the *mre* genes was assessed. RT-PCR analyses showed that the expression of this operon is down-regulated in the FdBk14 strain (Figure 3.7), which exhibits spherical cells independent of the light conditions under which it is grown (Bordowitz and Montgomery, 2008). Additionally, the *mre* genes are more highly expressed in the WT UTEX481 and SF33 cells (Figure 3.7); specifically, *mreB* is up-regulated in UTEX481 GL-grown cells (Figure 3.7A), which display a more elongated morphology. These results further indicate that MreB expression is correlated with the regulation of cell shape in *F. diplosiphon*. These results also suggest that RcaE regulates the expression of the *mre* genes in *F. diplosiphon*, and that *mreB* could be an important factor in the RcaE-dependent photoregulation of cellular morphology.

The work presented in this chapter demonstrates a novel role for the photoreceptor RcaE in the regulation of the morphogene *mreB* in cyanobacteria. While the role of *mreB* and its counterparts (*mreC* and *mreD*) in cell shape determination is well-studied and widely accepted, regulation of these factors remains to be fully elucidated. The results in this chapter provide novel insight into the photoregulation of cell shape in cyanobacteria. However, it is evident that *mreB* is not the only factor involved in RcaE-dependent photoregulation of cellular morphology, as illustrated by the

previously mentioned microarray studies (Stowe-Evans *et al.*, 2004). Recent data also has identified a role for FdTonB, a novel member of the TonB family of proteins and a glycine-rich protein, as a novel effector in the GL-dependent regulation of cellular morphology in *F. diplosiphon* (Pattanaik and Montgomery, submitted). This discovery of RcaE-dependent photoregulation of *mreB* now serves as initiating groundwork towards the identification of additional components involved in the CCA-dependent regulation of cell shape in *F. diplosiphon*.

REFERENCES

1. **Bean, G. J., S. T. Flickinger, W. M. Westler, M. E. McCully, D. Sept, D. B. Weibel, and K. J. Amann.** 2009. A22 disrupts the bacterial actin cytoskeleton by directly binding and inducing a low-affinity state in MreB. *Biochemistry* **48**:4852-7.
2. **Bennett, A., and L. Bogorad.** 1973. Complementary chromatic adaptation in a filamentous blue-green alga. *J Cell Biol* **58**:419-35.
3. **Bordowitz, J. R., and B. L. Montgomery.** 2008. Photoregulation of cellular morphology during complementary chromatic adaptation requires sensor-kinase-class protein RcaE in *Fremyella diplosiphon*. *J Bacteriol* **190**:4069-74.
4. **Cabeen, M. T., and C. Jacobs-Wagner.** 2005. Bacterial cell shape. *Nat Rev Microbiol* **3**:601-10.
5. **Cabeen, M. T., and C. Jacobs-Wagner.** 2007. Skin and bones: the bacterial cytoskeleton, cell wall, and cell morphogenesis. *J Cell Biol* **179**:381-7.
6. **Carballido-Lopez, R.** 2006. Orchestrating bacterial cell morphogenesis. *Mol Microbiol* **60**:815-9.
7. **Chomczynski, P.** 1992. One-hour downward alkaline capillary transfer for blotting of DNA and RNA. *Anal Biochem* **201**:134-9.
8. **Cobley, J. G., E. Zerweck, R. Reyes, A. Mody, J. R. Seludo-Unson, H. Jaeger, S. Weerasuriya, and S. Navankasattusas.** 1993. Construction of shuttle plasmids which can be efficiently mobilized from *Escherichia coli* into the chromatically adapting cyanobacterium, *Fremyella diplosiphon*. *Plasmid* **30**:90-105.
9. **Daniel, R. A., and J. Errington.** 2003. Control of cell morphogenesis in bacteria: two distinct ways to make a rod-shaped cell. *Cell* **113**:767-76.
10. **Divakaruni, A. V., C. Baida, C. L. White, and J. W. Gober.** 2007. The cell shape proteins MreB and MreC control cell morphogenesis by positioning cell wall synthetic complexes. *Mol Microbiol* **66**:174-88.
11. **Gitai, Z., N. A. Dye, A. Reisenauer, M. Wachi, and L. Shapiro.** 2005. MreB actin-mediated segregation of a specific region of a bacterial chromosome. *Cell* **120**:329-41.
12. **Grossman, A. R., P. G. Lemaux, and P. B. Conley.** 1986. Regulated synthesis of phycobilisome components. *Photochem Photobiol* **44**:827-37.

13. **Hu, B., G. Yang, W. Zhao, Y. Zhang, and J. Zhao.** 2007. MreB is important for cell shape but not for chromosome segregation of the filamentous cyanobacterium *Anabaena* sp. PCC 7120. *Mol Microbiol* **63**:1640-52.
14. **Jones, L. J., R. Carballido-Lopez, and J. Errington.** 2001. Control of cell shape in bacteria: helical, actin-like filaments in *Bacillus subtilis*. *Cell* **104**:913-22.
15. **Karczmarek, A., R. Martinez-Arteaga, S. Alexeeva, F. G. Hansen, M. Vicente, N. Nanninga, and T. den Blaauwen.** 2007. DNA and origin region segregation are not affected by the transition from rod to sphere after inhibition of *Escherichia coli* MreB by A22. *Mol Microbiol* **65**:51-63.
16. **Kehoe, D. M., and A. R. Grossman.** 1996. Similarity of a chromatic adaptation sensor to phytochrome and ethylene receptors. *Science* **273**:1409-12.
17. **Kehoe, D. M. a. G., A.R.** 1998. Use of molecular genetics to investigate complementary chromatic adaptation: advances in transformation and complementation. *Methods Enzymol.* **297**:279-290.
18. **Osborn, M. J., and L. Rothfield.** 2007. Cell shape determination in *Escherichia coli*. *Curr Opin Microbiol* **10**:606-10.
19. **Sambrook, J. a. R., D.W.** 2001. *Molecular Cloning: A Laboratory Manual*, New York.
20. **Seib, L. O., and D. M. Kehoe.** 2002. A turquoise mutant genetically separates expression of genes encoding phycoerythrin and its associated linker peptides. *J Bacteriol* **184**:962-70.
21. **Shih, Y. L., and L. Rothfield.** 2006. The bacterial cytoskeleton. *Microbiol Mol Biol Rev* **70**:729-54.
22. **Stowe-Evans, E. L., J. Ford, and D. M. Kehoe.** 2004. Genomic DNA microarray analysis: identification of new genes regulated by light color in the cyanobacterium *Fremyella diplosiphon*. *J Bacteriol* **186**:4338-49.
23. **Wu, X., Zarka, A. and Boussiba, S.** 2000. A simplified protocol for preparing DNA from filamentous cyanobacteria. *Plant Molecular Biology Reporter* **18**:385-392.

CHAPTER FOUR

In vivo Biochemical Characterization of RcaE

4.1 Introduction

CCA is a photomorphogenic process utilized by some cyanobacteria in order to optimally grow and thrive in their changing light environment. As explained in detail in section 1.2, this particular process is predominantly responsive to GL and RL.

Cyanobacteria adapt to these different wavelengths by accumulating the appropriate PBPs in their light-harvesting rods to optimally absorb these wavelengths, and thereby support maximal photosynthetic efficiency. As a result, the cyanobacteria exhibit a color phenotype that is indicative of the wavelength of light to which they have adapted (revisit Figure 1.1)

Although the CCA signaling mechanism has been the topic of multiple recent reviews, the actual biochemical function of the photoreceptor RcaE has yet to be determined (Kehoe and Gutu, 2006; Montgomery, 2008). Much of what is known about CCA has been elucidated through molecular genetic characterization of key components of the complex two-component system (TCS) that has been proposed to regulate the CCA process. Despite the detailed transcriptional analyses of the expression of operons which encode the light-regulated PBPs (Li *et al.*, 2008; Sobczyk *et al.*, 1993; Li and Kehoe, 2005) and the work that has been done to characterize the phosphorylation status of RcaC (Li and Kehoe, 2005), direct evidence of the biochemical mechanism utilized by RcaE is still lacking. After identifying multiple conserved domains (revisit Figure 1.2), which implicate possible biochemical and molecular function(s) of RcaE, it is clear that mutational analyses of key residue(s) within these domains could shed light on RcaE's role in regulating CCA.

The identified GAF domain of RcaE comprises the chromophore-binding domain (CBD) which is a part of the N-terminus of phytochrome and phytochrome-like proteins. The CBD of RcaE contains residues that are necessary for chromophore attachment, specifically a conserved Cys residue (C198), which has been shown to be required for chromophore attachment by mutational analyses (Terauchi *et al.*, 2004). Zinc blot analyses confirmed that this residue was indeed required for RcaE to bind a bilin chromophore *in vivo* (Terauchi *et al.*, 2004). However, in these same studies, the RcaE-C198A variant, which was hypothesized to lack light-sensing capability, fully complemented the pigmentation defect of the FdBk14 mutant in RL but not in GL. This suggests that in RL RcaE function could be independent of covalent bilin attachment, dependent upon associated proteins, or that there is another intramolecular chromophore attachment site important for RL responsiveness.

As previously introduced (section 1.8.1), another important activity/function of the GAF domain is its role in chromophore-binding specificity, as well as chromophore conformation, both of which contribute significantly to photoreceptor photochemical activity. For example, as previously discussed (section 1.4) the Pr and Pfr isomers of plant phytochromes result from differing chromophore conformations (reviewed in Chen *et al.*, 2004; Rockwell *et al.*, 2006). The ability of the chromophore to undergo photoisomerization is what allows phytochrome molecules to absorb different light wavelengths, and thus affects the function of the holoprotein.

Previously described studies ascribe a conserved role in chromophore conformation (and as a direct result, photochemistry) to a highly conserved tyrosine (Tyr) residue (Fischer and Lagarias, 2004; Fischer *et al.*, 2005). Their work showed that this

residue was responsible for the same photochemical function in phytochromes of *Arabidopsis*, *Synechocystis*, and *Pseudomonas aeruginosa*. RcaE contains a conserved Tyr in the GAF domain at position 137 (Y137; Figure 1.5, box #2). To gain further insight into RcaE function, it is important to determine whether RcaE uses similar tyrosine-dependent photochemistry to distinguish between RL and GL.

RcaE also contains a PAS domain, which is adjacent to the CBD. Typically PAS domains are involved in signal sensing and protein-protein interactions (Taylor and Zhulin, 1999). This region of RcaE could be involved in sensing the signal that initiates the light-signaling cascade. Also, since the C198A mutation is a loss of function mutant under only one light condition, the PAS domain could be a potential site for chromophore attachment or facilitate binding of an associated protein(s).

Another residue of interest is a conserved histidine (His) at position 430 (H430) located in a conserved Hbox domain in the C-terminal portion of RcaE. Hbox domains are motifs conserved in the kinase domains of HKs. The conserved His residue is the site for autophosphorylation in HK dimers, which are important for signal activation. Various studies have shown that mutation of the conserved histidine in HKs inhibits responses to stimuli (reviewed in Vierstra, 2003). As described previously (section 1.6.1), HKs play an important role in sensing and responding to environmental cues in bacteria via two-component systems (TCS). Therefore, the conserved H430 is a potential site for autophosphorylation of RcaE, and thus the initiation of the CCA phospho-transfer cascade. The hypothesis that this region of RcaE may be involved in phospho-transfer is supported by results obtained when insertional mutants, which resulted in truncations of RcaE's HK

domain, elicited a red colored phenotype (Kehoe and Grossman, 1997), allowing the speculation that this domain is responsible for the kinase activity.

In order to determine the role of these residues in RcaE biochemical function, and by extension the domains in which they are located, a mutational analysis approach was taken. The conserved Y137 residue in the GAF domain, a portion of the PAS domain which contains 9 of the most highly conserved residues, and the conserved H430 within the Hbox domain have been targeted for alanine substitution mutagenesis (Figure 4.1). These studies were designed to determine whether these residues and domains are critical for RcaE function and the regulation of pigmentation and cellular morphology during CCA.

4.2 Methods

4.2.1 Strains and culture conditions

The wild-type (WT) pigmentation strain used in these experiments refers to the shortened-filament strain (SF33) of *F. diplosiphon* (Cobley *et al.*, 1993). FdBk14 is an *rcaE* null mutant previously described (Kehoe and Grossman, 1996). For comparative studies, FdBk14 was transformed with pPL2.7 (Cobley *et al.*, 1993), pPL2.7GWRcaE (Bordowitz and Montgomery, 2008), or pPL2.7GWRcaE mutant variants (this study). The strains were grown in BG-11 (Fluka; Sigma-Aldrich) with 10 mM HEPES, pH 8.0, (BG-11/HEPES) at 28°C, shaking at 175 rpm with or without 20 µg/mL kanamycin (Kan₂₀) in monochromatic RL or GL, as described (Bordowitz and Montgomery, 2008).

4.2.2 Construction of RcaE mutant variants and transformations

The Gateway[®] converted pPL2.7 shuttle vector containing the full length RcaE driven by its native promoter, pPL2.7GWRcaE (Bordowitz and Montgomery, 2008), was used as a template for mutagenesis using a QuikChange[®] Lightning Site-Directed Mutagenesis Kit (Stratagene). The primers indicated in Table 4.1 were used in order to yield the desired mutant variants, RcaE-Y137A (Y137A), RcaE-Y137H (Y137H), RcaE-PAS (PAS), and RcaE-H430A (H430A). Mutagenesis was conducted according the manufacturer's instruction. The RcaE-C198A (C198A) variant was produced by restriction digestion of a pASKRcaE-C198A construct (Teruachi *et al.*, 2004) and sub-cloning into the pDONZeonpRcaE by ligation (Montgomery, unpublished). The final construct was produced by cloning into pPL2.7GW (Bordowitz and Montgomery, 2008) via Gateway[®] Technology. RcaE constructs were transformed in triplicates into FdBk14 cells via electroporation as described (Bordowitz and Montgomery, 2008).

4.2.3 Whole-cell spectral analysis

Complementation of mutant strains was observed spectrophotometrically as previously described in section 2.2.3.

4.2.4 Chl *a* and PBP quantification

Chlorophyll *a* (chl *a*) and PBPs were extracted and analyzed as described in section 2.2.4. The levels of phycobiliproteins are reported as the grand average (\pm standard deviations) of at least 3 independent experiments and normalized to their respective levels of chl *a*. Significance values are reported as results of an unpaired two-tailed t-test, using a 95% confidence interval.

primer name	sequence 5'-3'
5'FLRcaE_GWC	GGGACCAAGTTTGTACAAAAAAGCAGGCTATGAGGAI1TTGGACCGCTGAGTG
3'FLRcaE_GWC	GGGACCCACTTTGTACAGAAGAGCTGGGTTTCATTGGATATTGGCCGTACTCAAG
RcaEY137A_QC_2	CTCCAAGCCGATCGCGTGCTAATTAGCCATGTATTGCCCTGATGGTACAGGC
RcaEY137A_QC_2-r	GCCTGTACCATCAGGCAATACATGAGCAATTAGCACGCCGATCCGGCTTGAG
RcaEY137H_QC	CTCCAAGCCGATCGCGTGCTAATTCATCATGTATTGCCCTGATGGTACAGGC
RcaEY137H_QC r	GCCTGTACCATCAGGCAATACATGATGAATTAGCACGCCGATCCGGCTTGAG
PAS_QC_Part1	GCGATTGATTACCAATGCCGACAGCAGTACTGCCCGCTTATGTAGACGAGC
PAS_QC_Part1-r	GCTCGTCTACATAAGCGCCAGTACTGCTGCCGCA1TTGTAATCAATCGC
PAS_QC_Part2	GCAGTACTGGCCGCTTATGCAGCCGCCAACAGCAATATCGC
PAS_QC_Part2-r	GCGATATTGCTGTTGCCGGGCTGCATAAGCGGCCAGTACTGC
RcaEH430A_QC	GGATGAAAAGATGAATTCATTTCTATCATTAGCCGTGAACCTGCCGACTCCCTAACTTCC
RcaEH430A_QC r	GGAAAGTTAGGGAGTCCGCAGTTCCAGCGCTAATGATAGAAAATGAATTCATCTTTCATCC

Table 4.1. Primers Used for RcaE Cloning and Mutagenesis

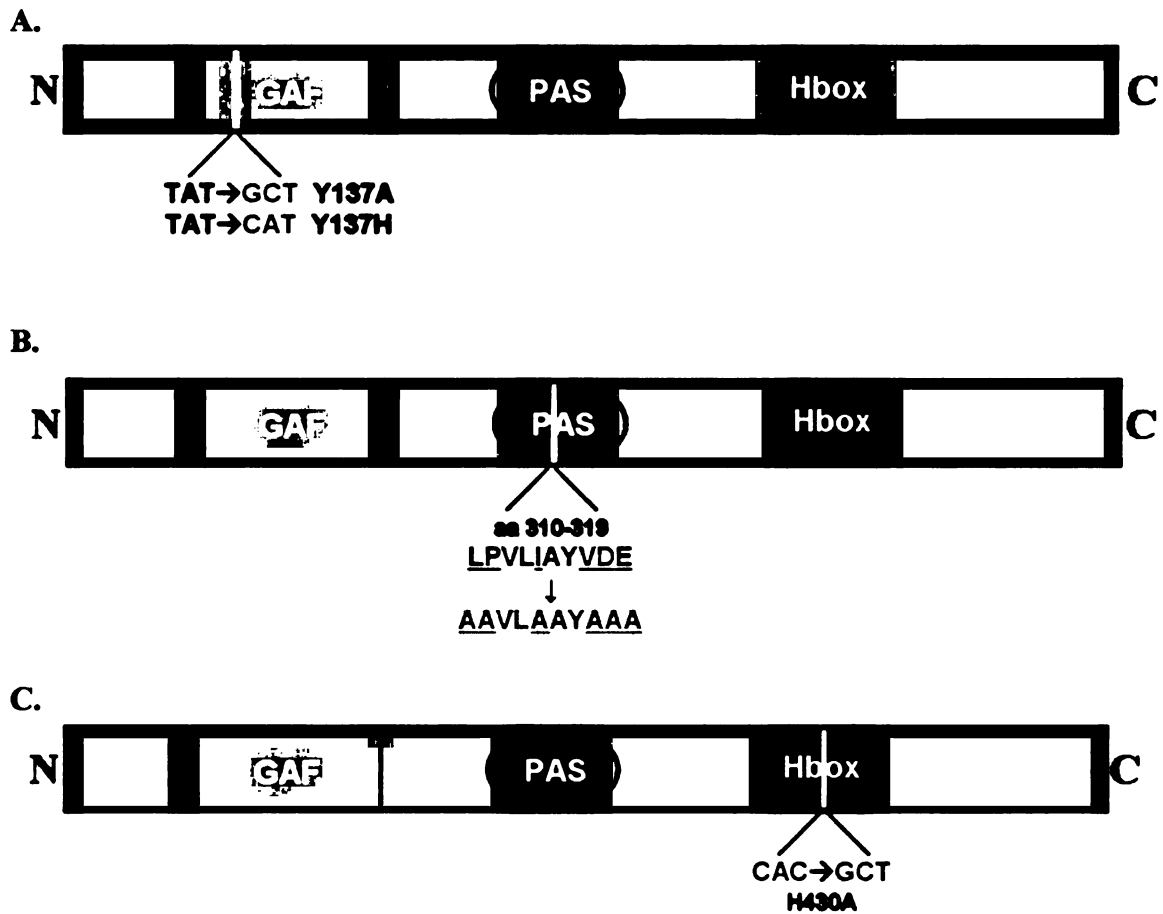


Figure 4.1. Depiction of newly constructed RcaE mutants. A.) The Y137 residue in the GAF domain was changed to either an alanine (A) or histidine (H). B.) The conserved underlined residues in the PAS domain (from amino acid 310 to 319) were changed to alanines (A). C.) The conserved H430 residue within the Hbox domain was changed to an alanine (A). Changes were made using primers shown in Table 4.1.

4.2.5 Protein extraction and immunoblot analyses

Soluble protein extracts were obtained and 250 µg used for anti-RcaE immunoblot analyses as described in section 2.2.5. Antibody was detected using SuperSignal® West Dura Extended Duration chemiluminescent substrate (Pierce), on a Bio-Rad Versadoc 4000MP imaging system (Bio-Rad Laboratories, Inc., Hercules, CA). RcaE expression was quantified using Quantity One 1-D Software (Bio-Rad Laboratories, Inc., Hercules, CA).

4.2.6 Microscopy

Slides of immobilized *F. diplosiphon* cells were prepared and imaged as described in section 2.2.6. Cell length measurements were made by utilizing the calibrated measurement tools of the Zeiss LSM Image Browser (LSMib). At least 50 cells were analyzed for each individual transformant. The lengths reported represent the grand median, and data were subjected to two-tailed Mann-Whitney U-tests in order to determine statistical significance.

4.3 Results

4.3.1 CCA Pigmentation Response

To determine whether the RcaE mutants restore the ability of an FdBk14 strain to adapt to its light environment, accumulation of PBPs was assessed via whole-cell spectral scans. The degree of the ability of the mutants to complement the CCA defective phenotype of FdBk14 can be seen in Figure 4.2. As previously explained, WT cells (i.e. SF33, Figure 4.2A) accumulate PE in GL (black arrow) and PC in RL (grey arrow). The

RcaE mutant, FdBk14 (Figure 4.2B) accumulated both PE and PC at almost equal levels under both light conditions, as did the empty vector control (Figure 4.2C). When full length RcaE was transformed into the FdBk14 background, CCA was restored, as indicated by the light-dependent accumulation of PE and PC (Figure 4.2D). As previously reported, a C198A mutation did not complement the FdBk14 background in GL (indicated by the lack of PE in GL) (Figure 4.2G; Terauchi *et al.*, 2004), and resulted in green-colored cells under both light conditions (data not shown).

The Y137A and Y137H mutants (Figure 4.2E and F, respectively) seemed to display WT, or WT-like CCA phenotypes, however there were some subtle differences. There were the expected light-dependent PE and PC peaks for these mutants, but the peak heights varied, indicating a phenotype slightly different from the WT RcaE construct (Figure 4.2D). In GL especially, the PE peak was lower for both Y137A and Y137H, when compared to that of the WT RcaE construct. Notably, the level of RcaE accumulation under GL for Y137H was undetectable (Figure 4.4, lower panel), which indicates less functional RcaE, and therefore only partial complementation. It is also worth noting that for the Y137A mutant, there was a small peak for PE in RL (which was not seen in any other constructs aside from FdBk14 and the vector control), which also indicates only partial complementation for this construct in RL. However, immunoblot analyses showed that RcaE is accumulating at ~98% of WT levels, indicating that the observed partial complementation is not due to lack of RcaE (Figure 4.4, lower panel). Interestingly, the cell color of the Y137A mutant was only subtly different from that observed for SF33 cells grown in RL; instead of displaying the normal green phenotype, the Y137A cells were slightly darker (data not shown).

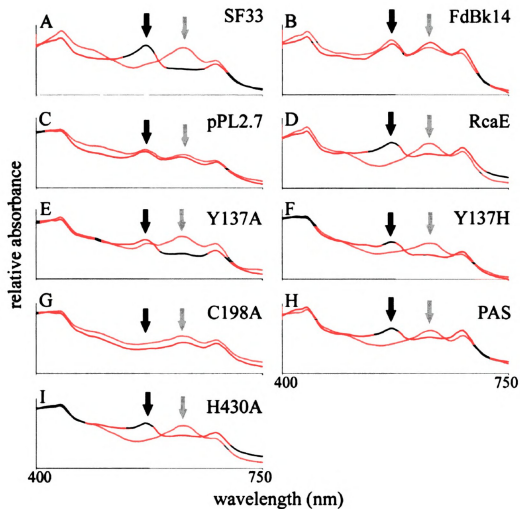


Figure 4.2. CCA pigmentation analyses in SF33, FdBk24, and RcaE mutants. Whole-cell absorbance spectral scans from wild-type pigmentation SF33 cells (A), the FdBk14 mutant (B), the FdBk14 mutant transformed with: pPL2.7 (C), GWpPL2.7-RcaE (D), or the pPL2.7GWRcaE variants: Y137A (E), Y137H (F), C198A (G), PAS (H), and H430A (I). Cultures were grown in RL or GL, as indicated by line color. Black arrows, PE absorption maxima, grey arrows, PC absorption maxima.

In the Y137H GL scan, there appeared to be a slight peak to the immediate left of PE (around 500 nm) which does not exist in the SF33 and WT RcaE, nor the FdBk14 or vector control scans (compare Figure. 4.2F with A, D, B, and C), indicating that this mutant is accumulating an additional pigmented protein. However, there was no detectable RcaE accumulation (Figure 4.4, lower panel); these results could correlate with the lack of functional RcaE in this mutant.

Interestingly, mutating the clustered conserved residues in the PAS domain, or the conserved H430 residue in the Hbox domain, did not result in a disrupted CCA phenotype, as seen by the light-dependent PE and PC peaks (Figure 4.2H and I). The PAS domain mutant displayed SF33-like pigmentation under both GL and RL conditions, however, showed no RcaE accumulation under either condition in the soluble protein fraction (Figure 4.4, lower panel). The H430A mutant however, displayed cells with a slight difference in the red color when grown in GL which may be attributed to the slightly lower PE peak. When compared to SF33 cells (which are brick red in color) the H430A mutant cells had more of a brownish tint to them (data not shown). It was predicted that knocking out this residue may interfere with the phospho-transfer cascade that is proposed to occur for regulation of CCA, and as such, the cells would most likely mimic that of the FdR mutants (i.e., appear red under both growth conditions).

Taken together, these data indicate that alone, none of the mutated residues in any of these domains are absolutely essential for the ability of the organism to adapt, with the exception of the previously described C198A mutation in GL (Terauchi *et al.*, 2004). However, these results do not rule out the possibility of a quantitative impact on PBP accumulation. Despite the prevalence of the expected PE and PC peaks in these strains, it

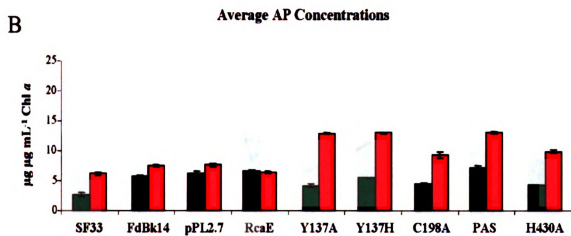
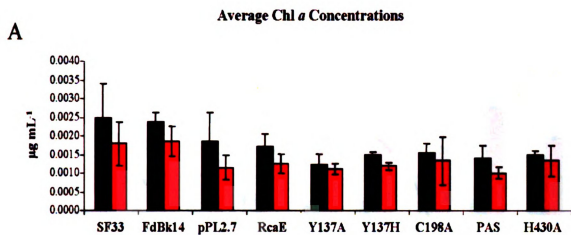
is quite possible that there could be quantitative differences in the levels of PBP accumulation, especially since there was an observed difference in the heights of the peaks.

4.3.2 Phycobiliprotein Accumulation

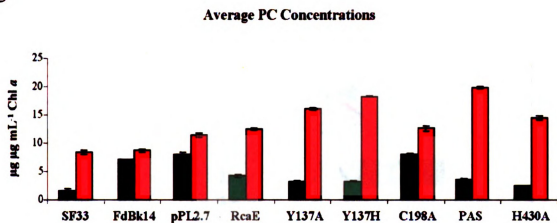
To further characterize the effect of the RcaE mutants on the CCA pigmentation phenotype, quantification of light-dependent PBP accumulation was conducted. The levels of chl *a*, as well as the individual PBPs in each strain are indicated in Figure 4.3, while the ratio of PE/PC accumulation for each strain is represented by Figure 4.4. The quantification of chl *a* (Figure 4.3A) indicate that all of the RcaE variants accumulated levels similar to that of the WT RcaE strain, and therefore are not likely compromised in their photosynthetic efficiency.

As previously explained in section 1.2, WT *F. diplosiphon* cells accumulate PE under GL conditions and PC under RL conditions (revisit Figure 1.1), while the FdBk14 mutant accumulates both PBPs, regardless of light condition (Terauchi *et al.*, 2004). As shown in Figure 4.3 C and D, recovery of the expected GL vs. RL trend in PC and PE accumulation in the RcaE variants indicates that these mutants are functional, or partially functional. Since this response was observed, higher PE/PC ratios were expected in GL, with lower PE/PC ratios expected in RL. This was the also the case, as seen in SF33 and the WT RcaE complemented FdBk14 line, as well as all of the RcaE mutant variants, with the exception of the C198A variant (Figure 4.4, upper panel). When compared to the WT RcaE transformant, the C198A mutant showed a 94% lower PE/PC ratio in GL, which is significantly different from the WT RcaE construct ($p < 0.0001$), which could be

Figure 4.3. Chl *a* and phycobiliprotein levels in SF33, the FdBk14 mutant, and FdBk14 transformed with RcaE mutant variants. The color of the bar indicates the color of light under which the strains were grown, and the bars indicate the averages (\pm standard deviation) of results from at least 3 independent transformants.



C



D

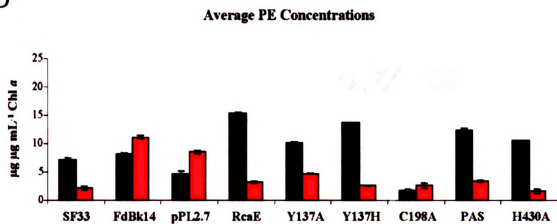


Figure 4.3 continued

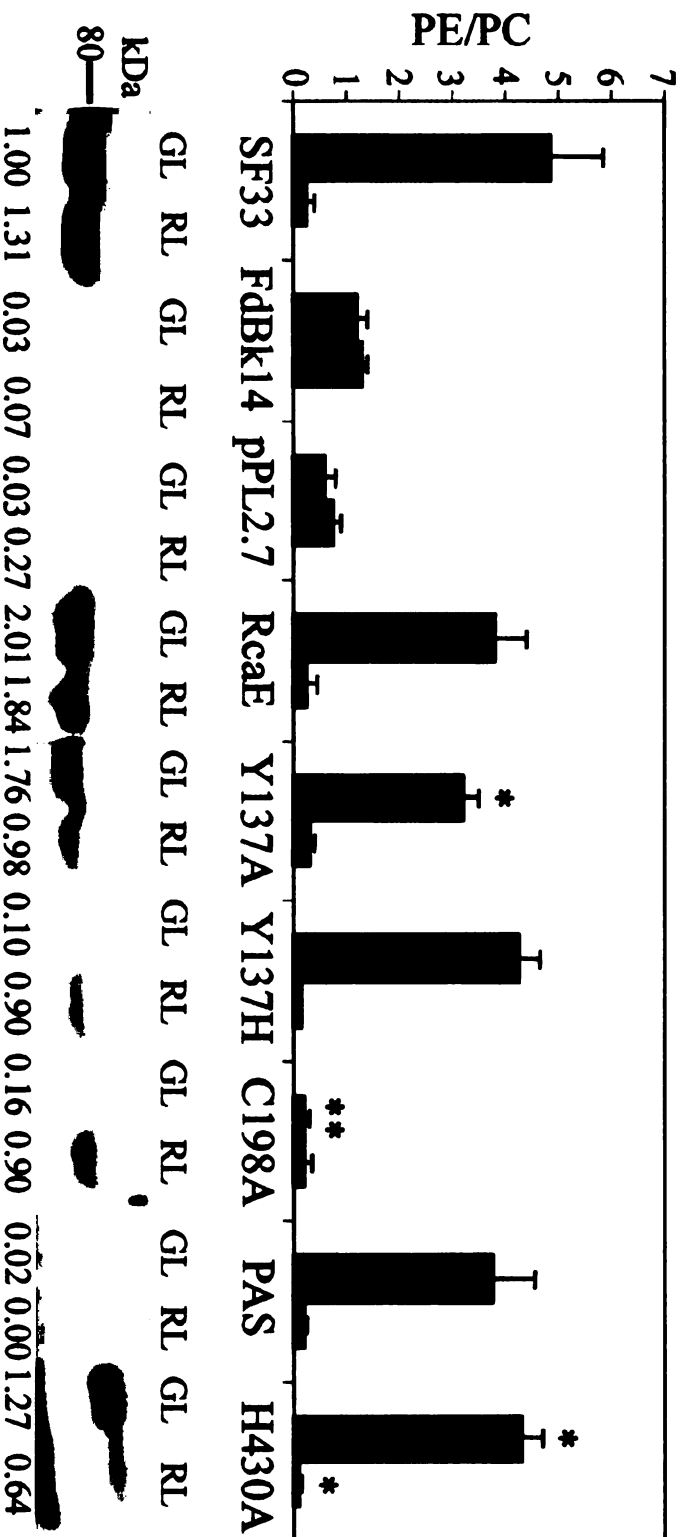


Figure 4.4. Phycobiliprotein ratios and immunoblot analysis of RcaE in SF33, the FdBk14 mutant, and FdBk14 transformed with RcaE mutant variants. Upper panel, PE/PC ratios for *F. diplosiphon* strains. The color of the bar indicates the color of light under which the strains were grown, and the bars indicate the averages (\pm standard deviation) of results from at least 3 independent transformants. *, $P \leq 0.05$, and **, $P \leq 0.001$; unpaired, two-tailed t-test, with a 95% confidence interval, comparing each mutant strain to the wild-type RcaE construct. Lower panel, representative immunoblot results for RcaE accumulation in the GL- and RL-adapted *F. diplosiphon* strains. Numbers indicate RcaE expression relative to SF33 GL levels.

attributed to the low accumulation of PE for this mutant (Figure 4.3 D). These results confirm what has been previously shown; this mutation does not complement the pigmentation phenotype of the FdBk14 mutant in GL, and therefore is not able to undergo CCA (Terauchi *et al.*, 2004). However, there was noticeably lower RcaE accumulation in this mutant in GL, with only ~20% of what is seen for SF33 (Figure 4.4, lower panel). Additionally, the Y137A mutant shows a 16% lower PE/PC ratio in GL, which is also significant ($p=0.0057$), and could be attributed to the lower levels of PE accumulation in this light condition (Figure 4.3). These results suggest that this mutant may only be partially complemented in GL. Since RcaE is shown to accumulate for this mutant (Figure 4.4, lower panel), it is possible that this pigmentation difference demonstrates a partial loss of function. While the Y137H mutant had a higher PE/PC ratio in GL, this 10% increase as compared to the WT RcaE construct, was not found to be significant ($p= 0.0636$). What is more interesting, however, is that none of these GAF domain mutants elicited significant effects in RL when compared to the WT RcaE construct, suggesting that alone, the function of these residues may not be required for CCA in this light condition; perhaps under RL conditions, a chromophore or light-induced alterations in chromophore photochemistry is not necessary (a situation similar to the C198A mutant). This hypothesis is supported by findings that *F. diplosiphon* cultures grown in dark conditions when supplemented with glucose still accumulate PC (Diakoff and Scheibe, 1975).

As there was no alteration in the whole-cell spectral scans of the PAS domain mutant (FdBk14 is complemented; Figure 4.2H), there were also no significant differences in the PE/PC ratios in either light condition when compared to WT RcaE

(Figure 4.4, upper panel). These results indicate that the cluster of conserved residues in the PAS domain is not required for the CCA pigmentation response. It was expected that RcaE accumulation would be correlated with the complemented pigmentation responses. However, this was not the case, as immunoblot analyses with total soluble protein indicated levels that equaled those of the FdBk14 strain. Possible explanations will be proposed in section 4.4.

By contrast, when compared to the WT RcaE strain, the H430A mutant yields both a 12% increase in GL (Figure 4.4, upper panel) which is significant ($p=0.0348$), and a 58.3% decrease in RL which is also significant ($p=0.0389$). This suggests that in GL, there was a slight gain of function, and that in RL there is only partial complementation of pigmentation accumulation for this mutant. RcaE accumulation in the soluble extracts of the H430A mutant (Figure 4.4, lower panel) indicates functional protein, which correlates with the pigmentation complementation described above. In GL, this mutant accumulated RcaE to levels similar to that of SF33, and ~1.5 fold less than the WT RcaE. By contrast, the levels in RL were ~2 fold and ~3 fold less than SF33 and WT RcaE, respectively. Therefore, the noted significant decrease in the PE/PC ratio in RL could be attributed to this lower level of RcaE accumulation. Based on these results, it is clear that the H430 residue plays a role in the regulation of PBP accumulation, and that this role could be linked to the proposed kinase/phosphatase activity.

4.3.4 Cellular Morphology Response

As has been previously presented (chapter two; Bordowitz and Montgomery, 2008), light-dependent cellular morphology is RcaE-dependent in *F. diplosiphon*.

Therefore, microscopy analyses were carried out in combination with the above-described pigmentation analyses, in order to determine if the conserved domains of RcaE contribute to regulation of cellular morphology. As previously demonstrated, SF33 exhibited elongated cells in GL, whereas in RL cells were shorter and more oval in shape (Figure 4.5 A and B). Quantitatively, SF33 cells were significantly longer in GL than in RL (Table 4.2) also as previously reported (Bordowitz and Montgomery, 2008). The FdBk14 mutant displayed round, bubble-like cells under both GL and RL conditions (Figure 4.5 C and D); with cell lengths similar to what was previously reported in Bordowitz and Montgomery, 2008. Also, RcaE complemented the FdBk14 mutant morphology (Figure 4.5 E and F), while the vector only control, pPL2.7, exhibited FdBk14-like morphology (Figure 4.5 F and G; Bordowitz and Montgomery, 2008).

As was described for the pigmentation responses, the GAF domain mutants differed in their ability to complement the FdBk14 mutant morphology. The C198A mutant only complemented the FdBk14 morphology in RL (compare Figure 4.5 N to B). In GL, the cells remained round, though they were a bit more elongated than that of FdBk14 (compare Figure 4.5 M to C). It is important to note that the level of RcaE accumulation in GL was less than 20% than in SF33, so lack of RcaE could be responsible for the observed phenotype (Figure 4.4, lower panel). While there was no difference in cell length between GL and RL, there were significant differences when this mutant was compared to the WT RcaE strain (Table 4.2). In GL, the C198A mutant cells were 8% longer ($p < 0.01$) while in RL the cells were ~5% shorter ($p < 0.05$). While these differences were subtle, they indicate that the ability to bind a chromophore, and hence continue through CCA signaling, is a contributing factor to RcaE's role in

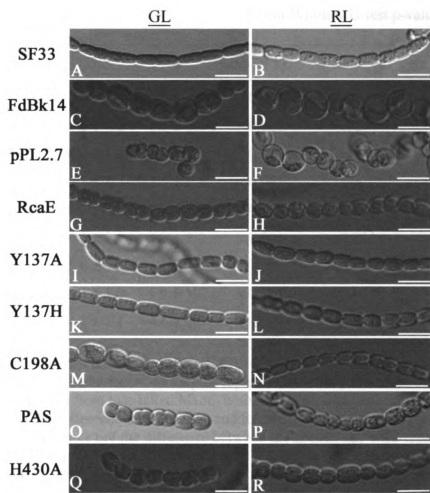


Figure 4.5. Morphological differences between of SF33, FdBk14, and FdBk14 transformed with RcaE mutant variants in GL and RL. Representative slices from a Z-series of DIC images of GL- and RL- adapted filaments of SF33 (A and B), FdBk14 (C and D), FdBk14 transformed with: pPL2.7 (E and F), RcaE (G and H), Y137A (I and J), Y137H (K and L), C198A (M and N), PAS (O and P), or H430A (Q and R) were captured at a 40X oil immersion lens objective, with a 2X zoom. Bars, 10 μ m.

Strain	Cell length (μm) under:		Mann-Whitney U-test p-values:		
	GL	RL	GL vs RL	vs RcaE GL	vs RcaE RL
SF33	5.6 \pm 1.6	4.8 \pm 1.0	< 0.001	n/a	n/a
FdBk14	5.2 \pm 1.0	6.3 \pm 1.7	< 0.001	n/a	n/a
pPL2.7	4.7 \pm 1.0	4.9 \pm 1.2	< 0.001	n/a	n/a
RcaE	5.1 \pm 1.2	5.5 \pm 1.1	< 0.001	n/a	n/a
Y137A	5.3 \pm 1.5	4.8 \pm 1.0	< 0.001	≥ 0.05	< 0.001
Y137H	4.6 \pm 1.0	5.3 \pm 1.1	< 0.001	< 0.001	< 0.05
C198A	5.6 \pm 1.3	5.2 \pm 1.1	≥ 0.05	< 0.01	< 0.05
PAS	4.4 \pm 1.0	5.6 \pm 1.2	< 0.001	< 0.001	≥ 0.05
H430A	4.7 \pm 1.1	4.6 \pm 1.3	≥ 0.05	< 0.001	< 0.001

Table 4.2. Median cell lengths for SF33, FdBk14, and FdBk14 transformed with RcaE mutant variants in GL and RL. Cell lengths represent median \pm standard deviation. P values are the results from two-tailed Mann-Whitney U-test comparison, and indicate: whether or not the difference between GL- and RL- adapted cell lengths is significant, (GL vs. RL), whether or not the difference between the mutant and wild-type RcaE in GL-adapted cell lengths is significant (vs. RcaE GL), and whether or not the difference between the mutant and wild-type RcaE in RL-adapted cell lengths is significant (vs. RcaE RL). N= 178-315 cells, from at least 3 independent transformants.

controlling cell length. These results correlate with what has been presented about the inability of this particular mutant to function in the regulation of pigmentation in GL conditions.

The Y137A mutant displayed similar cellular morphologies under both GL and RL conditions (Figure 4.5 I and J); in both cases the cells looked more elongated and brick-like in shape than what was seen for the WT RcaE strain grown in either condition. This visual morphology was most similar to what was seen for SF33 in GL (Figure 4.5A). However, when compared to the WT RcaE strain, the Y137A mutant showed no significant difference in cell length in GL. Additionally, there was a 12% significant decrease in length in RL ($p < 0.001$) when compared to the WT RcaE RL-grown strain; though this could be attributed to the slightly lower levels of RcaE accumulation (Figure 4.4, lower panel).

The Y137H variant also complemented the FdBk14 mutant morphology under both light conditions; however, the cell shapes slightly differed between GL and RL (Figure 4.5K and L). Under GL conditions, the cells of this mutant resembled the more elongated shape of SF33 in GL, though they were more cylindrical in shape, than brick-like, and 10% shorter in length ($p < 0.001$) than the WT RcaE strain. Under RL conditions the cells resembled the shorter, rounder shape of SF33 in RL, and only had a marginal 4% decrease in length ($p < 0.05$). Taken together, these results indicate that the individual C198 and Y137 residues in the GAF domain contribute to the regulation of RcaE-dependent morphology. While the C198 residue was shown to be especially important for recovery of GL-dependent morphology, the Y137 was shown to have an effect on cellular shape and length for both GL and RL-dependent morphology.

The PAS domain mutant also differed in its ability to complement the FdBk14 mutant. In GL, the PAS mutant displayed a morphology that resembled what was seen for FdBk14 or the vector control in the same light condition (compare Figure 4.5 O to C and E). When compared to the WT RcaE strain, cells were significantly 13% shorter ($p < 0.001$; Table 4.2). In RL, this mutant seemed to only partially complement the FdBk14 morphology; the cells were not quite the same shape seen for SF33 in RL conditions (compare Figure 4.5 P and B), but they were also not as round and bubble-like, as seen for FdBk14 (compare Figure 4.5 P and D). However, when compared to the WT RcaE strain, there was no significant difference in cell length.

Even though the CCA pigmentation response was complemented, the lack of RcaE protein accumulation in the soluble fraction for the PAS domain mutant renders interpretation of these results difficult. However, the morphology results alone provide grounds for speculation that the PAS domain in RcaE could be necessary for the correct photoregulation of cell length, at least in GL. If the PAS domain serves as a site for protein-protein interactions, it is possible that mutating the cluster of conserved residues results in the lack of the ability for this domain to interact with partner(s) that could perhaps be required for GL induced morphology.

That the H430A mutant also displayed an FdBk14-like morphology in GL (compare Figure 4.5 Q and C) indicated that this particular residue may also contribute to the regulation of RcaE-dependent morphology. This was another case where the RcaE variant was unable to complement the FdBk14 morphology in GL, but in RL displayed an SF33-like morphology (compare Figure 4.5 R and B). This mutant resulted in no difference between the cell lengths in GL vs. RL (Table 4.2). However, when comparing

this mutant to the WT RcaE, there was a significant decrease in cell length in both GL and RL of ~9% and ~16%, respectively ($p < 0.001$). Clearly this residue plays a role in RcaE's ability to regulate cell morphology, as there was lack of morphological complementation in GL (figure 4.5K), and decreased cell lengths under both light conditions (Table 4.2).

4.4 Discussion

In summary, mutational analyses of conserved residues in RcaE has shown that the GAF, PAS and Hbox domains all contribute to the regulation of CCA. Though the degrees to which each mutant vary with respect to complementation, results indicate that both the CCA pigmentation response, as well as the cellular morphology is impacted. Further, the results presented in this chapter indicate that each of these domains have different roles in contributing to RcaE's regulation of CCA, and will be discussed in more detail below.

The mutational analyses of residues within that GAF domain have shown that chromophore attachment and conformation is crucial to the pigmentation response, particularly in GL. This was shown with the C198A mutant; in GL, both spectral analyses and PBP quantification showed severely decreased levels of PE accumulation, which had been previously established (Terauchi *et al.*, 2004). However, novel microscopy analyses revealed that this conserved Cys residue was also crucial for GL-mediated morphology. Additionally, mutations of the conserved Tyr (Y137) showed that this residue was also necessary for CCA pigmentation response, again particularly in GL.

Since the Y137 mutants did not elicit RcaE-deficient cellular phenotypes, it is likely that this residue alone may not be completely necessary for regulation of cellular morphology. While rendering the Y137 residue presumably non-functional (Y137A) resulted in the inability to produce GL and RL specific cellular morphology (as described in section 4.3.4), this mutant still displayed SF33-like cell shapes (as opposed to the FdBk14 mutant morphology). Further, the Y137H mutant was also capable of complementing the FdBk14 mutant morphology, resulting in cell shapes that were GL and RL specific. If the function of the Tyr residue is conserved, i.e., plays an important role in chromophore conformation, then it is likely that these mutations have affected RcaE's ability to properly respond to the differing light conditions, hence the inability to completely establish GL- and RL-dependent morphologies.

While the GAF domain proved to be important for both CCA pigmentation response, as well as the cellular morphology response, mutation of the PAS domain proved to have an effect only on regulation of cellular morphology. Mutating this portion of RcaE's photosensory domain did not show differences in PBP accumulation (revisit Figures 4.2 and 4.4); however, the GL morphology response was significantly impacted. As presented in section 4.3.4, GL-grown cells resembled those of the vector only control, and were significantly shorter in length when compared to the WT RcaE strain.

These results were particularly interesting, given the lack of accumulation of RcaE in the soluble fraction. However, it was clear that the PAS mutant variant was functional *in vivo*, due to the recovered pigmentation response. It is possible that mutating the span of residues within the PAS domain could have resulted in improper folding of the protein, resulting in no detection of RcaE in the soluble fraction. If this

was the case, then it is possible that the function of the PAS domain is not important for pigmentation response, but that this domain could be involved with unidentified factors that contribute to the regulation of cellular morphology, especially in GL.

Finally, mutation of the conserved H430 residue resulted in both pigmentation as well as morphological defects. As presented in section 4.3.4, PE/PC ratios were significantly increased in GL, while decreased in RL. Also, the H430A mutant failed to complement the FdBk14 morphology in both light conditions, yielding significantly shorter cells that resembled the vector only control. Immunoblot analyses confirmed the accumulation of RcaE in these cells, with higher than SF33 expression in GL, and lower than SF33 and WT RcaE expression in RL. Therefore, if the proposed CCA signaling model is correct, and RcaE acts as a kinase in RL, then the PE/PC ratios could be lower than in wild-type because the ability to suppress the *cpeCDE* and *cpeBA* operons could be interrupted due to the lack of phospho-transfer through the CCA mechanism. In which case, the phosphatase activity (proposed in GL) may be the ground state for RcaE activity, and thus maintains the induction of those operons, yielding a slightly higher ratio of PE/PC in GL.

In total, mutational analyses served as a useful tool for initial characterization of RcaE, and its role in regulating CCA. Through this approach, specific roles have been identified for the conserved residues and domains which were studied. Characterization of the mutants in the GAF domain provided insight into its importance not only for chromophore attachment, but also chromophore photochemistry. The importance of these residues showed the GAF domain to not only be involved in the previously established pigmentation response (Terauchi *et al.*, 2004), but also in the regulation of

cellular morphology. Analyses with the PAS mutant determined that this part of the RcaE's photosensory domain is essential for GL-regulated cellular morphology. Further, analyses of the H430 residue in RcaE's Hbox domain showed that this residue indeed contributes to the *in vivo* biochemical activity of RcaE, as both pigmentation and morphology were affected. Together, all of these domains proved to be important in RcaE's role in CCA. Further and more detailed analyses of these residues and domains will undoubtedly yield additional insight into what specific contributions these domains lend in the CCA signaling pathway. A more comprehensive discussion about such analyses will be presented in the next chapter.

REFERENCES

1. **Bordowitz, J. R., and B. L. Montgomery.** 2008. Photoregulation of cellular morphology during complementary chromatic adaptation requires sensor-kinase-class protein RcaE in *Fremyella diplosiphon*. *J Bacteriol* **190**:4069-74.
2. **Chen, M., J. Chory, and C. Fankhauser.** 2004. Light signal transduction in higher plants. *Annu Rev Genet* **38**:87-117.
3. **Cobley, J. G., E. Zerweck, R. Reyes, A. Mody, J. R. Seludo-Unson, H. Jaeger, S. Weerasuriya, and S. Navankasattusas.** 1993. Construction of shuttle plasmids which can be efficiently mobilized from *Escherichia coli* into the chromatically adapting cyanobacterium, *Fremyella diplosiphon*. *Plasmid* **30**:90-105.
4. **Diakoff, S., and Scheibe, J.** 1975. Cultivation in the Dark of the Blue-green Alga *Fremyella diplosiphon*. A Photoreversible Effect of Green and Red Light on Growth Rate. *Physiol. Plant* **34**:125-128.
5. **Fischer, A. J., and J. C. Lagarias.** 2004. Harnessing phytochrome's glowing potential. *Proc Natl Acad Sci U S A* **101**:17334-9.
6. **Fischer, A. J., N. C. Rockwell, A. Y. Jang, L. A. Ernst, A. S. Waggoner, Y. Duan, H. Lei, and J. C. Lagarias.** 2005. Multiple roles of a conserved GAF domain tyrosine residue in cyanobacterial and plant phytochromes. *Biochemistry* **44**:15203-15.
7. **Kehoe, D. M., and A. R. Grossman.** 1997. New classes of mutants in complementary chromatic adaptation provide evidence for a novel four-step phosphorelay system. *J Bacteriol* **179**:3914-21.
8. **Kehoe, D. M., and A. R. Grossman.** 1996. Similarity of a chromatic adaptation sensor to phytochrome and ethylene receptors. *Science* **273**:1409-12.
9. **Kehoe, D. M., and A. Gutu.** 2006. Responding to color: the regulation of complementary chromatic adaptation. *Annu Rev Plant Biol* **57**:127-50.
10. **Li, L., R. M. Alvey, R. P. Bezy, and D. M. Kehoe.** 2008. Inverse transcriptional activities during complementary chromatic adaptation are controlled by the response regulator RcaC binding to red and green light-responsive promoters. *Mol Microbiol* **68**:286-97.
11. **Li, L., and D. M. Kehoe.** 2005. In vivo analysis of the roles of conserved aspartate and histidine residues within a complex response regulator. *Mol Microbiol* **55**:1538-52.

12. **Montgomery, B. L.** 2008. Shedding new light on the regulation of complementary chromatic adaptation. *Central European Journal of Biology* **3**:351-358.
13. **Rockwell, N. C., Y. S. Su, and J. C. Lagarias.** 2006. Phytochrome structure and signaling mechanisms. *Annu Rev Plant Biol* **57**:837-58.
14. **Sobczyk, A., G. Schyns, N. Tandeau de Marsac, and J. Houmard.** 1993. Transduction of the light signal during complementary chromatic adaptation in the cyanobacterium *Calothrix* sp. PCC 7601: DNA-binding proteins and modulation by phosphorylation. *Embo J* **12**:997-1004.
15. **Taylor, B. L., and I. B. Zhulin.** 1999. PAS domains: internal sensors of oxygen, redox potential, and light. *Microbiol Mol Biol Rev* **63**:479-506.
16. **Terauchi, K., B. L. Montgomery, A. R. Grossman, J. C. Lagarias, and D. M. Kehoe.** 2004. RcaE is a complementary chromatic adaptation photoreceptor required for green and red light responsiveness. *Mol Microbiol* **51**:567-77

CHAPTER FIVE
Conclusions/Perspectives

5.1 Light-Dependent Regulation of Cellular Morphology in *F. diplosiphon*

The results presented in chapter 2 show that in addition to the previously established regulation of PBP accumulation during CCA (Kehoe and Grossman, 1997; Terauchi *et al.*, 2004), RcaE also has a regulatory role in the light-dependent changes in cell shape and filament morphologies in *F. diplosiphon*. The finding that RcaE is the photoreceptor responsible for regulating these responses represents a novel role for the phytochrome-like protein RcaE in this organism and provides a molecular link for the pigmentation and morphological aspects of CCA first documented over 30 years ago.

As described in section 1.2, the regulation of PBP accumulation during CCA is largely dependent upon the Rca signaling system (revisit Figure 1.4). In addition to characterizing the RcaE-deficient cellular morphology, preliminary microscopy analyses showed an inability to recover the RL-dependent cellular phenotype in *rcaF* and *rcaC* mutants, suggesting that functional RcaF and RcaC are also required for correct regulation of cell shape in *F. diplosiphon*, at least in response to RL (Bordowitz and Montgomery, unpublished). Further microscopy analyses need to be completed in order to determine whether the proposed kinase activity of RcaE and subsequent phosphorelay to RcaF and RcaC (revisit Figure 1.4) are required absolutely for the photoregulation of cell and filament morphologies. Since initial observations revealed morphological differences, the cell and filament lengths of the *rcaC* and *rcaF* mutants, as well as their complemented counterparts, should be quantified and compared to the cell and filament lengths presented in chapters 2 and 4.

To determine if additional factors were required for light-regulated cellular morphology in *F. diplosiphon*, the role of RcaE in cell-shape determination was further

explored in chapter 3. Previous microarray results from *F. diplosiphon* indicated differential regulation of 17 novel genes not known to be associated with PBS components (Stowe-Evans *et al.*, 2004). These data strengthened the prediction that RcaE could be controlling the expression of genes associated with cell wall composition, given the morphological differences between SF33 and the RcaE-deficient strain FdBk14. Further, in Hu *et al.*, (2007), it was reported that MreB mutants of the cyanobacterium *Anabaena* displayed a round morphology, as opposed to the more elongated rod shaped WT cells. The authors determined that the round morphology was correlated with a higher susceptibility to treatment with the cell-wall degrading enzyme lysozyme, which indicated an altered cell-wall composition.

Given the similarity of the FdBk14 round mutant morphology to the *Anabaena* mutant, as well as other known *mreB* mutant morphologies (section 3.1), it was hypothesized that cell wall composition and the activity of components such as MreB may be under light- and/or RcaE-dependent regulation in *F. diplosiphon*. The work presented in chapter 3 established a light-dependent cell wall alteration associated with the change in cellular morphology (section 3.3.1), as well as demonstrated that *F. diplosiphon* WT strains are affected by a known MreB inhibitor, A22. The elicited changes in WT cell lengths and widths (section 3.3.2) when treated with A22 further indicated the involvement of *mreB* in the light-regulated cellular morphology of *F. diplosiphon*. As RT-PCR results showed lower *mre* gene expression in the FdBk14 mutant, the combined results of chapter 3 thus presented a novel role for RcaE in the regulation of the morphogene *mreB* in cyanobacteria.

While RT-PCR analyses confirmed down-regulation of the *mre* genes in the RcaE-deficient mutant, additional analyses need to be conducted with an FdBk14-RcaE complemented line in order to confirm definitively RcaE's regulation of the *mre* operon. Also, although preliminary Northern analyses indicated that the *mreBCD* operon was co-regulated (data not shown), additional RT-PCR analyses with primers for *mreBC* and *mreBCD* need to be completed in order to confirm these results. As proposed above, the regulation of cellular morphology may be dependent on the RcaE, RcaF and RcaC signal transduction cascade, however, RT-PCR analyses on the *mre* genes has yet to be completed in the *rcaF* and *rcaC* mutants. If differential regulation of the *mre* genes is observed in the *rcaF* and *rcaC* mutants, it would indicate that indeed the photoregulation of cell-shape determination is dependent upon the known RcaE-dependent signaling cascade.

In addition, a more quantitative approach should also be considered for studying the regulation of the *mre* genes. Preliminary studies were conducted utilizing a quantitative real time polymerase chain reaction (qRT-PCR) approach. However, these efforts failed, due to the inability to standardize against the ribosomal control gene. As indicated in Figure 3.7, *F. diplosiphon* 23S ribosomal mRNA expression is highly abundant in comparison to the *F. diplosiphon mre* genes. This made optimization of the early qRT-PCR parameters difficult, since cycle thresholds varied dramatically. For future studies, a more suitable reference gene, expressed in lower abundance, should be used in order to have a more comparable standard.

During the biochemical characterization of RcaE presented in chapter 4, some of the conserved residues and domains of RcaE were shown to contribute to RcaE's role in

regulating cellular morphology (revisit Figure 4.4). It would be particularly interesting to subject these mutant strains to *mre* gene expression analyses, and compare to results obtained with analyses of the *rcaE*, *rcaF* and *rcaC* mutants. This would aid in further determining whether cell shape is regulated by the known CCA signaling pathway, or if RcaE participates in cross-talk and/or contributes to separate regulatory pathway(s).

5.2 Biochemical Characterization of RcaE

Mutational analyses of conserved residues within the previously described conserved domains of RcaE (section 4.1) provided additional insight into the regulation of CCA. Mutating the conserved Y137 and C198 in the GAF domain provided insight into the importance of these residues not only in the previously established pigmentation response (C198A; Terauchi *et al.*, 2004), but also in the regulation of cellular morphology. While the role of the C198 residue had been previously demonstrated to be required for a wild-type CCA pigmentation response in GL, as well as for chromophore attachment, its contribution to regulation of cellular morphology (in GL) was a novel function established in chapter 4. Further, the novel pigmentation and morphological characterization of the Y137 mutants indicate that this residue may also have a conserved function in billin-regulated light sensing, similar to that demonstrated by Fischer *et al* (2005).

Analyses with the PAS mutant determined that this part of the RcaE's photosensory domain is essential for GL-regulated cellular morphology, yet it does not contribute significantly to the CCA pigmentation response. However, as indicated in Figure 4.3 (lower panel) RcaE accumulation was undetectable for soluble protein extracts

of this strain. Since the CCA pigmentation response was complemented, it is likely that functional RcaE is present in this strain. However, it is possible that mutating the cluster of residues within this domain could have affected the native folding of RcaE, and caused it to associate with the insoluble fraction. Crystallization of the GAF-PAS (chromophore-binding domain; CBD) portion of the *Deinococcus radiodurans* bacteriophytochrome, DrBphP, has revealed that the GAF and PAS domains closely interact in order to maintain a tight pocket for chromophore-binding (Wagner *et al.*, 2005). Homology modeling of these two domains of RcaE demonstrated a similar predicted structure (compare Figure A3.2 A and B). Unfortunately, the mutated PAS domain residues fall within an area of the modeled protein that shows no structure, due to poor sequence conservation with the parental structure (1ZTU, Wagner *et al.*, 2005). Therefore analyses on the insoluble fractions of the PAS domain mutant strain is required in order to reveal whether or not this mutant accumulates RcaE.

While the homology model suggests the GAF and PAS domains to be important for chromophore attachment and configuration, direct evidence of this relationship is still lacking. Chromophore attachment has only been established for the C198 residue (Terauchi *et al.*, 2004); therefore, future studies should focus on determining whether or not the Y137 residue is involved in chromophore attachment. In order to address this, zinc blot analyses should be employed, as described by Berkelman and Lagarias (1986), which can detect *in vivo* chromophore attachment in soluble protein extracts after SDS-PAGE analyses. However, it is clear that crystallization of RcaE and/or its functional domains (as done with DrCBD) will aide in truly understanding how the folding of this

protein affects its activity, and how the GAF-PAS domains may interact to elicit signal-sensing and proper photochemistry.

Analyses of the H430 residue in RcaE's Hbox domain showed that this residue indeed contributes to the *in vivo* biochemical activity of RcaE, as both pigmentation and morphology were affected. In GL conditions, this mutant displayed a significant increase in pigmentation accumulation while in RL conditions there was a significant decrease (revisit Figure 4.3, upper panel). As discussed in section 4.4, these results indicate that the proposed kinase and phosphatase activity of RcaE is required for proper regulation of the downstream PBP-encoding genes as well as factors associated with regulation of cellular morphology.

While the results provided in chapter 4 support the model that this H430 residue is needed for CCA signaling, these analyses do not fully elucidate biochemical activity of RcaE, as *in vitro* studies will need to be completed. In order to establish the kinase and/or phosphatase activity of RcaE, studies with purified protein will need to be employed. Such *in vitro* assays would allow both the basal kinase and phosphatase activity of RcaE to be assessed, and determination of whether or not the H430 residue contributes to such activity.

5.3 Perspectives

During CCA, *F. diplosiphon* enhances its photosynthesis by altering the PBP composition of its light-harvesting antennae, in order to efficiently utilize the light in its environment. In addition to the pigmentation phenotype associated with CCA, the organism also displays different cell morphologies under GL and RL conditions (Bennett

and Bogorad, 1973; Bordowitz and Montgomery, 2008). The biological relevance of the adaptive changes in pigmentation that occur has been linked to where the organism resides in the water column and in turn, the wavelengths of light to which it is exposed (Postius *et al.*, 2001). Since the initial observation of CCA-regulated cellular morphology over 30 years ago (Bennett and Bogorad, 1973), little speculation about the biological significance of this phenomenon has existed.

After the detailed microscopy analyses of the RcaE-specific photoregulation of *F. diplosiphon* cellular morphology presented in chapter 2, a working hypothesis has begun to emerge. The noticeably larger cells of the GL-grown UTEX481 WT strain (revisit Figure 2.6A) may be due to a need for a greater thylakoid membrane surface area in order to increase the total levels of PBPs under GL conditions. This is because in GL, PE is the sole active photosynthetic light-harvesting pigment. By contrast, the smaller, rounder cells observed for the RL-grown UTEX481 WT strain (revisit Figure 2.6B) contain both PC and chl *a* to absorb red light for photosynthesis. As described in Postius *et al.* (2001), in nature, cyanobacterial strains that grow deeper in the water column are exposed to lower levels of light, and display high levels of PE accumulation. Therefore, the more elongated GL cells could be a direct result of the need to maximize their thylakoid membrane surface area in order to optimally accumulate a larger PBP content for efficient photosynthesis under these lower light conditions.

The work presented in this dissertation has significantly contributed to understanding RcaE's role in regulating CCA. Characterization of the cellular morphology of the FdBk14 mutant as well as the RcaE mutant variants indicated a novel role for this photoreceptor, in addition to its established role in the regulation of

pigmentation accumulation (Kehoe and Grossman, 1996; Terauchi *et al.*, 2004). Further, lysozyme-sensitivity assays and gene expression analyses identified RcaE's role in cross talk with non-photosynthetic signaling pathways, as it regulates the expression of the cell-shape-determining genes *mreB*, *mreC*, and *mreD*. Although previous microarray analyses had identified 17 non-photosynthetic related genes to be differentially regulated in GL- vs. RL- conditions (Stoew-Evans *et al.*, 2004), microarray analyses with the FdBk14 mutant strain should be conducted in order to provide a more direct approach towards identifying additional genes directly impacted by RcaE. Additionally, since RNA for the FdBk14 strain is available (prepared for studies done in chapter 3), RNA sequencing studies could be immediately implemented. In any case, as the sequence of this organism becomes publicly available, such genomic approaches will greatly aid in these efforts.

As discussed above, there is still much to be done in order to identify RcaE's direct role in cell-shape determination, as well as its specific biochemical activity in the CCA pathway. Future work should be aimed at identifying the branch-point (if any) in CCA-regulated pigmentation and morphological responses, by focusing analyses on mutants in the downstream components, RcaF and RcaC, as well as identification of additional downstream effectors. Additionally, construction and characterization of RcaE double mutants may provide further insight into the roles of identified residues and domains in the regulation of both responses. Also, morphological and biochemical analyses of double mutants could indicate whether or not there is interaction between the conserved domains in RcaE, as was shown to be the case for the GAF and PAS domains of the *D. radiodurans* bacteriophytochrome (Wagner *et al.*, 2005).

In conclusion, characterization of the light-regulated function of the photoreceptor RcaE was undertaken in order to provide insight into how photosynthetic organisms sense and respond to their light environments. As summarized, the work presented in this dissertation has not only contributed significantly towards understanding the molecular basis of the photoregulation of cellular morphology in *F. diplosiphon*, but has also advanced our knowledge of the biochemical mechanisms utilized by RcaE in its regulation of CCA.

REFERENCES

1. **Bennett, A., and L. Bogorad.** 1973. Complementary chromatic adaptation in a filamentous blue-green alga. *J Cell Biol* **58**:419-35.
2. **Berkelman, T. R., and J. C. Lagarias.** 1986. Visualization of bilin-linked peptides and proteins in polyacrylamide gels. *Anal Biochem* **156**:194-201.
3. **Bordowitz, J. R., and B. L. Montgomery.** 2008. Photoregulation of cellular morphology during complementary chromatic adaptation requires sensor-kinase-class protein RcaE in *Fremyella diplosiphon*. *J Bacteriol* **190**:4069-74.
4. **Fischer, A. J., N. C. Rockwell, A. Y. Jang, L. A. Ernst, A. S. Waggoner, Y. Duan, H. Lei, and J. C. Lagarias.** 2005. Multiple roles of a conserved GAF domain tyrosine residue in cyanobacterial and plant phytochromes. *Biochemistry* **44**:15203-15.
5. **Hu, B., G. Yang, W. Zhao, Y. Zhang, and J. Zhao.** 2007. MreB is important for cell shape but not for chromosome segregation of the filamentous cyanobacterium *Anabaena* sp. PCC 7120. *Mol Microbiol* **63**:1640-52.
6. **Kehoe, D. M., and A. R. Grossman.** 1997. New classes of mutants in complementary chromatic adaptation provide evidence for a novel four-step phosphorelay system. *J Bacteriol* **179**:3914-21.
7. **Kehoe, D. M., and A. R. Grossman.** 1996. Similarity of a chromatic adaptation sensor to phytochrome and ethylene receptors. *Science* **273**:1409-12.
8. **Postius, C., Neuschaefer-Rube, O., and Boger, P.** 2001. N₂-fixation and complementary chromatic adaptation in non-heterocystous cyanobacteria from Lake Constance. *FEMS Microbiology Ecology* **37**:117-125.
9. **Stowe-Evans, E. L., and D. M. Kehoe.** 2004. Signal transduction during light-quality acclimation in cyanobacteria: a model system for understanding phytochrome-response pathways in prokaryotes. *Photochem Photobiol Sci* **3**:495-502.
10. **Terauchi, K., B. L. Montgomery, A. R. Grossman, J. C. Lagarias, and D. M. Kehoe.** 2004. RcaE is a complementary chromatic adaptation photoreceptor required for green and red light responsiveness. *Mol Microbiol* **51**:567-77.
11. **Wagner, J. R., J. S. Brunzelle, K. T. Forest, and R. D. Vierstra.** 2005. A light-sensing knot revealed by the structure of the chromophore-binding domain of phytochrome. *Nature* **438**:325-31.

APPENDICES

APPENDIX A1

Sequencing of *F. diplosiphon* shuttle vector pPL2.7

A1. Sequencing of *F. diplosiphon* shuttle vector pPL2.7

Shuttle vector pPL2.7 (Chiang *et al.*, 1992) was used as a vector only control in these experiments, since the Gateway[®] converted version (pPL2.7GW; Bordowitz and Montgomery, 2008) contains a *ccdB* suicide cassette, which does not allow for Kan selection of transformants. As a result, the entire vector was sequenced in order to confirm integrity. The previous sequence of the *F. diplosiphon* expression vector pPL2.7 was obtained by sequencing of various sub-cloned fragments. This sequence was used as a starting template to design primers at known restriction sites *Bam*HI and *Pst*II which have been previously used for cloning, to begin sequencing of the entire plasmid. Sequencing reactions were submitted to the Research Technology Support Facility (RTSF) at Michigan State University, and data were analyzed using Lasergene 6 software. Consecutive sequencing reactions were done using primers designed to complement the DNA sequence obtained from the previously analyzed reads. 18-mer oligos were designed by scanning in ~20 bps from the end of each read, and then reading in both a forward (5') as well as a reverse (3') direction. This strategy was created to produce reads that would provide multiple overlaps in order to obtain an accurate consensus. The final pPL2.7 consensus sequence was obtained by using the Lasergene 6 SeqManII program, aligning a total of 33 sequence reads (Table A1.1). The final consensus was then transferred to Gene Construction Kit software in order to produce the plasmid map. Upon comparison with the previously obtained vector sequence, there were three segments missing in the newly obtained sequence which ranged in sizes of 27 bps, 66 bps, and 50 bps. The plasmid DNA was then subjected to various restriction

enzyme digests to confirm the absence of these segments, as well as to confirm the integrity of the overall sequence.

primer name	sequence (5'-3')	region of pPL2.7	read length
RpPL2.7BamHI	TTAGGCATAACAAAGTAT	<i>Bam</i> HI site; bp 5044	860 bp
FpPL2.7PstI	AATCGCGGCCTCGACCTG	<i>Pst</i> I site; bp 2452	895 bp
pPL2.7JRB1	GTTGAAGGATCAGATCAC	bp 3923	28 bp
pPL2.7JRB3	AATTCCAACATGGATGCT	bp 2433	38 bp
pPL2.7JRB5	TTTGCTCACATGTTCTTT	bp 3371	905 bp
pPL2.7JRB6	AAGGCCAGCAAAGGCCA	bp 3354	937 bp
pPL2.7JRB9	CGACCGAGCGCAGCGAGT	bp 3465	649 bp
pPL2.7JRB10	TTCGGCTGCGGCGAGCGG	bp 3447	822 bp
pPL2.7JRB11	CTAGTAGCAGTGGAAACA	ori; bp 1708	926 bp
pPL2.7JRB13	TTTATACCCATATAAATC	bp 2415	56 bp
pPL2.7JRB15	GAGCCTATGGAAAAACGC	bp 3310	807 bp
pPL2.7JRB16	CGCCCCCTGACGAGCAT	bp 3292	852 bp
pPL2.7JRB17	CGACCGAGCGCAGCGAGT	bp 3465	607 bp
pPL2.7JRB20	TAAACTTGGTCTGACAGT	bp 2563	887 bp
pPL2.7JRB21	CGCTCAACGTGTCTTTGG	pFdA; bp 963	917 bp
pPL2.7JRB24	TTAGCGATTTTAGAAGCC	ori; bp 1751	910 bp
pPL2.7JRB25	TATGGGTATAAATGGGCT	bp 2409	229 bp
pPL2.7JRB26	AAATTGCAAGCAATAAAT	bp 40	867 bp
pPL2.7JRB28	AGATTATCAAAAAGGATC	bp 2641	899 bp
pPL2.7JRB29	GGGGGAAACGCCTGGTAT	bp 3221	918 bp
pPL2.7JRB30	GAATTTATGCCTCTCCG	KanR; bp 4304	900 bp
pPL2.7JRB33	AATCTATCGATTGTATGG	KanR; bp 4192	662 bp
pPL2.7JRB34	CTGGCGGGGCGATTGCTG	bp 5249	414 bp
pPL2.7JRB36	TTCCCAGTAGCCGAAAC	bp 5543	961 bp
pPL2.7JRB41	TGCTGGCGGGGCGATTGC	bp 5247	915 bp
pPL2.7JRB42	GCCGCTAGAGAGCGGTAT	bp 5525	949 bp
pPL2.7JRB44	CTCCTAATTGAATTAAGG	bp 21	908 bp
pPL2.7JRB45	AAACTCCCAGCCGCCAG	pFdA; bp 921	911 bp
pPL2.7JRB46	TATTCACAGGCGATCGCT	bp 1592	850 bp
pPL2.7JRB47	TTAATACTTTGTTATGCC	bp 5041	941 bp
pPL2.7JRB48	GCACTTCAAATTTATGAT	bp 5509	893 bp
pPL2.7JRB50	AAATTTATGATAAGCGAA	bp 5502	879 bp
pPL2.7JRB51	CCGACACGGTACTATCAA	bp 5468	919 bp

Table A1.1. Primers used for sequencing *F. diplosiphon* shuttle vector pPL2.7. Sequences were designed off of previously obtained results, as described in section A1.1. The region of the construct where each primer anneals is indicated by the base pair number, as well as the identified cassettes present in the plasmid. The length of reads obtained from the sequencing reactions are indicated in base pairs (bp).

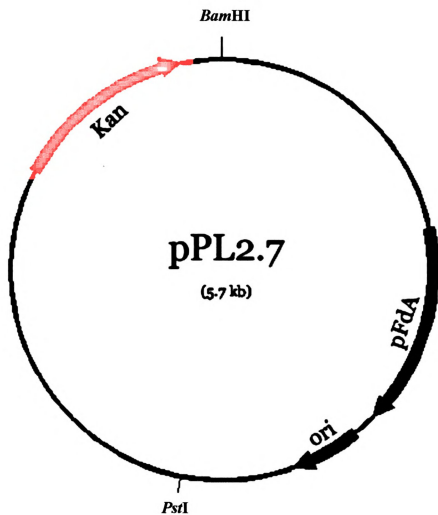


Figure A1.1 *F. diplosiphon* shuttle vector pPL2.7. The final vector plasmid is 5.58 kb in size, and contains a kanamycin resistance cassette (Kan^R) in red, a *F. diplosiphon* fragment used for maintenance which contains the origin of replication (pFdA), in blue, and a fragment containing the *E. coli* origin of replication (*E. coli* ori) in green.

APPENDIX A2

Determining Imaging Parameters for *F. diplosiphon* PBP Autofluorescence

A2. Determining Imaging Parameters for *F. diplosiphon* PBP Autofluorescence

In order to optimally capture PBP autofluorescence in *F. diplosiphon*, spectral imaging was done using the Meta scan-head on the CLSM. Image parameters were set using SF33 cells grown under either GL or RL conditions. A filament was focused under a Plan-Apochromat 63X oil objective and utilized for image parameter determination. To detect PBP autofluorescence, the filament was excited with three individual laser wavelengths: 488 nm, 543 nm, and 633 nm. An emission spectrum was then gathered at 10.7 nm increments as a lambda Z-series (Table A2.1).

The collected spectra were then analyzed for wavelengths where fluorescence reached maximum emission. The ranges of maximum PBP autofluorescence were compared between the three different excitation wavelengths in order to determine the best filter settings to use for subsequent imaging. Final autofluorescence was collected using a 543-nm laser for excitation and emission collected using a 560- to 615-BP filter and 640- to 753-nm Meta detector for GL-grown cells (Figure A2.1) and with a 615-nm LP filter for RL-grown cells (Figure A2.2). The fluorescence channels were falsely colored to reflect the PBS composition under each light condition; for GL-grown filaments, the autofluorescence observed using a band pass filter of 560-615 nm is indicated by pink, correlating with the accumulation of GL-inducible PE, as well as autofluorescence from AP using the meta scanning filter from 640-753 nm indicated by blue color. In RL-grown filaments, the autofluorescence observed using a 615-nm long pass filter is indicated by blue color, which correlates with the accumulation of PC, as well as PCc and AP.

excitation laser (nm)	maximum fluorescence emission ranges (nm)	
	GL	RL
488	~566-599 ~631-706	~652-716
543	~566-609 ~631-706	~641-716
633	~652-706	~614-716

Table A2.1 Spectral emission collections after excitation with 488, 543, and 633 nm laser lines. Maximum ranges of fluorescence emission collected at 10.7 nm increments after excitation of GL- and RL-grown filaments.

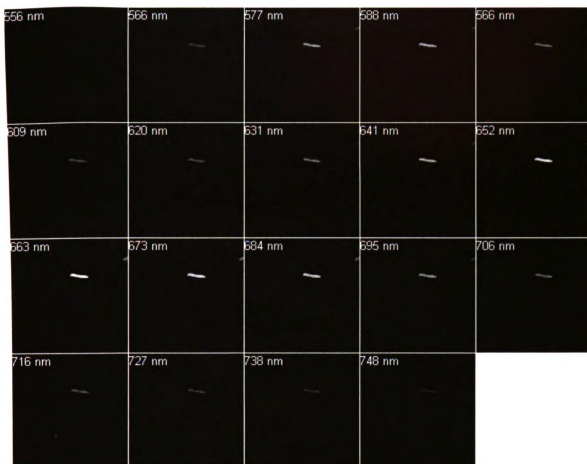


Figure A2.1. Spectral emission collection of SF33 GL-grown cells after excitation with 543 nm laser. An emission spectrum was gathered at 10.7 nm increments after excitation. Final imaging parameters include a band pass filter of 560-615 nm, selected to capture fluorescence correlating with the accumulation of GL-inducible PE (~566-609), and a 640-753 nm long pass filter, selected to capture fluorescence correlating with the accumulation of PCC and AP (~631-706 nm).

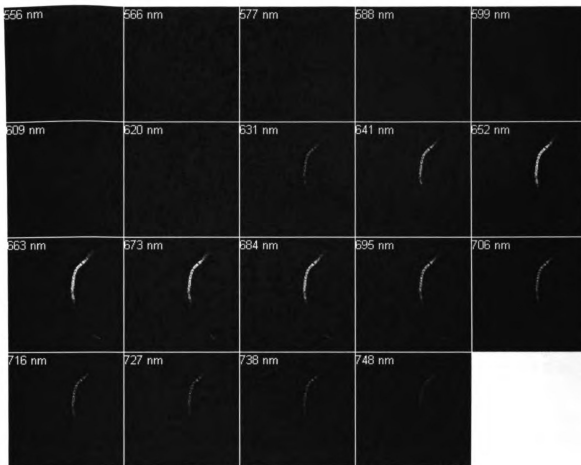


Figure A2.2. Spectral emission collection of SF33 RL- grown cells after excitation with 543 nm laser. An emission spectrum was gathered at 10.7 nm increments after excitation. Final imaging parameters include a 615-nm long pass filter selected to capture fluorescence correlating with the accumulation of RL-inducible PC, as well as PCc and AP (~641-716 nm).

APPENDIX A3

Homology Modeling of *F. diplosiphon* GAF-PAS Domain

A3. Homology Modeling of *F. diplosiphon* GAF-PAS Domain

To date, there is no known structure for full length phytochromes; however, in 2005 the Viestra lab was able to crystallize the GAF-PAS (chromophore-binding domain; CBD) portion of the *Deinococcus radiodurans* (Dr) bacteriophytochrome, BphP (Wagner *et al.*, 2005). Homology modeling of RcaE using this structure will help to determine how (and if) these two domains interact, and if these interactions are important to the signaling function of RcaE. The structure of the chromophore binding domain of DrBphP suggests that the GAF and PAS domain interact closely to produce a tight chromophore-binding pocket (protein data base: 1ZTU), and that there are key residues involved in this function. Experimental data from the Viestra lab have shown this to be the case (described in section 1.8.1; Wagner *et al.*, 2005, 2007).

After Psi-BLAST (5 iterations; Altschul *et al.*, 1997) analyses on a segment of the RcaE protein containing only the GAF and PAS domains (~311 residues; Figure A3.2 D), multiple sequence analyses yielded alignment with various phytochrome proteins (data not shown). The multiple sequence alignment (MSA) showed high sequence conservation amongst these two domains. Secondary structure predictions (Psi-PHRED, SAM, PROF-sec, and SABLE) of this segment of RcaE predicted a mixture of helices and beta sheets, which matched some portions of the CBD of the DrBphP structure (compare Figure A3.2A to B). Using the published structure of the DrCBD as a model, the structure of truncated RcaE consisting of the GAF and PAS domains was predicted and modeled and displayed as ray-traced images rendered in PyMOL (Figure 3.2 A and B). The conserved residues of the GAF domain (Y137 and C198) that were targeted for

mutational analyses in chapter 3, are highlighted in white (Figure A3.2 B #1 and #2, respectively). The conserved cluster of residues in the PAS domain that were targeted for mutational analyses in chapter 3, are highlighted in pink (Figure A3.2 B #3). Several unstructured areas exist within the model, which indicate areas of non-homology with the parent structure. These areas may need to be further analyzed by more complete matches available in PDB in order to get a more complete model.

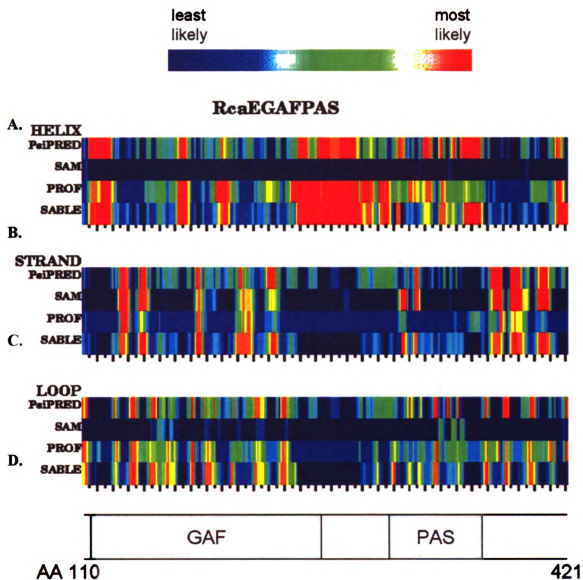


Figure A3.1 Secondary Structure Predictions of RcaE GAF-PAS domains. Secondary structure prediction programs PsiPHRED, SAM, PROF, and SABLE indicate the likelihood of these regions to be comprised of helices, A.) strands B.), connected by loops C.), similar to the DrCBD parent structure. The portion of the RcaE GAF-PAS domain conserved by the prediction servers is indicated in panel D.

A.



B.

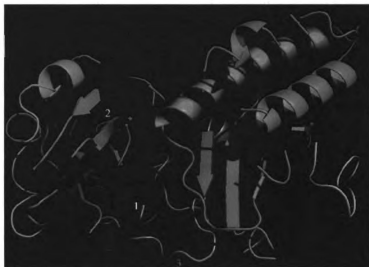


Figure A3.2 PyMOL images of DrCBD and homology modeled RcaE GAF-PAS domains. Homology modeling was completed using the published structure of the DrCBD (1ZTU) as a model A). The structure of truncated RcaE consisting of the GAF and PAS domains was predicted and modeled with residues of interest highlighted in white or pink B.) High-lighted in white: 1, Y137; 2, C198. High-lighted in pink: PAS domain residues 310-319.

REFERENCES

1. **Altschul, S. F., T. L. Madden, A. A. Schaffer, J. Zhang, Z. Zhang, W. Miller, and D. J. Lipman.** 1997. Gapped BLAST and PSI-BLAST: a new generation of protein database search programs. *Nucleic Acids Res* **25**:3389-402.
2. **Bordowitz, J. R., and B. L. Montgomery.** 2008. Photoregulation of cellular morphology during complementary chromatic adaptation requires sensor-kinase-class protein RcaE in *Fremyella diplosiphon*. *J Bacteriol* **190**:4069-74.
3. **Chiang, G. G., M. R. Schaefer, and A. R. Grossman.** 1992. Transformation of the filamentous cyanobacterium *Fremyella diplosiphon* by conjugation or electroporation. *Plant Physiol. Biochem.* **30**:315-325.
4. **Wagner, J. R., J. S. Brunzelle, K. T. Forest, and R. D. Vierstra.** 2005. A light-sensing knot revealed by the structure of the chromophore-binding domain of phytochrome. *Nature* **438**:325-31.
5. **Wagner, J. R., J. Zhang, J. S. Brunzelle, R. D. Vierstra, and K. T. Forest.** 2007. High resolution structure of *Deinococcus* bacteriophytochrome yields new insights into phytochrome architecture and evolution. *J Biol Chem* **282**:12298-309.

Secondary Structure Prediction Servers

1. **Adamczak, R., A. Porollo, and J. Meller.** 2004. Accurate prediction of solvent accessibility using neural networks-based regression. *Proteins* **56**:753-67. (SABLE)
2. **Adamczak, R., A. Porollo, and J. Meller.** 2005. Combining prediction of secondary structure and solvent accessibility in proteins. *Proteins* **59**:467-75. (SABLE)
3. **Karplus, K., C. Barrett, and R. Hughey.** 1998. Hidden Markov models for detecting remote protein homologies. *Bioinformatics* **14**:846-56. (SAM)
4. **McGuffin, L. J., K. Bryson, and D. T. Jones.** 2000. The PSIPRED protein structure prediction server. *Bioinformatics* **16**:404-5. (PSI PHRED)
5. **Porollo, A., Adamczak, R., Wagner, M., and Meller, J.** 2003. Maximum Feasibility Approach for Consensus Classifiers: Applications to Protein Structure Prediction. CIRAS (conference proceedings). (SABLE)
6. **Rost, B., G. Yachdav, and J. Liu.** 2004. The PredictProtein server. *Nucleic Acids Res* **32**:W321-6. (Prof-Sec)

7. **Wagner, M., R. Adamczak, A. Porollo, and J. Meller.** 2005. Linear regression models for solvent accessibility prediction in proteins. *J Comput Biol* **12**:355-69. **(SABLE)**

Homology modeling was done with the guidance of Dr. William Wedemeyer and using www.proteins.msu.edu

MICHIGAN STATE UNIVERSITY LIBRARY



3 1293 03063 199